Approaches for Improved Brain-Machine Interface Control Using High-Density Magnetoencephalography

DISSERTATION

zur Erlangung des akademischen Grades

Doktoringenieur (Dr.-Ing.)

angenommen durch die Fakultät für Informatik
der Otto-von-Guericke-Universität Magdeburg

von Dipl. Inf. Christoph Reichert

geb. am 07.01.1977   in Wippra

Gutachterinnen/Gutachter

Prof. Dr. Rudolf Kruse
Prof. Dr.-Ing. Hermann Hinrichs
Prof. Dr. Martin Bogdan

Magdeburg, den 01.12.2016

Zusammenfassung

Die Entwicklung von Hirn-Maschine Schnittstellen (engl.: Brain-Machine-Interface, BMI), ein interdisziplinärer Forschungsbereich aus Neurowissenschaften, Elektrotechnik und Informatik, gewinnt stetig an Bedeutung. Dies liegt vor allem an den mit dieser Technologie neu aufgekommenen Möglichkeiten, Personen mit schweren Schädigungen des zentralen Nervensystems durch Prothesensteuerung zu unterstützen, ihnen Kommunikation zu ermöglichen und klinische Anwendungen zu etablieren. Allerdings ist die Verlässlichkeit von BMI Systemen noch immer unzureichend, obwohl seit mehr als 25 Jahren intensiv in diesem Bereich geforscht wird. Dies liegt hauptsächlich an der Signalqualität der medizinisch risikoarmen Messmethoden. Im Gegensatz zu invasiven Verfahren können damit nur schwache Signale neuronaler Aktivität auf makroskopischer Ebene gemessen werden, die zudem von einem hohen Rauschsignal begleitet sind. Daher ist es nötig, Algorithmen für eine verlässliche Dekodierung zu entwickeln. Eines der Hauptziele der BMI Forschung ist die Entwicklung von Prothesen, die durch Hirnsignale gesteuert werden können, um ausgefallene motorische Funktionen, etwa eines Arms, gelähmter Personen wiederherzustellen. Aufgrund der geringen Informationstransferrate eines nicht-invasiv betriebenen BMIs, ist die kontinuierliche Steuerung eines künstlichen Arms wegen der großen Anzahl zu kontrollierender Freiheitsgrade nicht möglich. In dieser Arbeit werden Strategien untersucht, die es erlauben, mit einem Minimum von Informationstransfer einen Roboter zu steuern, der autonome Aktionen durchführen kann. Für diesen Zweck werden zwei typische Hirnsignale, die abhängig von visuellen Stimuli moduliert werden, untersucht, wobei die Stimuluspräsentation in einer virtuellen Umgebung integriert wurde. In Experimenten, in denen das Magnetoenzephalogramm in Echtzeit ausgewertet wurde, konnte eine mit Hirnsignalen gesteuerte Auswahl eines Objektes für einen späteren Greifprozess erfolgreich demonstriert werden. Anhand dieser Daten konnte ein signifikanter Anstieg des Dekodierungserfolgs gezeigt werden, wenn eine datengetriebene Konstruktion räumlicher Filter angewandt wird. Abschließend wird in dieser Arbeit die Implementierung eines asynchron arbeitenden BMIs vorgestellt, das es ermöglicht, eines von mehreren auswählbaren Objekten von einem intelligenten, virtuellen Roboter greifen und anheben zu lassen. Mit diesem abschließenden Experiment konnte auch gezeigt werden, dass das MEG potenzielle Vorteile gegenüber dem üblicherweise genutzten EEG bietet.

Abstract

As an interdisciplinary field encompassing neuroscience, electrical engineering and computer science, brain–machine interfacing (BMI) constitutes a research area of growing importance. For persons suffering from diseases affecting the central nervous system, new facilities arise with this concept, comprising prosthesis control, communication and clinical applications. However, despite extensive focus in the last 25 years, the reliability of BMI systems remains at an unsatisfactory level. The main reason is the signal quality achieved with measurement techniques involving minimal medical risk. Because only weak signals of macroscopic neural activity can be measured with existing noninvasive techniques, accompanied by a high level of noise, advanced processing algorithms are required to retrieve reliable decoding results. A major goal of BMI development is the brain-controlled use of a prosthetic device, restoring the mobility of paralyzed persons. Due to the low rate of reliable information a noninvasively operated BMI is commonly able to transfer, the continuous control of a prosthetic device, because it is required to have many degrees of freedom, appears to be impossible. In this thesis strategies are investigated, using a minimum of information transfer to control a robotic device, which autonomously performs an action. Two types of brain signals are considered for this purpose, depending on visual stimuli which are presented in a virtual reality environment. In experiments in which the magnetoencephalogram was instantaneously processed, a brain-controlled selection of objects for grasping was successfully performed. A systematic investigation of advanced signal processing and alternative classification techniques revealed a considerable increase of decoding accuracy when data-driven spatial filter methods are applied. Finally, an asynchronously working BMI implementation is introduced, facilitating the grasping and manipulation of one of several objects by an intelligent virtual robot. This final experiment also provides evidence for potential advantages of the MEG over the commonly used EEG.

Contents

1. Introduction

1.1 Aim of the Thesis

A considerable number of patients suffer from neurological disorders which induce severe paralysis. For example, in Germany 196,000 incidents of stroke were registered in 2008 [73]. Also, spinal chord injury can lead to extensive elimination of movement ability. Progressive diseases such as amyotrophic lateral sclerosis even can result in a so-called locked-in state, where no communication is possible due to complete paralysis. In the last decades, a novel technique evolved which provides the potential to restore communication and lost motor functions in paralyzed patients by interpreting brain activity measures [165]. This is achieved by decoding voluntarily modulated brain activity for controlling a device or for generating feedback. Hence, a system following this approach is known as a brain-machine interface (BMI) and brain-computer interface (BCI), respectively. Due to limitations in clinical rehabilitation and advancement of brain imaging techniques, BCI research increasingly moves into the focus of a wide research community. However, several challenges exist with the current state of the art technology. The main challenge is that brain signals are generally contaminated by a high level of noise originating from environmental distortions, disturbances from physiological processes and superimposed brain signals unrelated to the task. Furthermore, the signals of interest can only be acquired from a small fraction of the true network. Electroencephalography (EEG) is the standard technique for noninvasive signal acquisition in BCI research. Although some invasive brain recording techniques provide increased signal quality compared to EEG, and evidence has already shown them to be suitable for prosthesis control [78], the invasive nature of the intervention renders these modalities inapplicable for daily use and entails a high medical risk. In contrast, noninvasive techniques are uncritical for the patient's health but allow only for low information transfer rates and thus, for less reliable control. Since both invasive and noninvasive techniques are expected to achieve further development in the future, the trade-off between benefits and drawbacks have to be considered in future applications.

This work, however, will concentrate on the investigation of advanced approaches in the field of noninvasive BMIs, particularly in electrophysiological data recorded with a high number of sensors.

Although research in the field of BMI started more than three decades ago, developments still occur at a fundamental level and often are only evaluated under optimal laboratory conditions. The aim of this thesis is the development of strategies to extend existing approaches and to improve BMI use for prosthesis control. The most prominent brain signals to be reliably detected on a single trial level and thus commonly used in various paradigms to drive noninvasive BMIs are steady-state visual evoked potentials (SSVEP), the P300 potential and sensorimotor rhythms (SMR). Previous EEG studies based on SMR found support that reliable control with one degree of freedom is possible (cursor left vs right), but this is insufficient for controlling a robot arm with its several joints (shoulder, elbow, hand, etc). Moreover, this approach requires extensive training to appropriately modulate brain patterns, underscoring the need for alternative approaches for noninvasive prosthesis control, explained in the following. This work focuses the development of a BMI, controllable with only a few commands, that can be accomplished with the low information transfer rate of noninvasive modalities, and that can be applied to control an autonomous robotic system. Given the advantage of magnetoencephalography (MEG) over EEG due to its higher spatial and spectral resolution, MEG is the recording technique of choice for the investigations in this work. The high number of stationary sensors in MEG provides fast access to high density electrophysiological data. Therefore, this modality is suited to investigate potential informative brain sources, eventually also measurable in natural environments in the near future with advanced recording systems [181, 193]. Furthermore, well aligned and highly contrasted visual stimuli in a 2D plane, which are typical in common BMI experiments, will be transferred to a 3D virtual environment simulating a real world scenario. Importantly, the overall goal is the implementation of an interface enabling a user to asynchronously control a robot by voluntary brain wave modulation. Specifically, in the BMI implementations presented here, selection commands are triggered by decoding the P300 in one experiment and the SSVEP in another one. The direct comparison between EEG and MEG provides the opportunity to investigate the still open question, which of these methods yields a superior signal for successful decoding.

The main aims of the thesis can be summarized as follows:

- establish paradigms driven by visual stimuli in virtual reality

- exploit low information transfer rate for flexible movements of an actuator

- improve signal-to-noise ratio in high density electrophysiological data

- find optimal parameters for efficient control

- implement a framework for self-paced actuator control

- explore potential advantages of MEG compared to EEG

1.2   Advances in Prosthetic BMI Research

The major effort in movement related BMI control was translating movement related brain activity, commonly SMR, into commands for actuator control. Signals recorded during imagined movement were also decoded from noninvasive EEG to navigate a mobile robot [131] or a wheelchair [130], to control grasping and elbow movement of a robotic arm [142] and to control a hand orthosis [153]. However, the outcome of existing approaches based on SMR is "far from optimal" [130] and requires "some months of training" [153].

In the field of invasive recordings it has been shown that using subdural electrodes, i.e. electrodes with direct contact to brain tissue, arm movement trajectories can be predicted from electrocorticographic signals [158, 182]. Even more highly invasive electrodes (microelectrode array) penetrating the cortical surface of the brain have been used to perform reach and grasp movements of a robotic arm [78]. Although providing more accurate results compared to noninvasive EEG, invasively assessed BMI control is still not sufficiently reliable to be suited for daily use and requires intensive training. Furthermore, the measurement technique is accompanied by high medical risk and is not proved for safe long term use.

The approaches in this work follow the demands of Millán et al. [132] who suggest that BCI prototypes must be combined with assistive technologies, additional control channels must be considered, and development of algorithms is required. They also expect development of novel BCI technology and EEG devices. The review paper shows that current state of the art of noninvasive BCI is still at a laboratory level and requires new approaches to bring BCI technology out of the lab.

Chapter 3 deals with the manifold utilizability of brain-machine interfacing, accordingly providing a detailed overview of the current state of the art in BMI development.

1.3   Relationship of BMI and Mind-Reading

The term mind-reading is frequently used in the context of brain–computer interfacing. In fact, in multi-voxel pattern analysis studies, predicting a perceptual state of a subject by means of functional magnetic resonance imaging (fMRI), researchers were able to decode categories of perceived objects [43, 70], semantic categories of visually presented words [135] and natural photographs [95] from learned brain activity patterns. However, this kind of brain-reading is specialized to the task and therefore is only suited for reading the trained categories. An even stronger proof of reading the mind would be if perception of the environment were not clearly defined. In this respect decoding the actual percept of ambiguous visual stimuli [71, 171] is potentially more strongly related to mind-reading. Also, voluntarily modulated thoughts could be decoded from fMRI patterns such as attention to one of several moving patterns [91] and lie detection [49]. However, all the methods are limited to detecting only one of a few possible brain states. These sufficiently distinct states have to be learned by a machine learning algorithm using many repetitions of a stimulus or task generating prototype patterns of the states.

Thus, the decoding of brain states, which is also the tool in brain-machine interfacing, strongly requires the mindful cooperation of the test person.

Currently, the available technology merely permits us to distinguish a small number of well-defined, deliberately generated thoughts from brain activity recordings with moderate accuracy. Therefore, researchers are still far from the ability to read somebody's mind in the sense that free thoughts can be played back by a machine. The currently existing brain signal acquisition techniques and the limited knowledge of how the brain functions suggest that free thoughts will not be decipherable in the near future. Nevertheless, the ability to voluntarily control an assistive system by modulation of brain activity is a promising facility to enable disabled persons to restore mobility and communication by means of a BMI.

1.4   Outline of the Thesis

In this thesis I report new methods to efficiently decode high-density electrophysiological data for BMI control. A main focus lies on the effective reduction of the input signals by spatial filtering approaches. The optimal set of processing steps and parameters is evaluated using experimental data. Three experiments are employed in total to contribute advances in noninvasive BMI control. Experiments one and two investigate the feasibility to select targets in a virtual reality scenario by decoding brain signals elicited from overt and covert attention, directed to visual stimuli. The findings of the experiments are included in the third experiment which aims at the development of an efficient scheme for asynchronous initiation of robot commands for grasping. This final experiment, designed to require an intelligent, autonomous robot, demonstrates the noninvasive control of an assistive device.

This thesis is structured as follows:

- Chapter 2 outlines the neurophysiological background and presents fundamentals relevant to implement the data analysis performed in this work.

- Chapter 3 gives an overview of diverse variants of BCI applications and implementations. Existing approaches are introduced and the state of the art is illustrated.

- Chapter 4 explains approaches, considered to efficiently control noninvasively driven upper limb prosthetics. Methodological concepts are introduced that successively lead to the final BMI-controlled virtual demonstrator for autonomous grasping.

- Chapter 5 provides information about materials and methodological details of three experiments, performed to investigate the approaches.

- Chapter 6 presents the results of the planned investigations.

- In Chapter 7 these results are interpreted and discussed.

- Finally, in Chapter 8 the findings of this study are summarized and future perspectives are outlined.

2. Fundamentals

2.1 Neurophysiological Background

Controlling computers and machines by deliberately modulating brain activity is the basic principle of a brain–computer interface and a brain–machine interface, respectively. Such control is possible because techniques exist by which brain activity can be appropriately measured. These techniques are commonly restricted to electrophysiological measurement approaches such as electrocorticography (ECoG), EEG and MEG. The measured signal is an effect caused by superimposed electrical dipoles generated in the brain. In this section I will explain the fundamental background of how and where brain activity evolves.

2.1.1 Generation of Measurable Neuronal Activity

The human nervous system is composed of a vast number of special cells, known as neurons. Only the brain consists of approximately 10^{11} neurons [93] that are connected as a complicated network in which they send signals to communicate. Although a variety of neuron types exist, their basic structures are similar. In Figure 2.1 a pyramidal cell, one type of brain neuron among others, is shown with its basic components: cell body, dendrites, axon, and presynaptic endings. The metabolism of the cell takes place within the cell body, which contains the nucleus that holds genetic information. The dendrites commonly form a tree structure, receiving signals from other neurons. Those electrical impulses are transmitted by the axon of a presynaptic neuron. The connections between neurons are called synapses. Hence, the axon's tails are called presynaptic endings and the receiving dendrites are called postsynaptic dendrites. An axon can transmit a signal up to 2 m and branch to several neurons in different locations. The transmitted neuronal signal is known as an action potential.

The basic principle of the generation of an action potential begins at the plasma membrane of the cell body. Here, different electrical potentials are maintained outside and
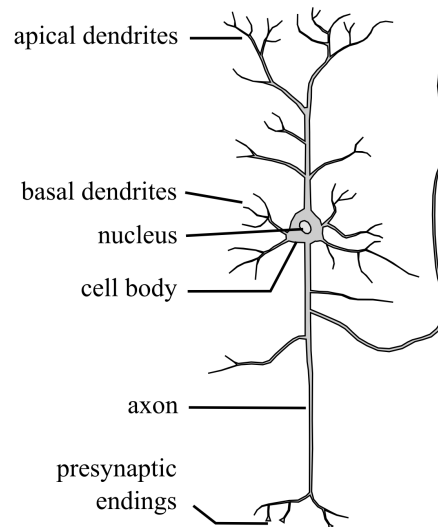
Figure 2.1: Structure of a pyramidal cell.

inside the neuron, resulting in the resting membrane potential. Typically, this potential is about -65 mV inside the neuron with respect to outer potential assumed to be zero. This potential difference is caused by an unequal distribution of positively charged Na^+ and K^+ ions as well as negatively charged amino acids and proteins and by the selective permeability of the cell membrane to K^+ ions. A membrane protein acts as an ion pump, keeping the Na^+ concentration in the cell low and the K^+ concentration high. Additionally, ion channels in the membrane that permit a much higher permeability to K^+ than to Na^+ ions cause the K^+ ions to leave the cell according to the gradient of concentration, resulting in a negative charge on the inner side of the membrane and a positive extracellular charge. When the neuron's membrane potential is reduced due to an excitatory event, Na^+ ions tend to flow into the cell, neutralizing the charge and even resulting in a positive charge of about 35 mV. Thus, an action potential of approximately 100 mV is generated. The action potential is conducted by the axon to another neuron or other cells (such as muscles) according to the all-or-none principle, meaning that the amplitude is maintained while it is propagated fast to its destination. The duration of an action potential is about 1 ms. At the presynaptic endings, neurotransmitters are released that serve as the input signal for the postsynaptic cell.

Typically, a single event processed in the brain induces activation of thousands of neurons that fire synchronously or consecutively. The neurons involved are dispersed over wide networks in the brain to enable functional organization of bottom-up and top-down processes and are organized in local clusters. Typically, specific functional processes in the brain can be attributed to parts of gyri and sulci (explained in Section 2.1.2) that represent general landmarks of the human brain. These circumstances facilitate the ability to measure localized brain activity accompanying neurophysiological processes. In a specific volume of brain tissue, all the electric currents that arise from cellular processes are superimposed, generating a potential with respect to a reference potential and inducing a magnetic field, respectively. This forms the basis of electrophysiological
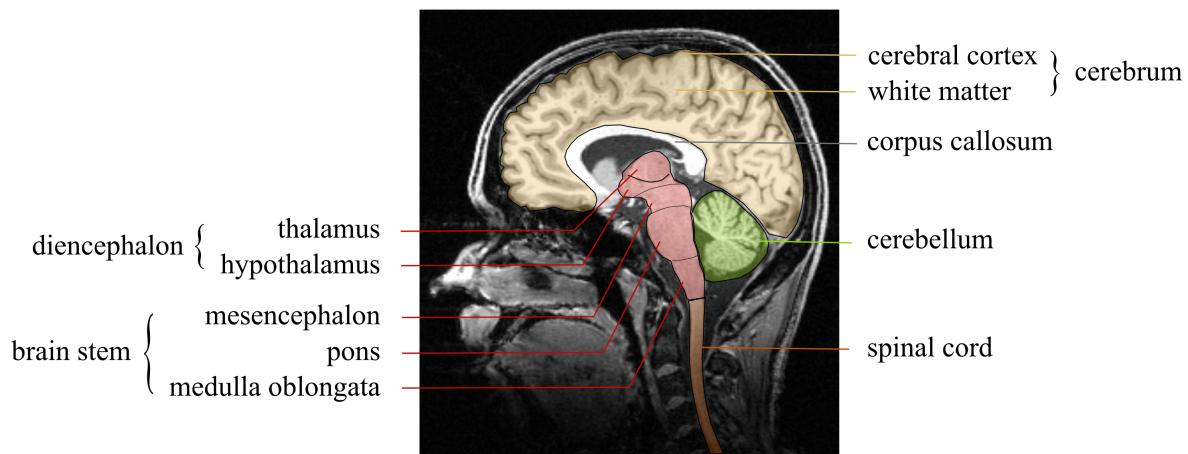
Figure 2.2: MR image showing a sagittal slice near the interhemispheric cleft. Parts of the central nervous system are marked by colored overlays.

measurement modalities, such as local field potentials, EEG and MEG. An introduction of modalities is given in Section 2.2 and a comparison with context to BCI in Section 3.2.

2.1.2 Functional Organization of the Brain

When we speak of the brain, usually the two cerebral hemispheres with their folded surface come to mind. In fact, the brain activity that we measure for BCI use, mainly does have its sources in the cerebrum. However, there are other important structures that are part of the human central nervous system, all with indispensable functionality. One of these components is the spinal cord, containing afferent and efferent pathways, i.e. the nerve tracts conducting signals from and to muscles and internal organs. The brain stem receives sensory information, contains motor neurons controlling head and neck muscles and plays a coordinating role for some sensory modalities and attention. Furthermore, the brain stem is involved in regulating vital functions as blood pressure and respiration. Another important brain structure is the cerebellum, which coordinates sensory information and motor functions, and so organizes movements and posture. Regions of the mesencephalon (midbrain) play an important role in eye movements and control of skeletal muscles as well as relaying auditory and visual signals. The diencephalon (interbrain) is composed of the thalamus and hypothalamus, responsible for coordinating sensory and motor information as well and having extensive connections to the cerebral cortex and the midbrain. Finally, the cerebral hemispheres consist not only of the cerebral cortex (gray matter) and the white matter but also include some subcortical nuclei and structures: the basal ganglia, the hippocampus and amygdala. Most axons that connect the two hemispheres run through the corpus callosum. In Figure 2.2 the locations of the main structures are shown, overlaid on a sagittal slice of an MR image.

The folding of the cerebral cortex results in inward folds (sulci) and outward folds (gyri). Large sulci divide the cerebral cortex into four lobes, all containing functional
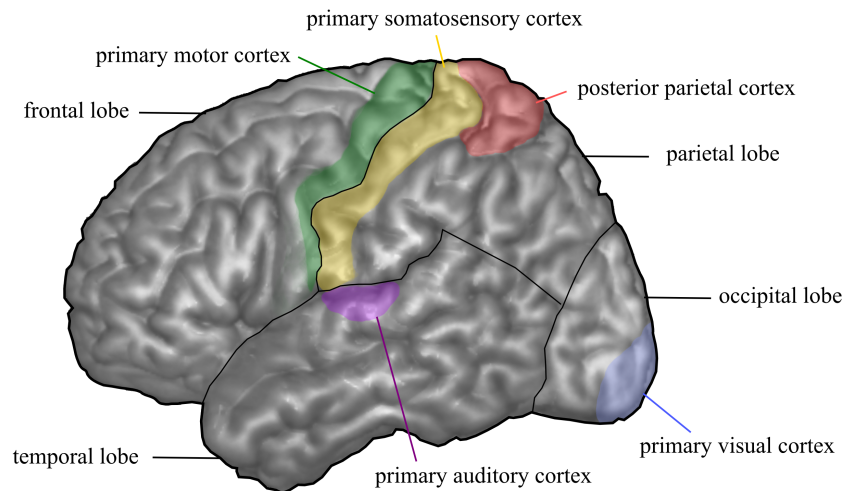
Figure 2.3: The four lobes, and the location of functionally specialized areas frequently approached in BCI control.

regions, specialized for particular functional processing and responsible for our cognitive abilities. See Figure 2.3 for the partitioning of the frontal lobe, temporal lobe, parietal lobe and occipital lobe. Importantly, sensory information and motor processes are primarily represented in the hemisphere contralateral to the side where sensation or movement takes place. Furthermore, although several regions exist where processing of left and right input and output is positioned symmetrically on the hemispheres, either hemisphere is also specialized for some functions (e.g. language processing). For the control of a BCI, focus is placed commonly on only a few prominent areas, which are considered to generate a control signal. One such ares is the primary motor cortex which is located on the gyrus precentralis, anterior to the sulcus centralis, which separates frontal and parietal cortex. The somatosensory cortex, located on the gyrus postcentralis, i.e. posterior to the sulcus centralis, on the parietal lobe, is also utilised. The motor cortex may be further partitioned into areas presenting several individual body parts. The location of these regions on the exterior surface of the cerebral cortex aids decoding of movement related brain activity. The primary auditory cortex in the temporal lobe and the primary visual cortex in the occipital lobe provide feasible access to the early processing of sensory input signals. Finally, the posterior parietal cortex and the frontal cortex play an important role in BCI implementations based on the detection of volitionally induced event-related potentials (see Section 3.3).

2.2 Brain Signal Acquisition Techniques

In the last decades several brain imaging techniques have been developed, which rely on different physical and biochemical properties that accompany neural activity in the brain. Acquisition techniques can be divided into two categories exploiting two dissimilar effects, one of which is the hemodynamic response. When a large population of

neurons is firing, the blood flow around this population increases and enhances the concentration of oxyhemoglobin and concurrently reduces the level of deoxyhemoglobin. On the one hand the oxygenation level changes the magnetic properties of the local cerebral blood flow which can be measured by functional magnetic resonance imaging (fMRI) [7]. This concept is called blood oxygenation level dependent (BOLD) contrast [145]. In fact, fMRI provides excellent spatial resolution and consequently precise localization of neural activation, but the hemodynamic response function (HRF) is slow, showing its peak between 4 and 6 seconds after the activation occurred. This delay combined with poor time resolution and the constrained measurement process in a shielded laboratory, mean that fMRI offers only limited application in BMI, although real-time fMRI has a wide field of interest as well [171, 179, 219]. On the other hand, the variation of the oxygenation level can be optically measured using near infrared spectroscopy (NIRS). The mobility and noninvasiveness of this technique is clearly an advantage but in addition to the poor temporal resolution caused by the HRF, the user is faced with a poor spatial resolution as well, which renders this method of low interest for BMI as well.

A second effect exploited by brain signal acquisition techniques is based on electrophysiological properties, i.e. the electrical potential differences and magnetic flux variation that result from increased and decreased neuronal firing as described in the previous section. While magnetic fields are solely measured noninvasively above the scalp using the MEG, electrical activity can be measured at several levels of spatial accuracy and signal strength, although some of them require invasive intervention. The highest spatial resolution provides single neuron recordings and local field potentials (LFP), which are measured within the cortex tissue [33]. The electrocorticogram is measured beneath the skull, either epidurally or subdurally [183]. The only noninvasive technique for acquiring electrical potentials is the EEG, which is recorded from the surface of the scalp, but is faced with the highest signal loss due to the skull and other tissues being between the sources and the sensors. The modalities used in this work are EEG and MEG, which is why I will describe these techniques more detailed in the following.

2.2.1 Electroencephalography

The existence of cortical electrical oscillations was already known at the end of the 19th century. Inspired by these findings from animal experiments, Berger [10] measured the first human electroencephalogram in 1924. He discovered that a rhythmic oscillation of about 10 Hz can be measured from the human cortex using an oscillograph. Today, this rhythm is well known as alpha waves (8–12 Hz) which are prominent in relaxation and are considered a fundamental rhythm at rest. Later, further rhythms were classified and can be attributed to cognitive states and functional processing, respectively. These are delta waves (below 4 Hz), which are often associated with deep sleep, theta waves (4–8 Hz), which are often related to learning and memory processes as well as sleep, beta/high beta waves (12–40 Hz), occurring during mental activity and gamma/high gamma waves (40–100 Hz) involved in learning, memory and information processing. It is important to understand, that these oscillations are macroscopic observations that
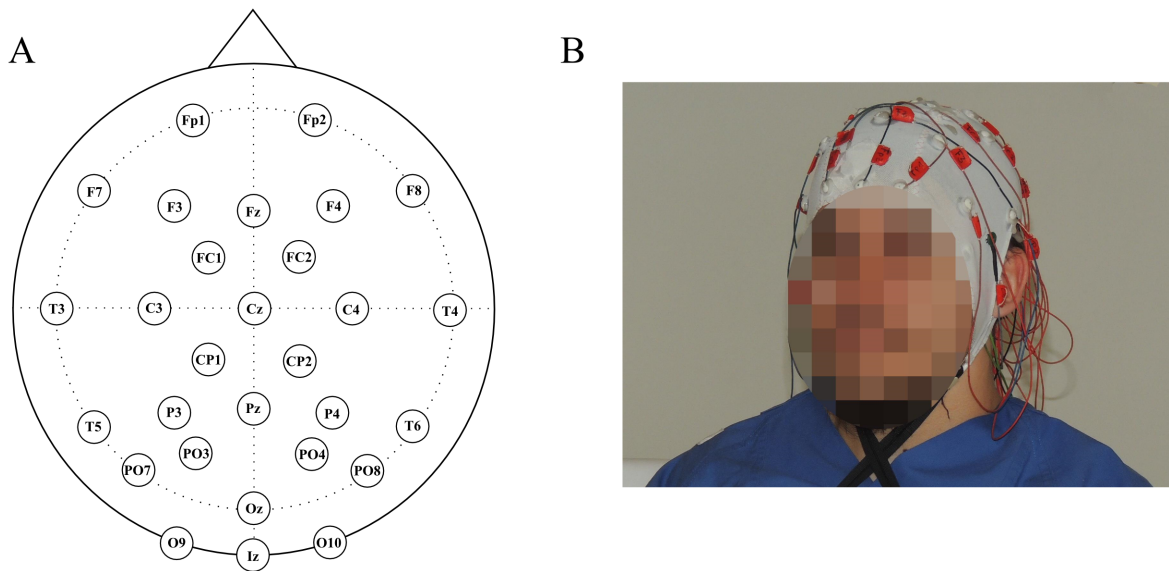
Figure 2.4: Sample of a standardized EEG montage (A). Electrodes are placed on a subject's scalp (B).

occur simultaneously, but vary in their amplitude at different spatial and temporal locations, depending on the tasks the brain is processing. Furthermore, the set of cognitive functions related to the different frequency bands is much wider than outlined above.

Noninvasive EEG signals are typically measured using silver chloride electrodes that are connected with the scalp by applying a conductive gel, which provides a constant reference potential to ensure a stable signal given the high impedance. The electrical potential at the electrode's position is measured relative to a reference electrode, attached distantly from the region of interest (e.g. over the mastoid process or at the ear lobe). A cap with standardized positions helps to generalize and reproduce the measurements over several sessions and between subjects. The skull, the cerebrospinal fluid, the dura mater and other tissues affect the spectral bandwidth and the spatial resolution of electrical potentials recorded from the scalp surface, blurring the signals. Thus, commonly 19 to 32 electrode positions distributed over the head, based on the 10–20 system, are sufficient to acquire scalp EEG recordings. Nevertheless, high density EEG montages of 64 up to 128 electrodes aid to improve the measurement by taking multiple simultaneous measurements of one signal source into account. Figure 2.4 shows an example set-up using standardized positions and labeling. Even numbers refer to the right hemisphere while odd numbers refer to the left hemisphere. Furthermore, F stands for frontal lobe, T for temporal lobe, P for parietal lobe, O for occipital lobe, C for central sulcus, z for zero and Fp for frontal polar, respectively.

EEG is widely used for clinical purposes such as diagnosis of brain disorders, sleep monitoring or localization of an epileptic focus. In research, it provides an important application for investigating brain processes. In addition to the spectral properties

that characterize brain processes, the event related potential (ERP) is the major phenomenon of investigation. An ERP is a typical low-frequent response to a stimulus that can be measured at certain EEG electrode positions. However, the signal-to-noise ratio of an EEG signal is too low to prove the existence in a single measurement interval. Thus, typically a considerable number of repetitive measurements is made after presenting the same stimulus and averaged afterwards. However, in recent decades the detection of ERPs and spectral changes in single recording intervals has been increasingly investigated using advanced preprocessing and feature extraction techniques as well as machine learning algorithms. Such pattern recognition approaches provide the basis for controlling a BCI, which has frequently been approached using EEG due to its obvious advantages regarding mobility and noninvasiveness (see Chapter 3).

2.2.2 Magnetoencephalography

Closely related to EEG, magnetoencephalography (MEG) is another noninvasive measurement technique, recording the magnetic fields induced by electrical currents resulting from neural activity. The development of the method began its course with the first measurement of magnetic fields of the human brain by Cohen in 1972 [41]. Because the magnetic fields that accompany brain activity are very weak, in the range of 10^{-13} Tesla, highly sensitive sensors are required and measurements have to be performed in a magnetically shielded room. Biomagnetic fields are measured by magnetometers, which measure the entire magnetic field variation at their positions and by gradiometers, which measure the gradient of the magnetic field, which is much higher for nearby sources than for distant sources and thus insensitive to background noise from outside the lab. In MEG the signals detected from superconducting detection coils are amplified by superconducting quantum interference devices (SQUID). Both measurement units only function properly at cryogenic temperatures and therefore are mounted in a dewar that stores liquid helium. The helmet-like part of the dewar is positioned directly over the subject's head. The detection coils are distributed over the head in a shape such that they are located approximately 2 cm away from the scalp when the subject is placed for measurement.

Although MEG provides a comparable temporal resolution to EEG and measures an effect that is proportional to electrical currents, there are important differences between the methods. First of all, in contrast to electrical potentials measured from the scalp, the magnetic fields are only minimally disturbed by fluids, bone and tissue. Therefore, the signals are less blurred and can be detected with higher spatial resolution, using denser sensor arrays. The absence of a filter effect induced by volume conduction also means that higher frequencies can be registered. Secondly, the locations of the responsible sources, for simplicity often assumed to be dipoles, are distinct in EEG and MEG. The reason is the sensitivity of either method to the orientation of the sources. In the brain, neurons are situated in the cerebral cortex, also known as gray matter, where they are arranged perpendicularly to the surface. Since the cortex is folded forming gyri and sulci, the orientation of a neuron depends on its position. Due to the orthogonal orientation of the magnetic field relative to the dipole direction, EEG and MEG field
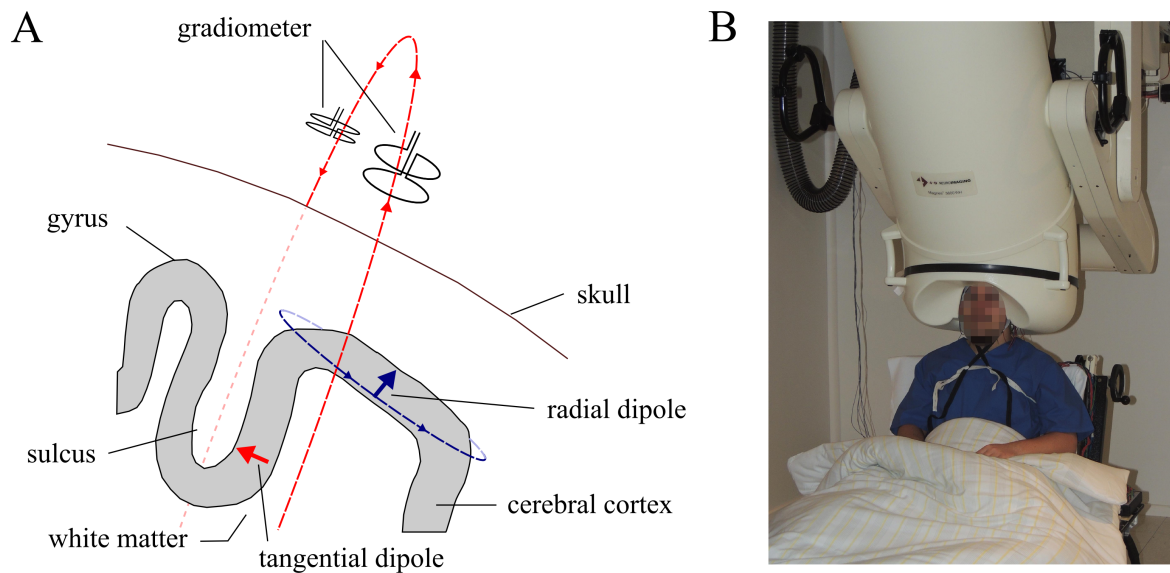
Figure 2.5: Principle of MEG measurement (A). MEG Dewar positioned over a subject (B).

distributions of a dipole are mutually orthogonal. According to the physical principle of magnetic field orientation relative to current orientation, the MEG is mainly sensitive to currents directed tangentially to the head surface, while radially directed currents can not be registered by the signal detection coils. In contrast, the EEG measures both electrical potentials originating from radially and from tangentially oriented currents but mainly from radial. Consequently, MEG registers activity of neurons located in fissures (sulci) but EEG measures electrical activity of neurons located primarily on the outer portion of cerebral cortex (gyri). For this reason, MEG not only measures similar activity with higher spatial resolution but also complements EEG investigations that fail to acquire signals sufficiently from within sulci and deeper brain regions. See Figure 2.5 for a demonstration of the MEG measurement principle. Dashed lines indicate magnetic field lines of the dipoles. Note that in the figure one detection coil is located in front of the depicted slice, measuring the outgoing magnetic field lines and the other coil is located behind the slice, measuring the ingoing magnetic field lines. Therefore, the measured signal change is inverted in either SQUID. This circumstance produces different signal distributions compared to EEG and is thus important for the interpretation of topographic maps.

2.3 Single-Trial Brain Signal Decoding

In classical neuroscience evidence for a theory is obtained by statistical testing of brain processes measured during distinct conditions. Generally, to obtain a sufficient test distribution for deriving statistically significant differences, a high number of trials is required in which the same task is repeatedly performed. However, in the last decades there has been growing interest in alternative analysis methods, yielding new oppor-

tunities to investigate brain function. Machine learning techniques provide interesting novelties to the field such as the multivariate view on the data rather than univariate significance calculations. Furthermore, the classification of single trials into one of several categories provides a direct measure for evaluation of separability of the investigated data. Most importantly, the possibility of deriving decisions, recognized in single data segments, facilitates the ability to provide neuro-feedback in real-time.

In order to control a BCI, the recorded brain signals have to be processed instantaneously. After extracting appropriate features that discriminate between brain states, these features can be used to represent the input space for a decoder function. For this purpose, statistical learning or machine learning techniques are applied.

Here I will briefly formally define supervised learning, which is the concept behind most classifiers applied in this work. A classifier learns some function $f(\mathbf{x}_i, \boldsymbol{\alpha})$ that maps input data $\mathbf{x}_i \in \mathbb{R}^N$, $i = 1, \ldots, l$ given a set of parameters $\boldsymbol{\alpha}$, to a set of c class labels $y_i \in \{1, \ldots, c\}$, where $\mathbf{x}_i$ is an input vector, N is the number of variables, also known as features, and l is the number of observations. The learning process is termed training, because data with known class labels are provided to construct the model. The class label $\hat{y}$ of a test data vector $\hat{\mathbf{x}}$ can then be determined by application of the learned model, which operates as a decision function:

$$\hat{y} = f(\hat{\mathbf{x}}, \boldsymbol{\alpha}) \tag{2.1}$$

One category of classifiers widely used in neuroscience is constituted by classifiers constructing a linear decision surface in the N-dimensional space, i.e. an $(N-1)$-dimensional linear hyperplane. These classifiers have in common that they can be defined by the linear discriminant function

$$y = \mathbf{w}^\mathsf{T}\mathbf{x} + b_0. \tag{2.2}$$

where $y = 0$ defines the hyperplane, and $y < 0$ denotes that $\mathbf{x}$ lies on one side, and on the other side if $y > 0$. The weight vector $\mathbf{w}$ and the bias parameter b_0 offer some useful properties. First of all, b_0 can be considered a threshold parameter that separates $-\mathbf{w}^\mathsf{T}\mathbf{x}$ into two classes. Geometrically, b_0 defines the normal distance from the origin to the hyperplane by

$$d = \frac{b_0}{\|\mathbf{w}\|}. \tag{2.3}$$

Furthermore, the hyperplane is oriented orthogonally to the weight vector $\mathbf{x}$. The perpendicular distance of a data point $\mathbf{x}$ from the hyperplane can be calculated as

$$r = \frac{\mathrm{sign}(y)(\mathbf{w}^\mathsf{T}\mathbf{x} + b_0)}{\|\mathbf{w}\|}. \tag{2.4}$$

The difference between the different approaches to construct linear classifiers is the algorithm that determines the weight vector $\mathbf{w}$ and the bias b_0. From the definition in Equation 2.2, it is obvious that linear classifiers are primarily suited to discrimination in binary classification problems.

2.4 Signal Processing

An essential factor for successful recognition of brain activity on a single trial basis, as required for BCI control, is the extraction of appropriate features, providing sufficient information to discriminate the control commands. Likewise, machine learning techniques often depend on sparse feature spaces in order to find generalizable solutions. This requires effective feature extraction, and a reduction of features. Often a substantial reduction of features can be achieved at the signal processing stage, where irrelevant and redundant features are removed. Generally, there are several basic steps that have to be applied to electrophysiological data, being commonly heavily contaminated with noise and artifacts. In the following sections I will describe some basic signal processing steps required in most BCI applications and largely applied in this work.

2.4.1 Preprocessing

Depending on the features on which the focus is placed for driving a decoding algorithm, essential preprocessing steps are required to remove unwanted content in the time varying signal. When processing signals representing electrical potentials, like EEG and ECoG, the potentials are measured relative to a reference potential. There are several possibilities for calculating re-referenced signals, in order to remove background noise. The method applied depends on the expected brain dynamics. Theoretically, all electrical charges within the brain sum up to zero. Provided a sufficient number of electrodes is available, the common signal over all electrodes represents background noise. Thus, in those measurements, especially in ECoG, this common signal is removed from each channel such that each channel primarily provides local signals rather than also involving global signals. This method is referred to as removing the common average reference (CAR). In the case in which a localized activity is of interest, differential signals between two electrodes are used, which can be calculated by simple subtraction of the two signals leading to bipolar signals. Several other methods of removing location dependent signal content are conceivable. This topic is closely related to spatial filtering, which is discussed in Section 2.5.1. In MEG, special reference sensors are available, which register environmental noise, considering magnetic field lines of several orientations. An algorithm for canceling out noise in MEG recorded with those reference sensors is provided in [177].

When analyzing brain activity, one is interested in the fluctuation of the signal in response to an event or dependent on a state. The channel signals obtained in EEG and MEG generally contain a constant signal offset, which is a multiple of the fluctuations. In some cases, it is an essential step to remove this DC offset of each channel. This operation can be performed without information loss in all cases. The DC offset is

removed by subtracting the signal averaged over a baseline interval, whose length and position relative to the processed interval depends on the task to be analyzed.

A further effective method for removing noise is the spectral filtering of a signal interval, where hypothetical or empirical knowledge is required. A basic step is to remove the line noise, which is done by applying a notch filter with cutoff frequencies around the line frequency and possibly also further harmonics. When analyzing event-related potentials, slow signal drifts are removed using a high-pass filter, and high frequencies by using a low-pass filter. Applying both cutoff frequencies simultaneously is known as a bandpass filter. With a spectral filter, signal changes assumed to be unrelated to the process can be removed. Finally, if a reduction of features is of interest, or the sampling rate is unnecessarily high compared to the low-pass cutoff frequency, down-sampling the signal to a lower sampling rate can be advantageous.

Finally, several kinds of artifacts play an important role in preprocessing electrophysiological data. Eye movements and muscle activity constitute the main sources of artifacts. For the investigation of neural processing these artifacts are often rejected by visual inspection. However, a BCI ought to deal autonomously with all kinds of signal distortions, without requiring additional input from an expert. A frequently applied method for artifact rejection is based on independent component analysis (ICA), where the signal is separated into several components assumed to originate from independent sources. However, the computational effort for this algorithm is high, and the reliability of this approach for removing solely the artifacts is questionable. A simpler approach is to exclude intervals from the training set that exceed a specific threshold in terms of amplitude or signal variance. Taking the artifact problem into account in the design of BCIs, it is of substantial importance to apply an algorithm that is capable of dealing with outliers in the data.

2.4.2 Event-Related Potentials

One characteristic of the brain is that macroscopic processing of controlled stimuli is detectable in electrophysiological signals as potential changes relative to a resting potential. These potential changes, also referred to as event-related potentials (ERPs) emerge as a typical pattern after stimulus presentation, often at several stages of processing at different locations. The occurrence of ERPs is usually in the range of tens to hundreds of milliseconds. For clear identification of an ERP, the channel data are adjusted such that a baseline interval, usually prior to the stimulus event, has zero mean. By conversion, positive and negative evolutions relative to a baseline potential are denoted with the letter P or N respectively, followed by a number indicating the time in ms or the number of the occurrence. Two prominent examples are the visual N1, occurring approximately 100 ms after a visual stimulus reaches the retina, and the P300 (see Figure 2.6 for an idealized depiction). A common approach in traditional statistical analysis is to average several hundred intervals, recorded after the same type of stimuli, to reveal significant results. In single trial analysis, as performed with BCIs, the reliable detection of an ERP is challenging, which is why several epochs usually
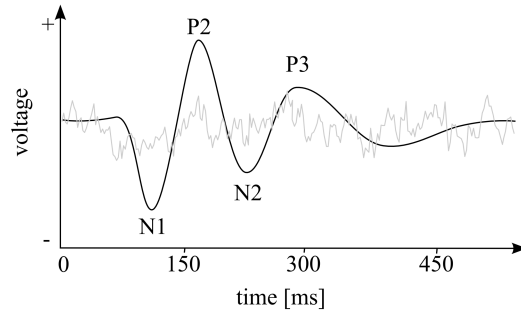
Figure 2.6: Schematic representation of an ERP.

are averaged before a decision is made. A realistic time course of a single trial EEG measurement is shown in Figure 2.6 as grey line. The challenge is to decide whether or not this curve is related to the expected ERP. Features that can be extracted from ERP measurements include spatial and temporal locations of extrema, the slope and average of hypothetically defined time segments, and template matching measures such as the Pearson correlation coefficient.

2.4.3 Frequency Analysis

As stated in Section 2.2.1, brain processes are accompanied by task-specific patterns of spectral activity, measurable in a frequency range of up to 200 Hz. Even when the brain is in a resting state, during relaxation and during sleep, there is a wide spectrum of oscillating activity all over the brain. The fact that event related synchronization (increase) and desynchronization (decrease) of specific frequencies at different locations compose a characteristic pattern according to a stimulus or task, renders the frequency domain a promising representation of features for classification of brain processes.

There are many approaches that have been developed for estimating the spectral density of a time series signal, ranging from parametric techniques such as the autoregressive model to non-parametric techniques, which are generally based on Fourier analysis. The basic approach is to estimate the spectrum using the squared discrete Fourier transform given by:

$$F(f) = \frac{\Delta t}{N} \|\sum_{n=1}^{N} x_n \mathrm{e}^{-2\pi i f n}\|^2 \tag{2.5}$$

where x_n is the nth value of the signal, Δt is the reciprocal sampling rate and frequency f is limited by the Nyquist frequency, which is half of the sampling rate. Several advanced spectral estimation techniques aim to reduce the shortcomings of this approach, frequently combining Equation 2.5 with window functions to reduce spectral leakage. Furthermore, reduction of variance of the spectral estimate is achieved for instance by combining multiple segments of the signal (Bartlett method) or multiple orthogonal window functions (Multitaper method). Because each of the various methods has its advantages and disadvantages, which method is the best choice depends on the signal characteristics that are the focus of the analysis.

2.5 Feature Extraction Techniques for Brain Signals with High Time Resolution

2.5.1 Spatial Filtering

In analysis of brain signals, one often is faced with activations that are distributed over several locations and are simultaneously distorted by diverse types of noise. A proven method for enhancing the signal-to-noise ratio is the application of spatial filters. For instance, in the field of magnetic resonance imaging, it is a common procedure to smooth the 3D-volume by applying a Gaussian filter, which is a well-known smoothing technique in conventional image processing. Furthermore, in EEG analysis a Laplace filter often is applied to extract local activity. This kind of filter is also adopted from conventional image processing, where it is primarily applied for edge detection. Several other methods exist for feature extraction from measured brain signals. I will introduce some of them in the next sections. In general, a spatial filter is a set of coefficients, which generate the filtered signal by composing the weighted sum of a set of values, originally distributed over several locations. Let $\mathbf{x} \in \mathbb{R}^C$ be a set of values measured at C spatial locations at an arbitrary point in time. The filtered signal $\hat{\mathbf{x}} \in \mathbb{R}^D$ is calculated as

$$\hat{\mathbf{x}} = \mathbf{W}^\intercal \mathbf{x} \tag{2.6}$$

where matrix $\mathbf{W} \in \mathbb{R}^{C \times D}$ is a set of D spatial filters $\mathbf{w}_j \in \mathbb{R}^C$, $j = 1, \ldots, D$. Consequently, the values in $\hat{\mathbf{x}}$, interpretable as filtered channels, are linear combinations of the values in $\mathbf{x}$ of all channels available. Importantly, the number of spatial filters must not necessarily match the number of sensor locations. Thus, spatial filtering provides not only the cancellation of noise but can also serve to reduce the number of informative signals. The way the values in $\mathbf{W}$ are determined depends on the particular spatial filter method.

2.5.2 Common Spatial Patterns

In the past, the common spatial pattern (CSP) method was frequently used as an optimal spatial filter in the decoding of EEG signals recorded during motor imagery [23, 167]. CSP filtering is actually a supervised method, since the class labeling must be known. The method decomposes the multichannel signals, constructing a filter that separates two classes by maximizing the signal variance of one class and simultaneously minimizing the variance of the other class. Generally, CSP analysis is applied to bandpass filtered signals using apriori knowledge (the frequency band expected to discriminate between the classes) to constrain the signal variation to specific frequencies. However, this step is not mandatory for the mathematical formulation of the method. Let $\mathbf{X}_1 \in \mathbb{R}^{C \times N}$ and $\mathbf{X}_2 \in \mathbb{R}^{C \times N}$ be matrices of N-point time series signals measured at C locations, where $\mathbf{X}_1$ holds measurements from one class and $\mathbf{X}_2$ from another class. Assuming that the matrices are centered, the covariance matrices $\mathbf{R}_1$ and $\mathbf{R}_2$ are given by

$$\mathbf{R}_i = \mathbf{X}_i \mathbf{X}_i^\intercal \quad (i \in \{1, 2\}). \tag{2.7}$$

The spatial filters $\mathbf{W}$ are determined by simultaneous diagonalization, such that

$$\mathbf{W}^{\mathsf{T}}\mathbf{X}_i\mathbf{W} = \mathbf{\Lambda}_i \quad (i \in \{1, 2\}, \mathbf{\Lambda}_i \quad diagonal) \tag{2.8}$$

and

$$\mathbf{\Lambda}_1 + \mathbf{\Lambda}_2 = \mathbf{I}. \tag{2.9}$$

The diagonalization can be solved with the generalized eigenvalue problem

$$\mathbf{R}_1\mathbf{w} = \lambda\mathbf{R}_2\mathbf{w}. \tag{2.10}$$

The generalized eigenvectors $\mathbf{w}_j$, $j = 1, \ldots, C$ represent the spatial filters in $\mathbf{W}$, where $\lambda_{i,j} = \mathbf{w}_j^{\mathsf{T}}\mathbf{R}_i\mathbf{w}_j$ correspond to the diagonal elements in $\mathbf{\Lambda}_i$. Importantly, in Equation 2.10, $\lambda = \lambda_{1,j}/\lambda_{2,j}$ and $\lambda_{1,j} + \lambda_{2,j} = 1$, while $\lambda_{i,j} \geq 0$. Consequently, a spatial filter $\mathbf{w}_j$ indicates high variance in the first class and low variance in the second class if $\lambda_{1,j}$ is close to 1 and vice versa. This property is beneficial for discrimination and qualifies CSP as a powerful feature extraction method. Note that although C spatial filter components are calculated ($\mathbf{W} \in \mathbb{R}^{C \times C}$), a selection of a few D components is sufficient in most cases, resulting in $\mathbf{W} \in \mathbb{R}^{C \times D}$. The filtered signal of a sample point can be calculated using Equation 2.6. Usually, a log transformation of the variance of the filtered signal $\hat{\mathbf{x}}$ is used as the feature for classification. Thus, CSP is potentially suited for extracting sparse feature spaces of dimensionality D if spatially distributed, time variant signals for two class problems have to be analysed. However, the CSP method tends to overfit [51] and hence is sensitive to instationarities of brain patterns.

2.5.3   Canonical Correlation Analysis

The Canonical Correlation Analysis (CCA) is a multivariate statistical method developed by Hotelling [87]. A canonical correlation determines the relationship between two sets of variables. Here I refer to the sets as the set of predictor variables and the set of outcome variables. It is an extension of the multiple correlation method which determines the relationship between a set of predictor variables and a single outcome variable, which furthermore is an extension of ordinary correlation. From this point of view, ordinary correlation and multiple correlation can be considered as special cases of canonical correlation.

Let $\mathbf{X} \in \mathbb{R}^{C \times N}$ be a matrix of predictor variables $\mathbf{x}_i$, $i = 1, \ldots, C$ keeping N observations each (e.g. N-point time series measured at C channels) and $\mathbf{Y} \in \mathbb{R}^{H \times N}$ be a matrix of outcome variables $\mathbf{y}_i$, $i = 1, \ldots, H$ keeping N outcomes each (e.g. N-point time series of H model functions). The aim of CCA is to determine two filter matrices $\mathbf{W}_x \in \mathbb{R}^{C \times \min(C,H)}$ and $\mathbf{W}_y \in \mathbb{R}^{H \times \min(C,H)}$ according to Equation 2.6, where $\mathbf{W}_x$ and $\mathbf{W}_y$ are determined such that the correlation $\rho_i(\hat{\mathbf{x}}_i, \hat{\mathbf{y}}_i)$, $i = 1, \ldots, \min(C, H)$ between the ith canonical variables in $\hat{\mathbf{X}} \in \mathbb{R}^{\min(C,H) \times N}$ and $\hat{\mathbf{Y}} \in \mathbb{R}^{\min(C,H) \times N}$ is maximal:

$$\hat{\mathbf{X}} = \mathbf{W}_x^{\mathsf{T}}\mathbf{X} \tag{2.11}$$

$$\hat{\mathbf{Y}} = \mathbf{W}_y^{\mathsf{T}}\mathbf{Y} \tag{2.12}$$

$$\max_{\mathbf{W}_x, \mathbf{W}_y} \rho_i(\hat{\mathbf{x}}_i, \hat{\mathbf{y}}_i) = \frac{E(\hat{\mathbf{x}}_i^\mathsf{T} \hat{\mathbf{y}}_i)}{\sqrt{E(\hat{\mathbf{x}}_i^\mathsf{T} \hat{\mathbf{x}}_i) E(\hat{\mathbf{y}}_i^\mathsf{T} \hat{\mathbf{y}}_i)}}. \tag{2.13}$$

The solution of the optimization problem is closely related to principal component analysis, where data are linearly combined such that variance is maximal in the first principal component. Here, the factorization is performed in parallel for both the predictor variable and the outcome variables, such that the correlation between both principal components is maximal. Since in practice; variance is not explained by only the first component, the remaining variance is explained by further components. This results in $\min(C, H)$ canonical variables and canonical correlations, respectively. The first canonical correlation is that which represents the strongest relationship between the linearly combined predictor variable $\hat{\mathbf{x}}_1$ and the linearly combined outcome variable $\hat{\mathbf{y}}_1$. Each of the vectors in $\mathbf{W}_x$ can be considered as a spatial filter, while the relevance of filter $\mathbf{w}_{x,i}$ decreases with increasing order i of the canonical variable. A comprehensive explanation of the mathematical background of CCA is given in [24].

For feature extraction of time series signals, two approaches for extracting features are conceivable. Either the CCA is applied separately to single trials and the canonical correlation coefficient represents the feature, or the CCA is calculated for a training set of aggregated trials and the spatial filter coefficients in $\mathbf{W}_x$ are used to reduce the number of channels and simultaneously enhance the signal-to-noise ratio.

2.5.4   Minimum Energy Combination

Minimum Energy Combination (MEC) was first proposed in a work by Friman *et al.* [59] for extracting SSVEP features from multiple channels. Similar to the previously described methods, this method calculates weights to determine a linearly combined signal from multiple channels, which can be considered a spatial filter.

Following the definitions of the previous section on CCA, we define $\mathbf{X} \in \mathbb{R}^{C \times N}$ as a matrix of N-point time series $\mathbf{x}_i$, $i = 1, \ldots, C$ measured at C channels and $\mathbf{Y} \in \mathbb{R}^{H \times N}$ as a matrix of H distinct model functions $\mathbf{y}_i$, $i = 1, \ldots, H$. Then the measured signals can be modeled as

$$\mathbf{X} = \mathbf{W}_y^\mathsf{T} \mathbf{Y} + \mathbf{W}_z^\mathsf{T} \mathbf{Z} + \mathbf{E} \tag{2.14}$$

where $\mathbf{W}_y \in \mathbb{R}^{H \times C}$ contains the amplitude coefficients that contribute to the portion with which the modeled signals in $\mathbf{Y}$ are represented in $\mathbf{X}$. Similarly, $\mathbf{W}_z \in \mathbb{R}^{C \times C}$ contains the weights that compose the interfering signals $\mathbf{Z} \in \mathbb{R}^{C \times N}$ in $\mathbf{X}$ and finally, $\mathbf{E} \in \mathbb{R}^{C \times N}$ is a matrix of noise. The idea of MEC is to cancel out the majority of the interfering signals. To achieve this, the potential model signals $\mathbf{Y}$ are first removed from the measured signal $\mathbf{X}$ by orthogonal projection:

$$\tilde{\mathbf{X}} = \mathbf{X} - \mathbf{X}\mathbf{Y}^\mathsf{T}(\mathbf{Y}\mathbf{Y}^\mathsf{T})^{-1}\mathbf{Y}. \tag{2.15}$$

The result is that $\tilde{\mathbf{X}} \approx \mathbf{W}_z^\mathsf{T} \mathbf{Z} + \mathbf{E}$ contains mainly interfering signals and noise. In order to minimize the resulting energy of the combined signals $\mathbf{w}^\mathsf{T} \tilde{\mathbf{X}}$, a weight vector $\mathbf{w}$ must be found by solving the optimization problem

$$\min_{\mathbf{w}} \left\| \mathbf{w}^\mathsf{T} \tilde{\mathbf{X}} \right\|^2 = \min_{\mathbf{w}} \mathbf{w}^\mathsf{T} \tilde{\mathbf{X}} \tilde{\mathbf{X}}^\mathsf{T} \mathbf{w} \tag{2.16}$$

constrained by the assumption $\|\mathbf{w}\| = 1$. The optimization can be solved by determining the eigenvalues of $\tilde{\mathbf{X}}\tilde{\mathbf{X}}^{\intercal}$. The solution is the eigenvector $\mathbf{v}_1$ corresponding to the smallest eigenvalue λ_1. Since the eigenvectors $\mathbf{v}_1, \ldots, \mathbf{v}_C$ are orthogonal, the signals in $\tilde{\mathbf{X}}$ are uncorrelated. Furthermore, the energy represented by $\lambda_1, \ldots, \lambda_C$ increases. Note that the lowest energy in λ_1 is determined by components containing the lowest amount of interfering signals. Thus, the first D eigenvectors represent the components removing most interfering signals. Normalizing the eigenvectors to equal energy, the spatial filter matrix $\mathbf{W}$ is obtained by

$$\mathbf{W} = (\frac{\mathbf{v}_1}{\sqrt{\lambda_1}} \ \ldots \ \frac{\mathbf{v}_D}{\sqrt{\lambda_D}})^{\intercal}. \tag{2.17}$$

Selecting the number of filtered signals D is a matter of empirical selection. A suggestion by Friman *et al.* [59] is to choose D as the smallest number for which the following holds:

$$\sum_{i=1}^{D} \lambda_i > \frac{1}{10} \sum_{i=1}^{C} \lambda_i. \tag{2.18}$$

This approach aims to discard 90% of interfering signals. After applying Equation 2.6, a signal with improved signal-to-noise ratio is extracted for further processing, given the measured signals contain the assumed model function.

2.5.5 Maximum Contrast Combination

An extension of the previously described method is the Maximum Contrast Combination (MCC), which was also introduced in the paper of Friman *et al.* [59]. The idea is to maximize the energy of the modelled signal $\mathbf{Y}$ simultaneously to minimizing the energy of the interfering signals $\mathbf{Z}$ in Equation 2.14. Considering the contrast function

$$\max_{\mathbf{w}} \frac{\|\mathbf{w}^{\intercal}\mathbf{X}\|^2}{\left\|\mathbf{w}^{\intercal}\tilde{\mathbf{X}}\right\|^2} = \max_{\mathbf{w}} \frac{\mathbf{w}^{\intercal}\mathbf{X}\mathbf{X}^{\intercal}\mathbf{w}}{\mathbf{w}^{\intercal}\tilde{\mathbf{X}}\tilde{\mathbf{X}}^{\intercal}\mathbf{w}} \tag{2.19}$$

we obtain the optimization problem of maximizing the generalized Rayleigh quotient of real-valued matrices and vectors. The maximum can be determined by finding the eigenvector with the largest eigenvalue. Thus, a generalized eigenvalue decomposition of the matrices $\mathbf{X}\mathbf{X}^{\intercal}$ and $\tilde{\mathbf{X}}\tilde{\mathbf{X}}^{\intercal}$ reveals the solution of the optimization problem, where the eigenvectors corresponding to the highest eigenvalues define $\mathbf{w}$. The generalized eigenvalue decomposition reveals C eigenvectors, where the vectors corresponding to the D highest eigenvalues are assumed to provide sufficient information to maximize the signal-to-noise ratio. Following the suggestion of Friman *et al.* [59], D is selected by the vectors $\mathbf{v}_i$ that satisfy $\lambda_i > N/(N-H)$, resulting in

$$\mathbf{W} = (\mathbf{v}_i \ \ldots \ \mathbf{v}_C)^{\intercal}, \text{ where } \{i|\lambda_i > N/(N-H)\}. \tag{2.20}$$

After applying Equation 2.6, the filtered signal contains D time series with increased signal-to-noise ratio, given the modeled signals are included in the measured signals. This is achieved by removing interfering signals and simultaneously enhancing the energy of modeled signals, i.e. by maximizing the contrast of an assumed signal and noise.

3. State-of-the-Art in Brain–Computer Interfacing

3.1 Intention of Brain–Computer Interfaces

The term brain-computer interface (BCI) refers to a category of implementations aiming to directly translate brain activity into device commands or feedback presentations. Various fields of applications are in the focus of this research area which emerged about three decades ago. Examples include communication devices for spelling [36, 54, 207] or software control [94, 136, 196], manipulation devices for motor substitution [61, 146], rehabilitation purposes [162], and attention training [117]. Due to the numerous conceivable applications, several synonymic terms exist in the literature, e.g. brain-machine interface (BMI), brain–neural–computer interface (BNCI) or simply neural interface. The general functionality of such a system is shown in Figure 3.1. A BCI can be considered as a closed–loop system: The user volitionally modulates, depending on sensory feedback, his neural activity to induce an intentional action. Brain activity is measured and instantaneously decoded in order to send control signals to an effector. The effector's feedback enables the user to respond appropriately, which closes the loop. The majority of BCI related literature reports findings obtained from offline analyses, where no connection to a brain was established and nothing was fed back. These so called open-loop BCIs investigate potential algorithms and speculate about a possible outcome in a closed-loop system. However, feedback has considerable influence on the course of an experiment, and consequently, the brain signals would differ from the activity used for the simulated system.

The target group of a BCI basically is represented by persons who have lost any ability to initiate muscle activity through the peripheral nervous system. Nevertheless, many approaches depend on minimal peripheral abilities like eye movements or even combine sustained peripheral function and brain activity to develop hybrid systems. Currently, there is strong interest in establishing BCIs in the field of neurorehabilitation (e.g. in

stroke) and neurofeedback (e.g. for treatment of attention deficit and hyperactivity disorders (ADHD) [201]). Thus, the target group is much larger than the commonly referred to locked-in patients. In this work, the focus lies on solutions for complete paralyzed persons and persons with minimally sustained peripheral functions.
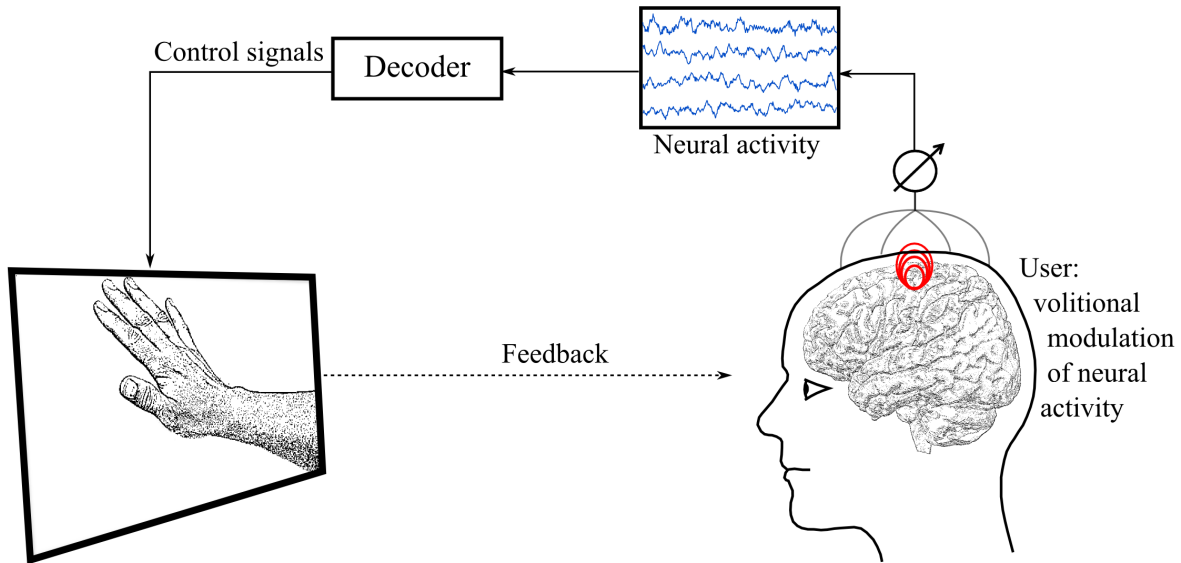
Figure 3.1: Schematic demonstration of a BCI's closed–loop.

3.2   Invasive BCIs and Noninvasive BCIs

Diverse recording techniques exist, and all have advantages and disadvantages. In general, the differences refer to signal quality, temporal and spatial resolution, practicability and medical risks. In order to acquire brain signals in the form of electrical fluctuations with a low signal-to-noise ratio and high spatial resolution, a derivation of electrical potentials directly from the surface of the cortex is required. An even more detailed mapping of neural network activity is provided by microelectrode arrays consisting of microwires. These kinds of electrodes are designed to measure single unit activity (SUA), which means that it is possible to determine the firing rates of individual neurons. Microelectrodes are positioned within the gray matter of the brain, which is why this technique is also termed intracortical recording. While SUA reflects intracellular or extracellular activity of individual neurons, multi unit activity (MUA) is the term for the recording of extracellular action potentials from several neurons in the vicinity of the electrode tip. A third application of microelectrodes is the recording of local field potentials (LFP). In contrast to SUA and MUA, which measure spike signals resulting from neural firings, this modality measures the superimposed electrical activity from a population of neurons in the vicinity of 0.5 up to several millimeters. The disadvantage of these highly invasive techniques is the fact that the brain tissue is penetrated, long-term use has not been approved, and the risk of an infection or

inflammation is extremely high. Due to the high invasiveness of micro electrodes they are, for obvious ethical reasons, mainly applied in animal research. In the field of BCI, spike activity driven manipulator control has been demonstrated with rats [38] and monkeys [34, 210, 220]. Despite the high medical risk, there are also attempts to apply microelectrode arrays for BCI control in humans [78, 79]. However, beside the problem of a sterile signal conduction, the main challenge is the fact that chronic implants suffer from tissue reaction. This means that the brain mounts an inflammatory immune response to foreign materials which causes the reorganization of neurons. Thus, there is considerable effort required in electrode design to establish biocompatibility of cortical electrodes (see Polikov *et al.* [160] for a review). The long term establishment of microelectrode driven BCIs for humans is an ambitious goal of the BrainGate project [194].

A more frequently used invasive intracranial, i.e. derived from inside the skull, measurement technique in humans is the electrocorticography (ECoG). ECoG electrodes are placed directly on the cortex tissue (subdural) or on the dura mater (epidural) which is a membrane enclosing the cerebrospinal fluid. The electrodes are typically arranged as grids or strips with electrode spacings of 1 cm or a few millimeters (high density grids). Thus, the spatial resolution is lower compared to LFP, MUA or SUA recordings. However, a larger part of the brain is covered providing insights into functional connectivity in the brain. Although a relatively large neural ensemble is represented in the electrical activity measured by these kinds of electrodes, the spatial resolution, the spectral bandwidth and the signal-to-noise ratio (SNR) are superior to noninvasive acquisition of electrical activity. Despite the fact that a craniotomy is required to place ECoG electrodes, meaning that a part of the skull is removed, this modality is more and more frequently applied in brain function research studies [45, 46, 58, 133]. However, the ethical limitations are similar to those of microelectrode implants. Experimental investigations with ECoG signals are only possible due to clinical procedures that require such kinds of intervention. For example, monitoring epileptic seizures for surgery planning is one possible clinical requirement for ECoG recordings. Some researchers recognize ECoG as a promising signal platform for BCI [183]. Consequently, there is much effort to use electrocorticographic signals in the field of BCI research in order to exhaust potential access to brain signals [30, 115, 184]. A key feature of ECoG is the advantageous characteristic that extraction of high gamma activity is possible (frequency range between 60 Hz and 150 Hz), which is not, or only with limited success, possible with measurements from the scalp. This kind of activity has been found to accompany many functional processes, like motor execution [45], auditory perception [44] and language processing [52]. Thus, valuable benefits would be available with the ECoG modality for development of BCI systems.

The term noninvasive BCIs refers to implementations that do not rely on measurements that induce any injury. Examples of noninvasive recording techniques include the electroencephalography (EEG), magnetoencephalography (MEG), near-infrared spectroscopy (NIRS) and functional magnetic resonance imaging (fMRI). Although NIRS and fMRI provide very low temporal resolution, there have been considerations of BCI

applications with these kinds of modalities in the past [39, 179]. A much better temporal resolution, which facilitates real-time processing in the sense of the human cognitive processing time scale, is provided by EEG and MEG. Both modalities measure the electrical activity of the brain indirectly by acquiring effects of the superimposed currents of relatively large population of firing neurons. Specifically, as explained in Section 2.2.1, the EEG measures changes in the electrical potential on the scalp surface with electrodes mounted to the skin. In contrast, the MEG measures changes in the magnetic field induced by the currents of electrochemical processes in neurons. The physical relationship between the direction of magnetic field lines and the electrical potentials of a dipole, as well as the theory of current flow in neurons and their alignment in the cortex, implies that EEG and MEG measure complementary signals [68]. The unique advantageous feature of EEG is the fact that this technique is currently the only noninvasive recording technique that provides mobile hardware solutions and is applicable outside a lab. For that reason, most BCI development concentrates on EEG signal acquisition, processing and decoding [123, 132]. However, EEG suffers concurrently from a very low spatial resolution and bad detection of higher frequencies, which have been shown to represent valuable information for BCI control. Reliable BCI control requires control strategies that rely on activations of spatially well-separated brain regions. Furthermore, the low signal-to-noise ratio requires repeated or prolonged execution of the control task to permit reliable detection. Thus, only a very small number of different conditions, obtained during long time intervals, can be distinguished in EEG measurements, leading to a low information transfer rate for the BCI. While the temporal resolution of MEG is comparable to that of EEG at less than 1 ms, the spatial resolution is advantageous in the sense that a denser array of sensors captures less distorted neuronal signals. The distortions in electrical potential recordings on the scalp stem from inhomogeneities in the head, since the different tissues between electrode and cortex have different electrical conductivities. In contrast, the magnetic permeability of these tissues is constant and thus has less influence on the magnetic fields. However, there is controversy in the literature concerning the accuracy of source localization with both modalities. This seems to originate in the methodological approaches applied. Some studies report comparable accuracy between EEG and MEG source localization [42], while others have found EEG to be superior to MEG [120] and vice versa [88, 110], with some able to improve the localization accuracy by combining EEG and MEG sensors [60, 120]. An uncontroversial aspect, however, is the fact that MEG records complementary signals, namely only tangential components of dipoles and no radial components as is the case with EEG. Consequently, MEG could serve to reveal sources not covered by EEG measurements. Nevertheless, due to its high expense and restrictions according to laboratory environments, MEG has rarely been considered for obtaining control signals for BCI [31, 128]. Development of new wearable magnetometers, which already is in progress, as initially demonstrated by Sander *et al.* [181], could change the view MEG, making it a potential modality to be used for BCI control.

In conclusion, the question whether invasive or noninvasive modalities are preferable for a specific BCI remains dependent on the goal of the project. For example, the med-

ical risk of an invasive BCI must be related to the benefit the user could achieve with the system. Finally, all of the recording techniques are accompanied by advantages and disadvantages. Consequently, for all modalities development towards beneficial features could render the technique more attractive for BCI systems. A summary of advantageous and disadvantageous features of modalities considered for BCI development is given in Table 3.1. The spatial resolution shown in this Table is an estimate of the accuracy in determining the source space, which is not necessarily the distance between the sensors. An important fact concerning NIRS and fMRI is that these modalities measure the haemodynamic response rather than electrical activity. Thus, neurofeedback would be delayed by at least four to five seconds. For completeness, the existence of further brain activity recording techniques has to be mentioned, e.g. invasive depth electrodes, noninvasive positron emission tomography (PET), and single-photon emission computed tomography (SPECT). However, these techniques have less importance in BCI development.

Modality	Invasiveness	Time scale	Spatial Resolution	Mobility
SUA	high	<1ms	0.01mm	bedside
MUA	high	<1ms	0.1mm	bedside
LFP	high	<1ms	0.5mm	bedside
ECoG	considerable	1ms	1.25mm	bedside
EEG	none	1ms	10mm	lab/home
MEG	none	1ms	5mm	lab
NIRS	none	0.1s	5mm	lab/home
fMRI	none	2s	1mm	lab

Table 3.1: Features of modalities

3.3 Typical Brain Responses for BCI Control

Although neuroscientific research has identified a large number of brain functions, which have been proved to show specific effects in certain brain regions, only a couple of brain signals are used to control neurofeedback systems. The main reason for the restricted pool of brain signals is that the measured signal must be strong enough to be detectable in single trials or at least in averages over a few trials. The classical approach to provide evidence of brain function is to average hundreds of single trials, recorded over several minutes in order to prove statistical significance of the effect to be verified. In contrast to the statistical approach, single trial analysis provides a direct measure of relevance, namely the accuracy with which a trial can be correctly detected. If this accuracy is too low, reasonable use of a BCI is impossible. A further criterion for a BCI control signal is that the user must be able to voluntarily induce the brain signal (active BCI) or must be able to influence the perception of an external stimulus (reactive BCI). Since those tasks require high attention, BCIs often demand a strenuous cognitive load for users.

3.3.1   Activity Induced by Real and Imagined Movement

Apparently, in the noninvasive domain only a few phenomena meet the previously defined criteria. A well-known idling rhythm of the brain comprises alpha waves, which occur in the frequency range around 10Hz and show strongest amplitudes over the visual cortex with the eyes closed. Alpha waves have been found to be an indicator of relaxation and, if decreased, of attention. Already in the 1970s biofeedback guided self-regulation of brain waves was propagated [144]. However, alpha waves are not suited to actively controlling a BCI; they were merely able to serve for monitoring purposes. A brain wave related to alpha waves is the sensorimotor rhythm (SMR), which appears over the sensorimotor cortex during rest and is present in most humans between 10Hz and 20Hz [14]. In the literature, sensorimotor brain waves between 8Hz and 15Hz are also referred to as the μ-rhythm [16]. When a person is moving or even imagines moving, the SMR amplitude decreases. This phenomenon is known as event-related desynchronization (ERD). Consequently, when the person resumes relaxation, event-related synchronization (ERS) can be observed [155]. Due to the similarity of brain activity during real movement and imagined movement, when targeting motor substitution applications, ERD/ERS is utilized in many BCI studies, e. g. [104, 156, 166, 224]. However, the SMR has also been used for BCI control in applications unrelated to movement, e. g. for spelling [19]. The advantage of this type of signal is that it can be spontaneously induced by the user and does not depend on external sensory stimulation, enabling active BCI control. However, the number of separable alternatives is low, allowing a maximum of three controllable degrees of freedom [125]. This is accompanied by intense user training. Another important fact is that the SMR is not detectable in a considerable proportion of people, while others are able to learn to modulate their SMR during extensive training.

A second type of brain signal, which is closely related to the SMR and was also initially applied for biofeedback self-regulation purposes [17], is the slow cortical potential (SCP). Technically, the SCP is a slow potential shift occurring over 0.5-10s [223]. Similarly to the SMR, a negative shift reflects cortical activation while a positive shift is associated with reduced activation [178]. The so-called thought–translation device, developed by Birbaumer and colleagues [15, 107], was the first BCI speller relying on SCPs and importantly, it was validated directly with the target group of users, namely locked-in patients. The proven complete independence from muscle activity is a clear advantage of this approach. One drawback of the approach, however, is the intense user training of more than 100 sessions of 5 to 10 minutes to achieve moderate self-control (70-80%). Furthermore, only one binary decision can be made within several seconds, which implies a very low information transfer rate. For communication purposes of locked-in patients, this might be acceptable, since it restores their ability to communicate at all.

3.3.2   Event-Related Potentials

Another type of brain signal applied for BCI control is the event-related potential (ERP). The most commonly applied ERP in this field is the P300 potential [76], which is

evoked approximately 300ms after an unexpected stimulus occurs and can be measured over anterior parietal sites. Classically, the P300 is evoked in the so-called oddball paradigm, in which a rare deviant stimulus is randomly presented in a series of irrelevant standard stimuli. The perception of the rare target stimulus elicits the typically 300ms delayed positive potential change. The first BCI using this paradigm was a matrix speller, introduced in 1988 [54]. In this speller a matrix is presented, consisting of a series of letters (typically 6 by 6) whereby stimulation is realized by shortly changing the colour intensity of letters in entire columns and rows. The user focuses on the letter to be selected and pays attention to the intensification of only the target letter while ignoring the remaining letters. The decoder detects whether or not a resulting P300 response was elicited and concludes, after a series of row and column stimuli, which was the intended target letter. This approach was followed by a vast number of studies aiming to improve the accuracy and the speed of the system [37, 80, 82, 90, 114, 143, 191, 206]. The fastest system was achieved using invasive recordings (113 bits/min) [30]. In most studies, the authors argued that the P300 based matrix speller does not depend on eye movements, due to the attention-based source of the signal. However, it has been shown that the accuracy of the speller decreases considerably if the user does not focus on the target letter but rather on a central fixation cross [29]. One reasonable rationale is the fact that perception and recognition of an intensification in the peripheral visual field is more difficult, but the main reason appears to be the contribution of stronger visual potentials that are evoked when fixating the target letter [30, 57]. The main advantage of the speller is the high number of symbols that can be selected after a short series of stimulus presentations. Primarily, the detection of the P300 is a binary classification problem, which reveals the presence or absence of the potential. Relatively fast yet numerous stimulus repetitions facilitate determination of the time points at which the P300 occurs. The attended symbol can be determined from these time points. Furthermore, the user does not need to train for the task or any kind of self-regulation. The popularity of the paradigm demonstrates the predominance of advantages relative to other item selection paradigms. Disadvantages of ERPs are the dependence on external stimuli and the difficulty to perform asynchronous control and detect the user's idle state, respectively. Furthermore, the duration needed for one selection is too long to facilitate continuous prosthesis control.

Another ERP relevant for BCI control is the so-called error potential. An early component, which is evoked in fronto-central regions after an error is recognized by a person, is the error-related negativity (ERN). Subsequently, a positive component can be measured over centro-parietal regions. A reliable detection of error potentials could facilitate the correction of errors made by the user (erroneous response) [20, 148] or by the system (erroneous feedback) [32, 56, 185]. Since the accuracy of error detection is moderate with current approaches, considerable development is required to establish error correction with beneficial outcome.

3.3.3   Visual Evoked Potentials

As mentioned above, the visual evoked potential (VEP) plays a sufficient role in gaze-dependent matrix spellers. The question then arises, whether the VEP alone can be used to control a BCI. Since the VEP is strongest when stimuli are projected onto the fovea, fixation of the target stimulus is required. Although efforts in VEP-guided BCI control based on covert attention have been made, e.g. selective attention [5] and spatial attention [97, 209], higher information transfer rates can be achieved in overt attention mode. Accordingly, the decoding of overtly attended VEPs is an indirect decoding of eye gaze. Similar to the P300 potential, the VEP is too weak in single-trial EEG to reliably detect a visual stimulus. Consequently, several successive visual stimuli with known temporal onset must be presented to decode the observed target area. Thus, transient VEPs [227] require sufficient time to be detected. However, it appears that rapidly repeated stimuli with constant delay evoke a steady state visual potential over cortical sites attributed to early stages of visual perception. The frequency of the visual stimulation produces an amplitude increase of the same frequency in the brain response [211]. These steady state visual evoked potentials (SSVEP) have been applied in many studies investigating BCI control [231]. Applications have also been implemented in the fields of mind speller [36, 212] and device control [216, 217, 230]. Also, demonstrations of brain-actuated control of prosthetic manipulators operating with two degrees of freedom have been reported [85, 140]. Some authors have substituted the frequency-based stimulation with presentations of binary coded flash sequences referred to as c-VEP and have reported improved information transfer rates (up to 144 bits/min) compared to SSVEP [12, 198]. Dependent on the stimulation equipment, a multitude of simultaneous oscillations are possible, providing a relatively high number of selectable targets [62]. Typically frequencies between 6 and 20 Hz are stimulated with BCI systems, but SSVEPs can be elicited up to 90 Hz [72] and have even been used for BCI control in the range of 37 to 40 Hz [50]. The high number of selectable items is one advantage. Another one is that no user training is required. Importantly, SSVEPs have the potential to be detected asynchronously to facilitate spontaneous BCI control [36]. Unfortunately, similarly to all the other noninvasively accessible brain responses, the speed of SSVEP detection is too slow to control prostheses continuously. A further drawback is that the perception of the flickering stimuli is unpleasant and can be sensed as annoying, stressing the user over time.

All the brain signals introduced so far are used in noninvasive BCIs and are primarily applied with EEG. In general, all the signals are global effects following complex cortical processes in the proximity of the electrode, where a vast quantity of neurons simultaneously respond to a specific stimulus or task. Due to the low signal-to-noise ratio provided by EEG, the low number of spatially distinctive patterns measurable, and the prolonged timing of the paradigms used, realistic control of a prosthesis is impossible. In contrast, if it is possible to acquire spatially highly resolved activity from a small population of neurons or even single neurons, a direct translation of an intended action could be instantiated. This invasive approach has already been demonstrated in studies where microelectrodes were implanted in primates [34, 210] and even humans

[78, 79]. The decoder is represented by a filter, commonly a linear model, that projects neural activity onto movement parameters. It has also been shown that features of high gamma activity in human ECoG are tuned to kinematic parameters [105, 133, 158, 182] and cognitive functions [52, 150]. A strong correlation between neural spike activity and ECoG high gamma activity has been shown in terms of firing rate and synchrony [168]. The advantageous spatial resolution of high gamma features is indicated by a more focal localization compared to lower frequency band features [133]. Concluding regarding the capabilities of the types of brain signals that have been investigated so far, invasive measurement techniques currently seem to be the only way to develop a prosthetic device that directly translates neural motor activity.

3.4   Dependent and Independent BCIs

The design of a BCI strongly depends on the requirements the system has to meet in order to be suited to the targeted user group. From a theoretical point of view, due to the poor signal quality compared to alternative communication channels, BCIs appear to be reasonable only if no other communication channel is available, i.e. the user has completely lost motor control and remains in a locked-in state. Otherwise, muscle activity signals from the electromyogram (EMG), speech recognition software or eye tracking systems could serve as more reliable communication channels. However, in a variety of applications, BCI research ignores the locked-in requirement. Rather, BCI is considered as an extension to existing assistive technologies [132], is developed for entertainment purposes, and is supposed to influence neuroplasticity in rehabilitation interventions. Nevertheless, only when the BCI is completely decoupled from peripheral neural activity, is it termed an independent BCI. Other BCIs often depend on eye gaze or even on further motor capabilities of the user and are termed dependent. Only a few implementations fulfill the independence constraint. Particularly speller devices often rely on directing eye gaze to target letters. Focusing attention on a target by eye gaze is also termed overt attention. In contrast, when a fixation cross is visually focused upon while a peripheral target is attended, spatial covert attention is applied. Another possibility for revealing independence from eye movements is to present targets and standards equally in the center of the visual field but at different points in time. This approach is called selective covert attention and was, for instance, the approach used by one study to reveal independence in a P300 based speller [208]. A non-controversial form of covert attention is applied in paradigms solely based on auditory perception. However, auditory stimulation yields a low information transfer rate, as demonstrated in some studies probing auditory BCI control [66, 100]. In summary, only mentally induced activity may be used to control an independent BCI. This is only possible with tasks where brain activity which is evoked by the processing of a stimulus itself is unlikely to be involved in the discrimination of categories, e.g. covert attention, or in absence of any stimulus, e.g. categorical imagery and mental tasks. Finally, as long as healthy subjects are employed to test a system, the independence of a BCI is not proven unless tested with locked-in patients. Some studies with patients suggest that BCIs considered to be independent, do not necessarily succeed in completely paralyzed

patients [74, 106]. In contrast, BCI performance appears to be independent by patient's physical impairment if residual abilities are present [106, 143, 190]. Consequently, the conscious abilities to control a BCI of patients who are caught in a completely locked-in state are not sufficiently identified and thus the need for completely independent BCIs is an open question [40].

3.5   Synchronous and Asynchronous BCIs

Most BCI systems present cues at defined points in time, expecting the user's command within a given interval. The rigid timing provides the advantage that the system is equipped with a very important piece of information which is very difficult to decode from brain activity: the onset of a spontaneous, volitional action intended to control the system. In such a synchronous mode, the user is constrained to perform an action, whether or not he or she wants to do so. Spellers often work synchronously. This is acceptable as long as the user wishes to communicate, but when the user relaxes, the systems turns to writing random text. Even the simplest form of movement initiation, moving a cursor on a screen, has only been shown in cue-based paradigms (e.g. Wolpaw and McFarland [224]) and often provides no option to rest. In real-life applications, a system would be required to determine not only which command is to be executed but also whether a command is intended at all. This is an important requirement for BCIs suitable for everyday use, particularly for motor substitution purposes. However, asynchronous BCIs have rarely been implemented due to the challenging detection of resting intervals and intrinsic activation onsets, respectively. Successful implementations of asynchronous BCI applications have been reported for SSVEP detection [36, 85, 140, 147], which is obtained by applying an amplitude threshold to the ongoing brain activity. Also, a P300 based asynchronous solution was proposed [229]. A more challenging task is the detection of a movement intention. An offline study of invasively assessed brain activity demonstrated the possibility of detecting intended movement onset and direction [218]. In an offline EEG study, the detection of self-paced reaching movement intention was demonstrated [116]. Although asynchronous control of a mobile robot [131] and a wheelchair [61] controlled by imagery tasks has been demonstrated, the accuracy of noninvasive BCIs is not suitable for reliable control of prosthetic devices in a continuous, asynchronous fashion. Nevertheless, asynchronism, i.e. the capability of spontaneous control, is an essential necessity for prosthetic BCI control.

3.6   Decoding Brain Activity Measurements

3.6.1   Feature Space Generation

An essential step for reliable decoding of brain activity is the translation of the input signal to an appropriate feature space. Commonly, measured brain activity is represented by several thousands of variables, involving redundancy and a high level of noise. Thus, the aim of feature extraction methods is to identify the informative signal and to

reduce the number of variables to a number reasonable for classification. For retaining the time-varying signal course as the feature space, a considerable amount of noise and redundancy can be removed by preprocessing steps like spectral filtering and resampling (see Section 2.4.1). For instance, such bandpass-filtered signals have been directly used as features by concatenating the time series of several channels [2, 57, 82] or by selecting peak values [9] or the averaged signal [188, 208] in hypothetically predefined time intervals.

A widely used representation of brain signals is the frequency domain. To translate time-varying signals to spectral features, methods based on the Fourier transform, like the power spectral density [61, 140, 152] and multi-taper [92, 164], as well as wavelet analysis [77] have been used. Another form of spectral analysis commonly used to recognize motor activity is the autoregressive model (AR) [103, 126] and its time-varying variant termed the adaptive autoregressive model (AAR) [64]. Also, connectivity measures such as the phase locking value have been shown to be suitable for classifying brain activity [28].

The translation of the raw data into a different representation is one part of feature space generation. Another part is the reduction and compression of the feature space, respectively. One prominent method known in the field of pattern recognition is principal component analysis (PCA), which is a linear transformation that retains the characteristics inducing highest variance in the data set, ordered in components. Despite the popularity of this effective dimensionality reduction, this method is only moderately used for BCI control [114]. Instead, because of the representation of the signal in several channels, in many studies the purpose of feature reduction lies in selecting informative channels. Often this is done by hypothetically selecting the channels that are located over brain regions where responses to the task are expected [4, 36, 102, 192]. An algorithmic solution for selecting channels is, for instance, recursive channel elimination [75, 109], which was derived from the more general approach termed recursive feature elimination [65]. As a nested method, the final feature set is found after multiple classification cycles. A similar procedure has been pursued by stepwise regression [29, 30].

Considerable improvements could be achieved by linearly combining the signals of several channels to concentrate the informative signal into a few channels. These spatial filter methods have been applied for classifying event-related potentials [199], frequency detection [13, 118] and for extracting ERD features [101, 102, 154]. Particularly when motor activity was to be classified, spatial filtering showed improved performance [139]. While there are various spatial filtering methods available, they can be divided into supervised and unsupervised methods, depending on the requirement of involving categorical information. The additional information provided for calculating supervised spatial filters permits higher accuracy as compared to unsupervised spatial filters as shown by Hoffmann *et al.* [81], who proposed a spatial filter, which is based on a solution to a generalized eigenvalue problem. Further examples of spatial filters have been shown by Rivet *et al.* [176], who propose an algorithm closely related to CCA and by Wang *et al.* [215], applying the so-called blind source separation algorithm. Further

feature extraction methods used for BCI are the matched filter approach [192] and template matching [9], generating a feature space that relies on correlations between the brain signal and a template signal.

All feature extraction and reduction methods described above can be applied in an automatic fashion. However, frequently the selection of features is performed by the experimenter's subjective experience, picking out manually a number of features showing statistical differences [97, 188]. Clearly, this approach makes a BCI impractical for independent, spontaneous use. Note, that the approaches described in this section provide an insight into the variety of methods used so far, but there are many more algorithms and modifications published in the field of BCI.

3.6.2   Decoding Algorithms

The core component of a BCI consists of an appropriate algorithm that translates a set of features obtained from brain signal recordings into an output signal. In general, two kinds of output signals can be distinguished, relying on different decoding approaches. The first kind of signal is a continuous output generated by a function that maps the feature input to a real-valued output value. Commonly, this is achieved by linear regression or state transition methods like the Kalman filter [124, 158]. For example, the reconstruction of hand position was obtained by a linear model that maps primate SUA/MUA [34] and human ECoG recordings [182], respectively, to spatial coordinates. However, the most commonly used, second kind of output signals is, due to the low signal-to-noise ratio in noninvasive recordings, the classification of the data samples into a few distinctive classes. In the majority of cases, only two discrete categories are distinguished, which is also known as binary classification. The most popular classifiers for BCIs are linear classifiers. This seems to be due to the high number of features which is accompanied by a low number of samples, making the training set easily linearly separable and providing insufficient information to model nonlinear relationships. Although diverse approaches using nonlinear classifiers exist, they have not yet been established for particular BCI applications. So far, a multitude of classifiers and deviated variants have been used for BCI research. The methodological reviews of Lotte *et al.* [123] and Bashashati *et al.* [8] together specify more than 40 classification algorithms, ignoring the diverse combinations with feature extraction methods or classifier combinations. Thus, only a subset of frequently used algorithms will be mentioned here. Linear discriminant analysis (LDA) [19, 53, 114, 156] and the related Fisher's linear discriminant [89, 102], including its regularized [21, 57, 137, 208] and stepwise [121, 206] variants, are the most frequently used learning algorithms in the field of BCI. A further popular classifier for BCIs is the support vector machine (SVM) algorithm [149, 164, 180, 204]. The option of using radial basis functions (RBF) and other nonlinear kernel functions [63] besides the standard linear kernel renders the SVM a flexible and powerful learning algorithm. The reason is that the number of features in brain signal decoding is often high compared to the number of samples. The SVM has proved to generalize well for this kind of data set (curse-of-dimensionality [18]) thanks to the regularization parameter. Neural networks (NN) have been applied in many variants

with multi-layer perceptrons (MLP) being the most frequently applied NNs [63, 89]. Furthermore, decision tree approaches [129] and the advanced method of random forest classifier [2] have been used for BCI control. In other studies, Bayesian and Gaussian classifiers [82, 131, 152] as well as the k-nearest neighbor (kNN) approach [96], have been probed. Another work used k-means clustering to identify the presence of SSVEP signals [161], showing improved accuracy in asynchronous control mode. In some cases a simple threshold detection approach appears to be sufficient to decode the brain state from a small set of features, as it was performed in several studies [9, 108, 184]. Finally, the choice of which decoding algorithm to use for a specific application depends on the type of signals to be classified, the feature set used, and the researcher's preferences.

3.7   Hybrid Approaches

All the characteristics described in the last sections offer advantages and disadvantages. The idea behind hybrid BCIs is to combine different methods, exploiting their beneficial features to improve accuracy, reliability, or speed of the system. In BCI development, a hybrid system could mean the combination of many sorts of methods: Different acquisition modalities, stimulation modalities, types of brain signals, decoding algorithms and even other biosignals unrelated to brain activity. In their review, Millán *et al.* suggest that BCIs might be used as additional channels to enhance conventional assistive technologies, due to the limitations of both BCIs and existing assistive products. To date, various constellations have been studied for improved brain–machine interaction. For instance, eye gaze input was combined with EEG-based motor imagery detection, intended to overcome the Midas Touch problem, which is typical in eye tracking systems working with the dwell time approach [228]. An indirect measure of eye movement is the electrooculogram, which has been combined with ERD detection for machine control [163]. In another study targeting alternative biosignals as additional input channels, the electromyography was fused with EEG activity [113], which was found to yield higher performance than individual modalities and was later evaluated in a clinical setting [152]. Zimmermann *et al.* [232] demonstrated that biosignal measures can improve the detection of motor execution with NIRS. In the field of multimodal brain imaging systems, only the combination of NIRS and EEG [55] has been investigated for BCI use. Consequently, the investigation of combined EEG and MEG,as targeted in this work, is due.

The greatest efforts have been made in combining multiple brain signals. Some examples are the combination of ERD and SSVEP [3, 4, 27, 86], SSVEP and P300 [214, 225, 226] and ERD and P300 [122], respectively. The combination can consist of simultaneous application of brain signals for the same task or separated application for distinct commands. Furthermore, the hybrid BCI can process the inputs simultaneously to increase the input band-width or sequentially to exploit task-specific suitability of the input signals. For example, one input signal could turn the actual communication device on and off, which is termed in the literature the so-called "brain switch". Also, the correction of erroneous mental commands by detecting error potentials [48, 197] as a complementary

brain signal can be considered hybrid. Finally, combining feature extraction methods [35] and classification methods [111] is termed hybrid as well. All studies referred to in this section report performance enhancement in at least some of their participants. The variety of hybrid approaches implemented so far, and the evidence for improvements that can be expected, indicate the significance of hybrid approaches.

3.8 Intelligence in Brain-Controlled Assistive Systems

The challenge in noninvasive BCI control is that only a limited number of brain states is available to perform complex tasks. Thus, one approach to improving communication is to equip the assistive system with intelligent algorithms. For instance, in spelling applications, intelligent prediction models, commonly applied in mobile devices, such as the predictive text entry system T9 [2, 83] or a prefix-based language model based on prediction by partial matching (PPM) [152], are used to enhance the speed of the system. Recently, a robotic system was introduced, which autonomously grasps a cup and executes the movement to the mouth [189]. The system is controlled by a single "go" command, induced by imagination of finger tapping. Although there is considerable development required to make such a system applicable for daily use, the concept points to the crucial trend of development. Another research group described the concept of shared control by driving a telepresence robot, which is remotely controlled by BCI commands on the one hand but is able to autonomously avoid obstacles on the other hand [205]. A similar concept was employed in [61], where users controlled an intelligent wheelchair with three commands induced by motor imagery. The wheelchair was equipped with sensors and assisted the user in uncertain situations.

A critical question in BCI research is the transferability of a system developed in a laboratory environment. Additional electromagnetic noise, as well as visual and auditory sources of irritation, could substantially influence the functioning of the system. One method to simulate this in the lab is the use of virtual reality (VR) techniques. For example, Leeb *et al.* [112] simulated a straight run with a wheelchair including interaction with avatars, where a tetraplegic patient could spontaneously initiate the forward movement. An important aspect is the fact that when moving through an environment, the motion in the visual field induces additional brain activity, which could affect the reliable control of the BCI. This is most critical when motor activity is used as the control signal, because mirror neurons induce activations similar to actual or imagined movement when movement is observed [157]. Using a VR environment, it was shown that navigation through a virtual world is possible using BCI commands based on motor imagery [186].

3.9 Summary of Existing Approaches and Methodological Challenges

In this chapter, I have revealed the variety of BCI applications and potential implementations that have been reported in this rapidly growing field of research so far. The

broad spectrum of approaches symbolizes the state of the art in this research field: The reliable decoding of brain signals, in particular of noninvasively acquired brain signals, is a challenging task which is not appropriately solved for daily use applications yet. The main challenges developers are faced with are based on physical and technical limitations. The primary problem is the low signal-to-noise ratio, which could be derived from several circumstances:

- brain signals are weak and require sensitive high quality amplifiers

- environmental noise contaminates the signal

- physiological activity such as heart beat and eye movements produce noise and artifacts

- one sensor measures superimposed signals from ongoing activity in the whole brain

- the skull and several tissues attenuate the signal

Thus, a main issue is the preprocessing of the noisy signal and the extraction of a small number of informative features from the typically high amount of data. The problems of low spatial resolution and low signal-to-noise ratio decrease with the employment of invasive techniques, albeit without vanishing. However, the risky circumstances and the unsolved problem of long-term bioincompability prevent the establishment of invasive BCIs.

An important fact to consider is that only a few tasks based on perception and attention produce brain responses that are measurable and discriminable in single trials with noninvasive methods. This means that the user has to perform relatively time consuming tasks for a simple outcome. Consequently, the current state of the art in noninvasive BCI does not permit practical continuous real-time control of an artificial limb. Instead, the research field is dominated by BCIs that operate with cognitive tasks in a scheduled, well controlled sequence.

Also in terms of classification some challenges exist. In many cases, the classification data set suffers from a few samples in a high dimensional feature space. Furthermore, artifacts produce outliers, and the features are often nonstationary over time. To solve these issues, appropriate feature extraction methods and classifiers are required. One approach to overcome the lack of reliable classification accuracy is the combination of several decoding algorithms or input signals, which is often referred to as a hybrid approach.

Considering the development of noninvasive BCI, the main focus is concentrated on performance improvements in various variants of a few classical paradigms. A weakness in BCI research is that the majority of studies investigate open-loop BCIs, which do not regard the effect of feedback. Secondly, almost all noninvasive systems are employed with EEG. From a practical point of view concerning home usability, this is most reasonable, however, the spatial resolution and spectral bandwidth are limited compared

to ECoG and MEG. The lack of spatial resolution in noninvasive BCIs is circumvented in this work by applying MEG recordings in a closed-loop BCI. Established classical paradigms, commonly applied with plane two-dimensional visual stimulation, are extended to work in virtual reality. Due to the low information transfer rate achievable with current techniques, signal processing and decoding algorithms, particularly pertaining to asynchronous limb control, need to be investigated with measurements of higher quality. The asynchronous control of an actuator is one of the central goals in this thesis. Electrocorticography, as an invasive method, allows only limited access to subject groups, which are comprised of patients suffering from brain diseases requiring ECoG for an established clinical purpose. In contrast, MEG provides the possibility of recruiting a wide range of subjects and performing experiments without risks, while simultaneously providing excellent spatial and temporal resolution. The efficient processing of such high-density sensor data, requiring noise reduction and suitable feature extraction, is in the focus of this work.

4. Approaches to Improve Brain–Controlled Upper Limb Actuation

In this chapter several methodological issues are described, and ideas for achieving more reliable decoding of brain signals are introduced, with the aiming of providing insights for advanced development of brain–controlled prostheses. The methods outlined in this chapter are presented as preparation to the experiments described in Chapter 5. In the following sections I will introduce the paradigms and algorithms that will be used to successively investigate the ability to drive a robotic device by noninvasive brain recordings. Details about the experimental set-up, subjects and materials used are explained in the next chapter.

4.1 Exploiting Low Information Transfer for Complex Tasks

In the last chapter various types of BCIs were described. Considering the features of the different recording modalities, invasive techniques obviously provide the highest signal quality and hence, are the most promising for development of accurately working BMIs. However, the medical risk of implantation, the inflammation risk of wired recording and the short-term biocompatibility of the state-of-the-art electrodes for cortical derivations prohibits the use of invasive recording. Furthermore, research work and BMI development are very limited due to the fact that, for obvious reasons, subjects can only be recruited if they have to undergo a clinical intervention. For this reason the majority of BMI development concentrates on EEG applications. For example, a large EU project denoted TOBI [151] focused on the design of noninvasive BCI prototypes for assistive technology and rehabilitation. The main drawback of noninvasive techniques is the slow information transfer rate which is at most 80bits/min [16]. This rate is much to

low to continuously drive a robotic device. In order to control three degrees of freedom (DF) for the pure end-point movement, one has to distinguish seven control signals (idle and two directions per DF) in short intervals. Due to the challenge in achieving this requirement with noninvasive techniques, no such system has yet been developed. Instead, the intention to do something, e.g. open or close a hand, was decoded from SMR modulation in previous studies demonstrating a two-state application [31].

One aspect of the present work is to simplify the noninvasive brain control of prosthetic devices. The requirement for this is the use of intelligent semi-autonomous robotics. The general idea is to exploit the low information transfer rate (ITR) of noninvasive techniques to build a brain–machine interface that can drive a robotic system able to autonomously grasp and manipulate objects. With the planned framework the control of the grasping device is reduced to the problem of decoding the intention to select a target object or the execution of a predefined robot command from voluntary brain activations. Interactions with a robot are simulated by presenting a VR scenario to the subjects. In this scenario, a CAD model of an industrial robot (Mitsubishi RV E2), equipped with a three finger gripper (Schunk Dexterous Hand SDH) is placed on a desk. Additionally, objects can be placed on the desk and assigned with areas for visual stimulation and feedback. Importantly, the virtual robot can simulate a grasp of the object by applying a grasp planning algorithm [172]. Furthermore, an example of manipulation, specifically picking up and presenting the object, can be simulated. The VR scenario and the grasping algorithm have been implemented by the Fraunhofer Institute for Factory Operation and Automation (IFF) who kindly provided the environment [98] for the experiments.

In order to use a preferentially high capacity of noninvasive brain signal acquisition, MEG is utilized in this work since it is the topographically most sensitive method. The higher number of sensors and the fact that MEG permits higher discrimination accuracy compared to EEG when activity of small structured brain areas is classified [164] suggests that a higher ITR is achievable with this modality. All experiments presented in this work are performed as a closed-loop BMI, with the MEG data processing done online. In the initial preliminary experiments only MEG is recorded due to the easier set-up and the fact that for technical reasons only the MEG data stream is accessible in real-time. However, EEG recordings simultaneous to MEG recordings are possible with this system. In the final experiment, this possibility is employed in order to investigate a potential increase of accuracy by combining both modalities in offline analyses. Analyses by means of pattern recognition have rarely been performed using MEG data (e.g. [164, 175]) and consequently even more rarely has a BMI been implemented [31]. Importantly, the brain responses obtained from MEG that are investigated in this study had not been analysed with pattern recognition techniques until now.

Providing a robotic system that autonomously performs complex movements of everyday tasks requires only a small set of commands that can be executed by pressing buttons. In a BMI set-up the button presses must be substituted with virtual selections. Common assistive technologies like speech recognition and eye-tracking are not options for the targeted group of users. Thus, mere brain activation is used to perform

the selection. One intuitional approach would be to set the focus virtually to one of the selectable items and shift it in a similar manner to shifting the focus in a GUI with the tabulator key. Motor imagery tasks would be the consequential control signal. A simple synchronously controlled version of this strategy would require only two commands (*next item* and *select*). As the ITR depends on the number of alternatives, more commands (e.g. *previous item*) would enhance the speed of the system. However, as mentioned above the number of distinguishable MI classes is very limited with noninvasive techniques. Furthermore, only a limited portion of people are able to successfully perform MI driven BCI control [22], a problem which is even more critical in disabled users [106, 154]. Although similar tree-based approaches have been performed in some speller implementations [138, 187], MI-control has rarely been used for selection purposes due to the better performance with paradigms that benefit from visual stimulation. Concerning the limitations of MI based selection and the presumption that users might have a damaged motor cortex, that approach is not part of this work. Instead, selections will be decoded by detecting electrical potentials in the brain resulting from visual stimulation and selective visual attention, respectively.

The first approach is based on the circumstance that the visual perception of a repeated flashing sequence elicits potentials in the visual cortex that are correlated with the stimulation. If the intervals between flashes are constant and in a specific range, the stimulated frequency is reflected in the brain response which is termed steady state visual evoked potentials (SSVEP). For this paradigm, the ability to direct eye gaze to the targets is required. The decoding algorithm detects which of several stimulation frequencies is projected on the retina's fovea by classifying the brain response evoked in early visual areas. The advantages of this method compared to MI classification are that i) it can be detected in relatively short intervals, ii) a high number of classes can be distinguished and iii) BMI control depends on visual perception rather than on activations in motor areas. Thus, SSVEP could be a potential brain response that can be used to perform fast multi-class selections in a VR environment. In a preliminary set-up the selection success of virtual realistic objects is tested by presenting flicker stimuli near objects and decoding the focused frequency from relatively short signal intervals.

The second approach, which is applied in this work in order to investigate brain controlled selection of VR items, utilizes a brain response established in many speller paradigms, called P300 response. As already outlined in Section 3.3.2, in the so called oddball paradigm the P300 can be measured over the parietal lobe as a positive deflection approximately 300 ms after a rare (deviant) stimulus occurred in a series of irrelevant (standard) stimuli. Compared to the SSVEP stimuli, longer stimulation intervals will be required but the number of selectable items is much higher and the flashing stimulus presumably is less annoying than a flickering stimulus [213]. Furthermore, again the activated brain areas do not depend on an intact motor cortex. The biggest advantage however, is the potential independence of eye movements. Directing gaze to the target item provides an additional early visual component which reflects a stronger perception of the target stimulus compared to the standard stimuli [57]. Conse-

quently, focusing on the target item provides more information and increases detection accuracy [29]. However, in the targeted set-up the aim is to be independent of eye gaze and to use only information evoked by selective attention responses. This renders the selection approach applicable to a wider range of users. Both approaches will reveal, depending on decoding accuracy, speed and number of alternative selections, an ITR accompanied by pros and cons of the paradigm. These results will be discussed from the perspective of enhancing the functionality of the selection set-up. The final system is intended to permit a user to asynchronously control a virtual grasping robot. In this case asynchronous control means that the system doesn't assign the point in time it expects a command (which is common in most current BMI implementations) but the user is free to decide when to perform an action.

The results obtained online during the experiments, i.e. the accuracy that is measured with the provided feedback is most likely not optimal. The initial implementation involves algorithms derived from current knowledge about similar experiments performed with EEG and ECoG. However, significant potential for improvement of the ITR by algorithm improvement can be expected. Particularly, the circumstance that MEG provides a higher sensor density and reflects alternative source locations leads to the hypothesis that there is potential in optimizing signal processing and feature extraction. In post-analyses, algorithm refinement will be investigated. This applies to the length of the stimulation interval, application of spatial filter methods, comparison of classifiers and dependence on the size of the feature set. The most promising combination for asynchronous selection will be subject to final system implementation. Even after the online evaluation of the final system, further improvements are conceivable. A potential interest exists in the comparison and combination of simultaneous EEG recordings in order to rank the results obtained and to evaluate the benefits of different modalities.

4.2 Detection of Perceived Steady State Visual Stimulation

4.2.1 Signal Emergence and application in BCIs

The human visual system processes a visual stimulus in a bottom-up fashion while two pathways are distinguished for higher order processing [134]. Early cerebral processing of visual information is performed in the primary visual cortex (V1), which is located in the posterior part of the occipital lobe. From there, the dorsal pathway travels to the parietal lobe, which processes spatial information and motion. The second stream is the ventral pathway, which mainly processes visual features and goes to the temporal lobe. A visual evoked potential (VEP) is a series of typical negative and positive deflections in brain activity measured over different brain areas following a visual stimulation onset. The positive and negative waves are attributed to different stages of processing. A first component typically is measured over the occipital cortex 50 to 80 ms after the stimulation of retinal receptors. With common measurement techniques, evoked potentials can be visually identified only after averaging numerous intervals of identical stimuli or tasks. Thus, the low but repeatedly occurring signal remains, while the

noise, although having much higher signal strength, is cancelled out. Responses to single brief visual stimuli are considered transient. In contrast, as Regan [169] has found in experiments presenting oscillating light, flicker stimuli produce a stable VEP which is known as the steady state visual evoked potential. The advantage of SSVEPs is the sustained amplitude and phase characteristic of frequency components over a long time period. Importantly, the spectral response in the frequency domain of the brain signal peaks at the stimulation frequency and harmonics. Consequently, spectral analysis of a sufficiently long stimulation interval facilitates the identification of the perceived flicker frequency.

In a BCI set-up targeting SSVEP detection, several flicker stimuli oscillating at different frequencies are presented simultaneously. The user focuses on one of the stimuli in order to execute a command associated with that stimulator. In the measured brain activity, the frequency component of the focused stimulator is larger than the frequency components of the unattended visual stimulation. This is because the receptors located in the fovea centralis, i.e. in the subjective center of the visual field, have the highest density in the retina as well as having a higher impact than peripheral receptors on processing in the visual cortex. By detecting the most prominent of the stimulated frequencies in the brain activity, inference of the attended stimulus can be made. The requirement of directing eye gaze renders this approach a dependent BCI. An approach independent of eye movements is theoretically possible by selective attention (presenting overlapping stimuli) [5] or spatial attention paradigms (presenting spatially distributed stimuli) [97] where the user pays attention to one stimulator while focusing on one fixation point permanently. However, such approaches exhibit reduced accuracy and limit the number of alternatives enormously. Consequently, independent BCIs based on SSVEP detection have rarely been implemented thus far and provide no option for the intended aim of this work. The range of frequencies suited to the evoking of SSVEPs as indicated in the literature is between 3 Hz and 50 Hz and above [72]. In fact, stimulation frequencies higher than 30 Hz are not perceived as flickers, suggesting that the stimulus is processed in early visual areas but that higher order processing fails. A potential advantage of this phenomenon is that decoding of a perceptually hidden and consequently non-annoying stimulus may be possible, although unfortunately, discrimination accuracy of EEG signals decreases with high stimulation frequencies [213]. Stimulation frequencies for BCI applications are commonly chosen between 5 Hz and 20 Hz [231]. This frequency range is also beneficial for virtual reality guided stimulation given the typical frame rates of 60 Hz and 75 Hz provided by TFT displays and projectors.

Although the theory of determining the frequency of an attended visual stimulus from SSVEP is comprehensible, reliable detection from spectral information is challenging. This is because the SSVEP is superimposed by spontaneous brain activity from many other sources, and accompanied by a high noise level. Spontaneous brain activity is often reflected in oscillations of similar frequencies which further complicates reliable detection. An advantage of SSVEP frequency analysis is that a priori knowledge is available, more specifically the information which frequencies are expected to be modulated by the stimulation. One approach to emphasize SSVEPs is to calculate a Fourier

based signal-to-noise ratio by dividing the Fourier power of the considered frequency by the average Fourier power of adjacent frequencies. While this seems advantageous for visualization purposes, there is no obvious advantage for classification since this method actually just normalizes the Fourier power to a scale which is better comparable between frequencies.

4.2.2   Employing SSVEP for Item Selection in Virtual Reality

The application of flicker stimuli in BCI set-ups was mainly performed in EEG experiments but never in MEG experiments, although MEG could provide supplementary information for a more reliable decoding. This part of the work will close this gap by probing the discrimination accuracy of MEG signals evoked by flicker stimuli in a virtual reality environment. A large number of dipoles arising from a population of neurons superimpose their electrical fields such that we are able to measure electrical potentials on the cortex and even on the scalp. Similarly, the superimposed magnetic fields induced by the dipoles can be measured outside of and distant from the skull, even though they are very weak. Therefore, similar to SSVEPs the magnetic equivalent can be obtained from magnetoencephalographic recordings: the steady state visual evoked fields (SSVEF).

In a first attempt, I investigate whether SSVEFs can reliably be discriminated, with the constraint that the stimulator is partly occluded by an object. The time needed to execute one command should be as short as possible. Here, the duration of the flicker stimulus is chosen to be 5 s. The number of simultaneously presented frequencies is four, allowing the discrimination of four different states. Stimulation frequencies are chosen at $6.67\,\text{Hz}$, $8.57\,\text{Hz}$, $10.0\,\text{Hz}$ and $15.0\,\text{Hz}$, such that the periodic time of stimulus onsets correspond to multiples of a frame duration ($1/60\,\text{s}$). Importantly, fundamental frequencies do not overlap with any harmonic frequency, which could introduce mutual disturbance. While the stimulation frequencies remain fixed at their positions, the objects randomly exchange their positions. This guarantees that frequencies can be detected independently of the occluding object and conversely that objects can be selected independently of the background oscillations. Furthermore, this provides the possibility of using the objects movement as a cue. For evaluation purposes the focused frequency must be known in each trial. Thus, the subject's task will be to select one specific object during the entire run. The randomization is performed such that each object is placed at each of the positions eight times, resulting in 32 trials. A green coloured ring around an object indicates the position of the frequency decoded by the SSVEP detection algorithm. All other positions are marked with a red ring indicating wrong decoding if actually focused upon by the user. In initial training runs random feedback with a confidence of $70\,\%$ is presented. The data of these runs are used for calibration and to train a classifier. Subsequently, the classifier is used to detect the frequency that most likely represents the attended oscillating stimulus. Importantly, all processing steps are performed in real-time, i.e. as soon as a sufficient amount of acquired data is available. The decoding result is presented in a manner analogous to

the training runs immediately after processing. This renders possible the approach of a closed-loop BMI capable of selecting one of four objects in a virtual reality environment.

4.2.3 Online Detection of SSVEFs

The onset of flicker stimulation is marked by an event code which is sent by the BMI software to the acquisition system, registering the code in an auxiliary digital channel. This channel operates in real-time in parallel to the MEG data provision to deliver the onset of events. Thus, the time window cut out for SSVEF detection starts at the position where the flicker onset event code was received and lasts for 4.5 s. Since SSVEFs are expected to essentially emerge in visual areas, only a sub array of the entire MEG sensor field is used, arranged by the manufacturer of the sensor array to capture activity from occipital brain regions. Therefore, only 59 out of 248 MEG sensor time series are used for online detection, which keeps the feature space comparatively small. As a first step, the DC offset is removed and environmental noise is reduced. The noise cancellation is performed by an algorithm introduced by Robinson [177], where the amount of signal common to both biomagnetic sensors and reference sensors is subtracted. Subsequently, spectral features are calculated. The mean amplitude of frequency f in signal Φ_B obtained from sensor s is determined as

$$F(f, s) = \frac{1}{N} \| \sum_{n=1}^{N} \phi_{n,s} \cdot \mathrm{e}^{-2\pi i f t_n} \|$$ (4.1)

where $\phi_{n,s}$ is the magnetic flux in sensor s at sample n. The time point t_n at sample n can be obtained by dividing n by the sample rate f_s. Each of the values $F(f, s)$ defines one feature while each interval (of a trial) represents one observation. Thus, the resulting training set $\{\mathbf{X}, \mathbf{y}\}$ consists of $k = 59 \times 4 = 236$ features and l observations which are labeled with an index denoting one of the four stimulation frequencies:

$$\mathbf{X} = \begin{bmatrix} x_{1,1} & \cdots & x_{1,k} \\ \vdots & \ddots & \vdots \\ x_{l,1} & \cdots & x_{l,k} \end{bmatrix}, x_{i,j} \in \mathbb{R}$$ (4.2)

$$\mathbf{y} = \begin{bmatrix} y_1 \\ \vdots \\ y_l \end{bmatrix}, y_i \in \{1, 2, 3, 4\}$$ (4.3)

The theory of SSVEP emergence presumes that the amplitude at the frequency f increases if a stimulus oscillating with this frequency is observed by the user. Thus, features representing this frequency may increase in several sensors. Consequently, a regression approach appears to be appropriate to distinguish the four classes. Therefore, for this purpose a regularized logistic regression algorithm is used for classification. The regularization parameter λ penalizes small weights having the effect of an implicit feature selection. The classifier determines the probability that stimulation frequency f is observed by the user. The frequency providing the highest probability is selected and fed back to the participant.

4.2.4 Optimizing SSVEF Detection for Improved Decoding with Dense Sensor Arrays

Optimal information transfer rate depends on both the time needed to send a command and the accuracy with which the decoder recognizes the intention. Furthermore, the decoding accuracy depends on the quality of the feature representation and the pattern recognition algorithm used. Some authors reported evidence that the involvement of harmonics, i.e. frequencies at a multiple of the stimulation frequency, increases the accuracy in SSVEP detection [141], suggesting another parameter for investigation. The following approaches aim to find an optimal set of parameters that maximize the information transfer rate. The data source is provided by the MEG data recorded during the BMI experiment following the methods in Section 4.2.3. The evaluation of diverse combinations of parameters and methods is performed in a validation framework that is compatible with BCI application, namely calibration of a training set is performed only with past data. This avoids an overestimation of accuracy as is potentially possible in a cross-validation framework where the amount of training data is consistently high in every validation cycle. Specifically, the first test set is constituted by the third run while the first two runs are used for calibration. Each following run is treated as a separate test set which is tested on a classifier trained on all previous runs but maximal on the past five runs. In the following I will refer to this validation scheme as simulated online validation (SOV). The measure applied for evaluation is the decoding accuracy which is calculated as percent correct detections.

As a common pool of raw data the time series are cut in single trials, starting at stimulation onset and lasting 5 s. The preprocessing steps are performed identically to the procedure in the BMI implementation, resulting in a set of 59 time series for each trial. Only those trials are included where the target frequency is known, i.e. the runs where the object to be selected was instructed (see Table 5.1). These preprocessed time series constitute the basis for all analyses. The methods used in the BMI implementation provide a benchmark for the optimization approach. Specifically, this is the Fourier transform of a 4.5 s data segment as defined in Equation 4.1 in combination with a regularized logistic regression (rLR) classifier. In cases of harmonics involvement in the Fourier feature space, the harmonic frequencies are simply considered as additional frequencies.

4.2.4.1 Spatial Filtering for SSVEF Detection as an Efficient Noise Reducer and Feature Extractor

There are several strategies existing in the literature, which can extract SSVEP features from EEG time series. One method, suitable for efficiently filtering EEG signals [23] recorded during motor imagery, is the common spatial pattern method (see Section 2.5.2). Since CSP also was successful in SSVEP detection from EEG recordings [1, 147], it qualifies for one of the feature extraction methods to be investigated with the recorded MEG data. For this purpose, the time series is first band-pass filtered using a 2nd order Butterworth filter centered at the frequency of interest (fundamental

stimulation frequency or optionally the 2nd and 3rd harmonic) where the bandwidth is 2 Hz. Since CSP is basically suited for binary separation, the spatial filter is calculated for each frequency using bandpass filtered signals of the examined frequency as the first class and all other frequencies as second class. Class sizes are balanced by discarding samples of all frequencies equally. Two filters effecting high variance in one class and two filters causing high variance in the other class are selected to spatially filter the bandpass filtered time series according to Equation 2.6. Afterwards, the log variances are calculated as features, resulting in a 16 dimensional feature space (four spatial filters by four frequencies).

Another approach, offering a promising method for SSVEP detection [118], is the canonical correlation analysis, described in Section 2.5.3. The advantage of paradigms evoking SSVEPs is that the stimulation frequencies are well known and thus, a reference function easily can be defined. Here we model the reference functions in $\mathbf{Y}$ of Equation 2.12 as pairs of sine and cosine waves for a target frequency and optionally its harmonics:

$$\mathbf{Y} = \begin{bmatrix} \sin(2\pi f t_1) & \dots & \sin(2\pi f t_N) \\ \cos(2\pi f t_1) & \dots & \cos(2\pi f t_N) \\ \vdots & \ddots & \vdots \\ \sin(2\pi h_n f t_1) & \dots & \sin(2\pi h_n f t_N) \\ \cos(2\pi h_n f t_1) & \dots & \cos(2\pi h_n f t_N) \end{bmatrix}, \ t_i = \frac{i}{f_s}, \ i = 1, \dots, N \qquad (4.4)$$

where the fundamental frequency f is the first harmonic and h_n is the number of harmonics to include. By involving sine and cosine functions simultaneously, the model is phase independent. The weights in $\mathbf{W}_y$ define the proportion of sine and cosine, respectively and regulate the phase shift between the measured and modelled signals. Obviously, this approach only applies to continuously recorded data since concatenation of measured data with different phase shifts would fail. Thus, for each stimulation frequency the CCA method is applied to single intervals of multi-channel MEG signals. The features extracted for classification are the correlation coefficients ρ_1 (see Equation 2.13) corresponding to the first component of a particular frequency. Thus, merely one feature characterises each frequency, independent of the number of harmonics involved.

The feature extraction methods MEC and MCC as introduced by Friman *et al.* [59] are promising tools for SSVEP detection. In Section 2.5.4 and Section 2.5.5 I described the two methods aiming to enhance the signal-to-noise ratio by determining and applying a spatial filter. The model signals $\mathbf{Y}$ in Equation 2.15 are identical to that in Equation 4.4. Consequently, the same properties and constraints concerning phase shift hold as for the CCA approach. The spatially filtered time series signals $\hat{\mathbf{X}}$ are further processed to obtain a single feature per frequency, comparable to the CCA feature space. The feature extraction is performed equally for both MEC and MCC according to Friman *et al.* [59] as follows. First of all, the SSVEP-cancelled signals $\tilde{\mathbf{X}}$ (see Equation 2.15) are transformed by the estimated filter matrix:

$$\hat{\tilde{\mathbf{X}}} = \mathbf{W}^\intercal \tilde{\mathbf{X}}. \qquad (4.5)$$

Afterwards, an autoregressive model of order $p = 15$ is fitted to the D time series data in $\hat{\tilde{\mathbf{X}}}$, yielding the model parameters $\alpha_{d,j}, \ldots, \alpha_{d,p}$ and the prediction error $\sigma_{E,d}^2$. The fitted models are used to interpolate the noise power in the SSVEP frequencies. The noise level for harmonic h in signal d is then calculated by

$$\hat{\sigma}_{h,d}^2 = \frac{\pi N}{4} \frac{\sigma_{E,d}^2}{\left| 1 + \sum_{j=1}^{p} \alpha_{d,j} \exp(-2\pi i j h f f_s^{-1}) \right|^2}. \tag{4.6}$$

Finally, the presence of an SSVEP of a specific frequency is tested by the following test statistic:

$$T = \frac{1}{D h_n} \sum_{d=1}^{D} \sum_{h=1}^{h_n} \frac{\| \mathbf{Y}_h \hat{\mathbf{x}}_d \|^2}{\hat{\sigma}_{h,d}^2}. \tag{4.7}$$

Here, $\mathbf{Y}_h$ is a pair of sine and cosine modeled signals according to the harmonic h of frequency f. The feature value determined as T is the average of signal-to-noise ratios across harmonic frequencies and spatially filtered signals. Thus, if an SSVEP signal at frequency f is present in $\mathbf{X}$, the feature value is higher than that of the other frequencies. Similarly to CCA, this approach is applied to single intervals of MEG signals. This is in contrast to the application of CSP, where an adequate number of intervals is required to estimate the filter matrix.

4.2.4.2 Validation of Harmonics Involvement for Enhanced Feature Robustness

So far, four feature extraction methods are the focus of investigation for the decoding of SSVEP emergence in the MEG: Fourier transform, common spatial patterns, minimum energy combination and maximum contrast combination. The last three methods provide the possibility of including several harmonics resulting in one measure per stimulation frequency. Since in the past evidence has been shown that involvement of harmonics improves SSVEP detection [141], the involvement of the second and third harmonics of a stimulation frequency is a further parameter to be investigated. With the CSP method this is performed by adding the additional bandpass filtered signals as input channels but keeping the number of output channels. Thus, the harmonics involvement does not increase the number of features. In contrast, the feature space of the Fourier transform method is extended by adding the harmonic frequency features.

4.2.4.3 Validation of Timing Parameters for Speed Optimization

A considerable impact on a successful detection of SSVEP is the duration of the stimulation. The longer a stimulation lasts, the more accurate is the frequency decomposition and the more reliable is the prediction. However, a long decision duration implies a low information transfer rate. Thus, a trade-off between accuracy and stimulus duration must be found. For this purpose, interval lengths starting from $0.5\,\mathrm{s}$ up to $4.5\,\mathrm{s}$ in steps of $0.5\,\mathrm{s}$ are used to evaluate the impact of stimulus duration on decoding accuracy and information transfer rate. In order to calculate the trade-off, the number of

bits is determined that can be transferred in one minute, given the number of possible commands n_c. This commonly used measure for BCI evaluation has been proposed by Wolpaw *et al.*[222]. Given the probability $P \geq 1/n_c$ the bit rate per trial of length t_{trial} is calculated as

$$B_{trial} = \log_2 n_c + P \log_2 P + (1 - P) \log_2 \frac{1 - P}{n_c - 1}, \tag{4.8}$$

assuming that the probability of each command is the same. The probability P can be interpreted as the decoding accuracy or the correct prediction rate. To obtain the information transfer rate per minute one has to multiply B_{trial} with the number of possible trials per minute:

$$B = \frac{60}{t_{trial}} B_{trial} \tag{4.9}$$

Thus, B can be higher for shorter intervals although P is lower. This implies that information is thus transferred faster but with more errors. Correction of the errors requires additional commands for the BMI application. This is an important point to consider when choosing the trade-off between accuracy and stimulation time.

4.2.4.4 Validation of Classifier Algorithms

Finally, beside the initially applied rLR, a variety of methods exists to recognize the attended frequency from the extracted feature space. Here, five additional procedures are considered to classify the data set into four classes. An easy and straightforward way to do this is to determine the frequency feature that reveals the highest value. I will refer to this approach as the argmax classifier:

$$f = f_y, \text{ where } y = \text{argmax}(\mathbf{x}), \; y \in 1, \ldots, n_c, \; \mathbf{x} = (x_1, \ldots, x_{n_c})^{\mathsf{T}}. \tag{4.10}$$

However, this method is only applicable if the features represent a direct measure of the frequency content in the signals. From the feature spaces considered here, this only applies to CCA, MEC and MCC. Further conventional classifiers eligible to naturally discriminate multiple classes are the linear discriminant analysis, the naïve Bayes classifier, the kNN classifier and the nCentroid classifier. All these classifiers are suitable for the discrimination of m-dimensional vectors while they vary in their tendency to overfit in higher dimensional feature spaces. Nevertheless, these are the classifiers among which the performance is to be compared in this offline analysis.

4.3 Attention Based Event Detection

The previous sections described how to decode the perception of a visual stimulus from the cognitive system. When using mere perception as a communication channel, the user has an active influence on his perception. In the case of visual stimulation, the perceptual change is induced by focusing on a specific stimulus which is performed by eye movements. However, BMIs conceptually strive for communication channels that

rely purely on conscious brain wave modulation independent of any peripheral movement. One strategy that satisfies this requirement is to employ the user's attention to communicate his or her intention. This can be performed by tracking the user's attention in response to specific events. Although with this approach external stimulation is still required to synchronize the brain responses, no activations of peripheral nerves are necessary. The only constraints are that the user is able to perceive the stimulus and that he or she is aware of how to perform the task of attention based communication.

4.3.1   P300 Generation and the Oddball Paradigm

In experiments involving stimulus uncertainty, Sutton *et al.* [203] discovered that expected stimuli are differently processed in the brain to unexpected stimuli. Specifically, when the subject's guess was different to the following stimulus, a positive EEG component has been found peaking about 300 ms after stimulus onset. Today this typical potential variation is known as the P300 or P3 response. Actually, it is composed of an early frontal component and a component occurring over parietal locations somewhat later [159]. Generally, the P300 is not the result of a single process but is thought to reflect a superposition of a distributed network of memory and attention related activations. Typically, a P300 is evoked in a so called oddball paradigm [200]. In this paradigm an infrequently presented target stimulus is detected by the subject while more frequently presented background stimuli are to be ignored. When subjects perceive the deviant stimulus, the typical P300 response is evoked. There are several theories about the underlying brain dynamics. The emergence of the P300 is proved to be evoked by the novelty of a stimulus [195] as well as being an update mechanism in passive perception, i.e. without attention to a task. However, the most important point is that an attentional component evokes a P300 after an anticipated stimulus occurs in a series of similar but otherwise ignored stimuli. This phenomenon is utilized in many BCI applications, mostly in matrix speller implementations. The general approach is to detect the presence of a P300 potential following a short visual stimulus. Due to the low signal-to-noise ratio, several intervals are averaged before classification or the classifier output is accumulated. Conceptually, the task of detecting a P300 response is a binary classification problem. For selection of multiple items, the actual selection is determined from temporal information pertaining to the stimulus occurrence.

4.3.2   Employing the P300 Potential for Item Selection

Although many P300 speller variants have been investigated using EEG data, only one study [11] has performed single trial detection of P300 potentials with MEG data so far, albeit not closed-loop. However, analogously to SSVEF detection, there are legitimate grounds to also investigate the magnetic fields of P300 activations for real-time detection. Here I employ an oddball task with the aim of selection of objects, presented in a virtual reality environment. Extending the first experiment, six objects are presented on a table that can be selected by mere attention to the visual stimulus near the target object. Furthermore, the scenario contains a CAD model of an industrial robot equipped with a three finger gripper. The virtual robot simulates the movement

of its original which is able to grasp an object with known position and shape [98]. To indicate a stimulus event serving for discrimination of standards from targets, the backgrounds of the objects are flashed in a random order. The randomization is performed such that two successive flashes of the same objects are prevented. A stimulus appears every 300 ms and lasts for 100 ms. Each of the objects is flashed five times per trial, leading to 30 flashes within 9 s. The user focuses on a cross in the centre of the item arrangement. The object to be selected is covertly attended by the user, which elicits a characteristic brain response after each perception of a flash behind the attended target object. For maintaining the user's attention, mental counting of the target flashes is beneficial. Grey rings around the objects are used to present a cue for an upcoming target object in order to be able to supervise the selections. Supervision of selections is required to reliably train a classifier. Finally, after the decoding is performed, a green ring indicates the decoded object, while all other objects are marked with red rings. For demonstration purposes a grasp of the decoded object by the virtual robot can be presented as feedback. Like the first approach, this experiment also works as a closed-loop BMI, processing MEG data in real-time.

4.3.3   Online Detection of the P300 Potential

For reliable synchronization of screen events, event signals are sent to the MEG system, which provides a digital marker simultaneously with the magnetic flux measurements. Based on these markers, a signal interval is cut out from the online data stream starting at the first flash onset and lasting 10 s, capturing all flash onsets of one trial and allowing sufficient time for the evolution of brain potentials after the last flash. This interval then is band pass filtered between 1 Hz and 12 Hz and down-sampled to 32 Hz. Subsequently, the preprocessed signals are cut in 1 s intervals starting at each flash onset. These preprocessing parameters are chosen according to Hoffmann *et al.* [82], who demonstrated good performance in EEG experiments and are in line with suggestions of Farquhar and Hill [53]. Since the P300 is typically evoked in parietal and frontocentral areas and thus is generally measured over the vertex, i.e. at the top of the head, only 152 sensors closest to the centre of the sensor array are involved. This serves as a first reduction of the amount of data. The separated intervals are labelled according to target and nontarget flashes. Afterwards, a support vector machine classifier is initially trained for feature selection. The highest sum of weights per sensor in the vector w of Equation 2.2 is used as a measure to select the 64 most discriminable sensors. This results in a feature set of 2048 features (64 channels $\times$ 32 samples). Linear SVM is chosen as the classifier, since the classification problem is binary and high dimensional. It has been shown that SVMs are well-suited for discriminating high dimensional brain signal data by self-regulation of feature importance [164, 175]. When single flash intervals of one trial are classified for the presence of a P300 response, the distance of the test sample to the separating hyperplane is calculated and summed for each of the six objects. The object with the maximum cumulated distance is assumed to be the attended object. If each of the intervals following a flash were classified correctly, the negative distances of standard stimuli would sum to a negative value

while the positive distances of target stimuli would sum to a positive and therefore maximal value.

4.3.4   Optimizing P300 Detection for Improved Decoding with Dense Sensor Arrays

4.3.4.1   Parameter Validation

A first step to achieving improved decoding accuracies is to explore different parameters to those used in the initial closed-loop system. The difference between MEG and EEG, in terms of the properties of the measured quantity could reveal different features that maximize separability. Essentially, the spectral filter coefficients and the length of the ERP interval could have a significant impact on the classification result. In an SOV as described in Section 4.2.4, several parameter sets will be evaluated starting with the parameters used during acquisition with the closed-loop BMI. The parameters to investigate are the interval length, which is set to additional values of 600 and 800 ms, and the highpass cut-off frequency which is set to additional values of 0.5 and 0.1 Hz. Time intervals from 600 to 1000 ms are common in P300 speller systems though it remains unclear which is the best choice for MEG data. While it is plausible that evoked potentials do not change faster than 10 Hz (in [53] 12 Hz has been found to be optimal), slow potentials could very well have an impact on classification results. Therefore, the two additional frequencies, permitting a longer evolution of brain waves, are taken into consideration, too. Furthermore, the impact of involving all MEG channels rather than hypothetically selected channels with a superior location is investigated although the dimensionality of the classifier feature space further increases. However, the feature selection method is applied analogously to the feature selection performed in the closed-loop BMI, keeping the 64 channels for the final classification constant.

The main challenge in detecting event-related potentials from noninvasive electrophysiological data is the low SNR measured at individual sensor positions. In many studies, this is solved by averaging across several trials at the expense of the time needed to transfer a symbol. The alternative approach is to classify single event intervals and pool the classifier output to make the final decision instead of pooling the data and classifying afterwards. This approach is pursued in the closed-loop BMI and is to be compared with the common approach of pooling the repetitions beforehand in this offline analysis.

4.3.4.2   Spatial Filtering for P300 Recognition as Efficient Noise Reducer and Feature Extractor

Another option to enhance the SNR is to average the signal from several channels. However, the ERP is most likely not equally distributed over several spatially distinct sensor positions. Thus, the coefficients that weight the contribution of a channel to enhance the signal strength of the brain response to be detected have to be determined optimally. I introduced such linear combinations of channels in Section 2.5.1 as a spatial filter. Given the high number of sensors in MEG and the extremely vague knowledge

about the sensors that capture the P300 response, an analytical determination of optimal spatial filter coefficients is advisable. Here I aim at testing five different methods to estimate the filter $\mathbf{W}$ that weights the MEG signals according to Equation 2.6. The first one applies the CSP method, the second method applies a whitening transform, and the other three methods are based on CCA but all applying different model functions that serve as reference signals. As was determined by Farquhar and Hill [53], best practice is to use as many channels as possible and let the machine decide which channels are important. Spatial filters do exactly this, which is why all MEG sensors available will be involved in the analyses. The preprocessing steps are applied as hitherto, but interval length and band-pass filter frequencies are set according to the most promising results of the parameter optimization previously performed.

All spatial filters that I will introduce in the following, have in common that they are represented by a matrix $\mathbf{W}$, which linearly weights the channel data by simple matrix multiplication (Equation 2.6). The estimation of $\mathbf{W}$ differs between methods in the assumptions made and in the analytical approach. Importantly, the transformed data can be considered virtual channels with specific properties, determining the number of informative virtual channels and with it the number of spatial filters. Thus, spatial filtering also serves as a means to reduce the feature space. All subspaces of virtual channels are classified equally as the original channel space using a linear SVM classifier. Filter matrix estimation and classifier training are performed using a set of training data and applied to a set of test data. Evaluation is performed by SOV again.

The first spatial filter to be applied for P300 extraction is the CSP method, introduced in Section 2.5.2. Let $\mathbf{X}_1 \in \mathbb{R}^{C \times N_1}$ be the concatenated MEG time intervals following a standard stimulus and $\mathbf{X}_2 \in \mathbb{R}^{C \times N_2}$ be the concatenated time intervals following a target stimulus, where C is the number of sensors and N_1 and N_2 are the total numbers of samples, i.e. number of trials involved $\times$ number of samples in the time interval. Then, the filter matrix $\mathbf{W}$ is determined as described by Equation 2.7 – Equation 2.10. Since the highest variance of the standard trials is represented by the first columns in $\mathbf{W}$ and the highest variance of target trials is represented in the last columns in $\mathbf{W}$, only the 32 first and 32 last spatial filters are selected to transform the original sensor space to a feature space consisting of 64 channels, comparable to the approach not applying spatial filtering. In contrast to the procedure used in motor imagery BCIs targeting oscillatory brain responses [23, 167], not the variance in the virtual channels but rather the entire virtual channel data are used as features, analogous to the feature involvement in the original sensor space classification. This is done because the variance is not an adequate measure to distinguish the P300 from ongoing brain activity. Rather, the time course of event-related components extracted by the spatial filter holds important information to distinguish the potentials. Once the filter matrix is determined from a training set of data, it is applied to each unseen data interval to transform the data to the new feature space.

For ERP classification in EEG data, Farquhar and Hill [53] found that spatial whitening led to the best performance in several data sets. Because they suggest whitening as the spatial filter in their best-practice guideline for BCIs, this method is also to be tested

with the MEG data from the current experiment. The procedure is quite simple: Let $\mathbf{X} \in \mathbb{R}^{C \times N}$ be the concatenated MEG time intervals, regardless of the stimulus. The filter matrix $\mathbf{W}$ is computed as

$$\mathbf{W} = (\mathbf{XX}^{\mathsf{T}})^{-1/2}. \tag{4.11}$$

The transformation $\hat{\mathbf{X}} = \mathbf{WX}$ reveals a virtual sensor space, where the virtual sensors in $\hat{\mathbf{X}}$ are all uncorrelated. Again, $\mathbf{W}$ is calculated from training data and applied to the new data to be validated.

A last method to be used as a spatial filter is the CCA (see Section 2.5.3). While this method has frequently been applied in detection of steady state brain responses [12, 13, 118, 174], there is only one study that applied CCA for ERP classification [199]. The application of CCA is rather different in steady state signal detection compared to ERP detection. When the task is to detect oscillatory signals of a well-defined frequency, CCA is applied to a single trial where a sine/cosine combination of reference signals is used to determine the correlation between the brain waves and the potential stimulus (see Equation 4.4). This approach is independent of the phase of the stimulus, because the CCA determines the weights regulating the phase, i.e. the ratio of sine and cosine coefficients, independently in each single trial. In ERP detection, the reference signals are unknown, i.e. a template of the expected shape of the event-related brain response can only be estimated. Furthermore, the information available in noninvasive brain recordings of a short time segment comprising the evoked potential of a single event is insufficient to reliably determine reliable canonical variates. Thus, to successfully apply CCA to ERP detection, it is necessary i) to provide an appropriate model function and ii) to estimate the canonical coefficients representing the spatial filter matrix from a sufficient amount of data. Three different model functions will be applied to estimate $\mathbf{W}$ with CCA, which will be explained in the next paragraph. The model functions are the only difference between the last spatial filter methods to be tested. However, the composition of the input variable sets is common for all methods. Analogous to the CSP approach, let $\mathbf{X}_1 \in \mathbb{R}^{C \times N_1}$ be the concatenated MEG time intervals following a standard stimulus and $\mathbf{X}_2 \in \mathbb{R}^{C \times N_2}$ be the concatenated time intervals following a target stimulus, where $N_1 = T_1 N$, $N_2 = T_2 N$ and T_1 and T_2 is the number of standard stimuli and target stimuli, respectively. Then a set of model functions is defined, such that $\mathbf{Y}_1 \in \mathbb{R}^{H \times N_1}$ is a concatenation of T_1 copies of a set of H model functions defining the ERP of a standard event, and $\mathbf{Y}_2 \in \mathbb{R}^{C \times N_2}$ holds T_2 copies of H model functions defining the ERP of a target event. For the final analysis, which estimates $\mathbf{W}_x$ from a set of training data using Equation 2.13, the matrices attributed to standard and target stimuli are concatenated once more, i.e. $\mathbf{X}$ is of size $C \times N_1 + N_2$ and $\mathbf{Y}$ is of size $H \times N_1 + N_2$. The remaining procedure is as usual: training data and test data provided in an SOV are transformed with the filter matrix $\mathbf{W}_x$, if more than 64 channels remain, the at most 64 best channels are selected using ranking of SVM weights, and the final SVM classifier is trained and tested on the unseen data.

4.3.4.3 Modeling P300 Reference Functions

A relatively naïve but the most intuitive approach is to model a hypothetical template as a reference function that incorporates the theory about the expected signal, which has widely been investigated in the literature. Although the event-related brain responses are not identical in individuals, the notion is that the correlation of the relative slow P300 potential and the optimally linearly weighted sensor data is higher in target related intervals compared to intervals following a standard event. Here we use a Gaussian function which peaks at μ=300 ms. The standard deviation parameter σ is chosen at σ_1=75 ms for the rising slope and at σ_2=150 ms for the falling slope:

$$f(t) = e^{-\frac{(t-\mu)^2}{2\sigma^2}} \text{ where } \sigma = \begin{cases} \sigma_1 & \forall t \leq \mu \\ \sigma_2 & \forall t > \mu. \end{cases} \tag{4.12}$$

Thus, a skewed Gaussian shape represents the model function for target events. The background of the skewness is that the processing of the visual stimulus can start, at the earliest, roughly 100 ms after onset, which is the time window for early visual processing. The other assumption is that the potential extends over a longer period than it requires to evolve. Furthermore, the prolonged descent of the model function also takes peak latencies later than 300 ms into consideration, which have been reported in many studies on oddball paradigms [119, 127]. For standard events, the model function is simply a zero signal. With these reference signals, the CCA method finds a spatial filter that transforms the sensor data to a component that best fits the template after target events have occurred and shows minimal variability after standard events. Note that only one model function is provided instead of a set of model functions, which reduces the CCA to the multiple correlation method and decomposes only one spatial filter, generating one virtual channel.

The second approach to generating a set of reference functions is that suggested by Spüler *et al.* [199], who determined the reference ERPs as an average over all standard trials and an average over all target trials, respectively. Thus, as many reference functions as available channels are generated, each representing a noise-reduced version of activity in that channel, following target and standard events, respectively. In contrast to the previously defined reference function, this approach is less hypothetical but more data-driven, because no assumptions about the course of the ERP's waveform are made. The basic assumption is that the average signal of single channels represents a good estimate of the channel's contribution to the ERP. The CCA combines the partial signals to components highly correlating with linear combinations of the single trial data. As a result, the spatial filter $\mathbf{W}_x$ defines the contributions of each channel to subcomponents determined from the averaged signals by $\mathbf{W}_y$.

A more data-driven approach has been developed during this work [170] by generating reference functions as follows. Analogously to the first solution of generating an ERP template as the reference, activity following standard trials is assumed to be a zero signal. For the activity following target trials, one model function for each time step in the interval of interest of size H is defined by setting the value at time point k, $k = 1, \ldots H$

after onset of a target trial to value 1. Thus, the model functions are easily generated by setting a zero matrix $\mathbf{0}_{H \times H}$ for all standard trials and an identity matrix $\mathbf{I}_H$ for all target trials. The concatenation of the respective matrices reveals a weight for each time step in $\mathbf{W}_y$ which is by definition identical to the components in $\hat{\mathbf{Y}}$ (Equation 2.12) at target onset. Due to the constraint that $\hat{\mathbf{X}}$ and $\hat{\mathbf{Y}}$ are composed such that correlation is maximal, $\mathbf{W}_y$ accounts for optimal temporal composition of sample points after onset and $\mathbf{W}_x$ accounts for optimal spatial composition of channels. Therefore, CCA combined with the suggested reference functions can be considered a spatio-temporal filter. The advantage of the method is that the evolution of ERP subcomponents is estimated implicitly by the method applied and thus free of hypotheses. In combination with high density MEG this could reveal new insights into the generation of target-related potentials in oddball paradigms, commonly denoted as P300 potentials.

4.4 Asynchronous Control of an Autonomous Effector with Low Transfer Rates

The design of the paradigms described in the previous sections already illustrates that ITR is low using noninvasive brain imaging techniques. Even if users perform perfectly, achieving 100% correct selections, the ITR would be 24 bit/min when selecting one out of four items every 5 s and 15.5 bit/min when selecting one out of six items every 10 s. This is definitely insufficient to continuously control an upper limb prosthesis with several degrees of freedom. Nevertheless, noninvasive control of artificial upper limbs could be possible if the continuous control part is transferred to an intelligent, autonomous device, which requires only a few commands to submit the user's intention. Here, a virtual reality system already introduced in Section 4.3.2 is employed that is capable of autonomously grasping and picking up an object. Communication between user and system is possible by visual stimulation and feedback and importantly, by voluntary brain wave generation. The drawback of the first two paradigms is that they are synchronously driven, i.e. a predetermined rigid timing scheme is applied, and the user has no option to determine the start of a grasp or to withhold a grasp and persist in a resting state. In this section, I will describe a framework, which facilitates the asynchronous control of an autonomously grasping robotic arm.

4.4.1 Framework for Effective Asynchronous Effector Control

An essential requirement for asynchronous control is that a new command can be transmitted at any point in time. Although the latency between intention and execution still is relatively high due to the duration of selection a noninvasively driven BCI permits, the BCI is considered to be asynchronous from the perspective of the onset of the user's intention. Regardless of this latency, the framework introduced in this section is controllable in real-time. Similar to the previous approaches, a selection has to be made which out of several objects has to be grasped. However, in contrast to the previous approaches, the grasp does not start immediately after the selection is performed, but rather the system waits for a start command or a reselection. For this purpose, two

virtual buttons, a start button and a stop button, are required, which can be selected similarly to the target objects. Furthermore, a fixation cross is required to permit resting intervals in which no command is transferred. To provide reasonable control options and to execute the respective commands, several states of the system are defined, which are denoted "start", "grasping", "grasped", "pick up object", "presenting", "replace object", "retract" and "break". The virtual scenario showing three of the states and a state diagram is shown in Figure 4.1. When the robot is in the start position, the
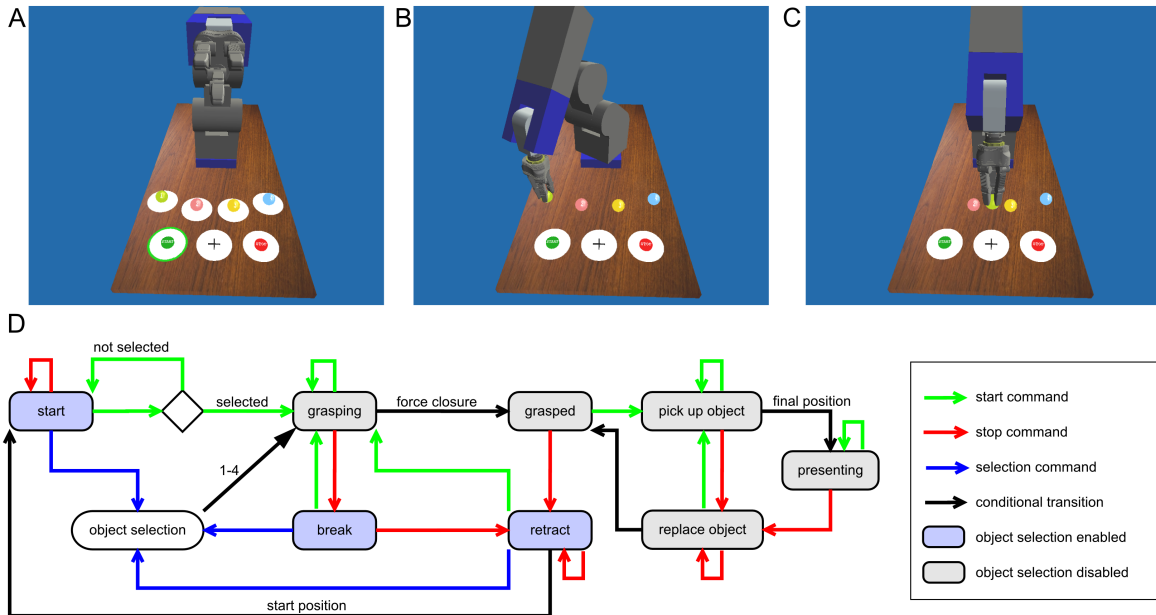

Figure 4.1: Virtual scenario showing the robotic gripper in the states *start* (A), *grasped* (B) and *presenting* (C) and the state diagram (D). The figure originally has been published in [173].

system waits for an object number to be selected for grasping. If an object selection is received, a green ring indicates the object decoded from brain activity. The grasp is only started, when the item "start button" is selected; otherwise reselection or resting is expected. Importantly, resting is possible in each of the states, suspending the delivery of commands. When the gripper is in grasping mode, visual stimulation for object selection is disabled, because only a stop command is a reasonable action, which will interrupt the movement. A further stop command retracts the gripper, while a start command continues the movement. After complying with the force closure condition, the gripper can be retracted by a stop command, or the object can be picked up by a start command. When the gripper is in the final position, each reversed movement can be initiated by the stop command, and each forward movement can be repeated by a start command. Visual stimulation of objects is only enabled in the states "start", "break" and "retract" to prevent user irritation and unwanted selections when object selection is not reasonable. With this framework it is possible to grasp and manipulate an object uning only three commands: select, start and stop.

4.4.2 Employing Flicker Stimuli for Self-Paced Effector Control

Irrespective of the results, the two approaches based on SSVEF detection and P300 detection reveal, SSVEP detection appears to be more suited to asynchronous control. Two reasons are that SSVEPs can be decoded in shorter intervals compared to P300 potentials and that the absence of an SSVEP is easier to decode than the overall absence of a P300 potential. Furthermore, in the targeted scenario in most cases only two selectable items are visually highlighted, which violates the concept of the oddball paradigm having an insufficient number of standard events. Therefore, the asynchronous BMI is to be controlled by SSVEP detection. Four virtual objects are tagged with stimulation surfaces flickering in object selection mode at frequencies 6.818 Hz, 7.5 Hz, 8.333 Hz and 9.375 Hz. The start and stop buttons flicker continuously at 10.714 Hz and 12.5 Hz, respectively. SSVEFs are decoded by means of CCA, according to the method described in Section 4.2.4, involving three harmonics. Classification is performed using the argmax classifier Equation 4.10 but with an extension which takes an idle state into account. The resting intervals are distinguished from the selection intervals by applying a confidence threshold th_f, which is determined from a set of calibration data for each of the frequencies f separately. The detection is performed asynchronously in intervals of 1000 ms involving an interval of the previous 2000 ms of data. The interval length is chosen to provide a compromise between achieving reliable decoding and ensuring an acceptable delay with the goal of achieving a high ITR. With respect to the uncertainty of a single prediction made from a 2000 ms interval, the constraint is constituted that three identical selections are predicted consecutively, while resting intervals are allowed between predictions. This results in a dwell time of at least 4000 ms for selecting an item. The stage of a prediction is indicated by colored feedback rings around the decoded item, ranging from light blue over cyan to green for the final selection. After a selection is made, the next decoding feedback is generated 3 s after the feedback appeared, to provide the user with a short break to plan the next action.

4.4.3 Validation of Measurement Modalities for SSVEP Detection

The MEG device provides the capability of simultaneously recording EEG activity. This feature facilitates the investigation of the information content in both physiological signals for decoding brain activity. Here the SSVEP and SSVEF induced during item selection as described in the previous section is to be compared. In contrast to classical statistics commonly used to investigate brain function in both modalities, the decoding accuracy which is determined from single trial classification provides a direct measure of the data quality that can be achieved with each of the acquisition methods. Since the CCA method has already been proven to provide good results in SSVEP detection [118], and this method is well-suited to determining the contribution of individual channels from among a number of channels, this method is used to systematically investigate the

contribution of the channels involved to the decoding accuracy. Both MEG and EEG signals reflect an electrophysiological measure of brain activity that emerges simultaneously. Thus, when sampled at the same rate and normalized to a common scale, MEG and EEG channels can be involved simultaneously in a CCA. The algorithm then finds the linear combination of channels that maximally correlates with the reference signal, i.e. an oscillation of a specific frequency.

To investigate the performance outcome after applying several sets of channels, the MEG and EEG data that were recorded during the robot control task in Section 4.4.2 are used in an offline analysis. For this purpose the data are segmented into intervals of 4.0 s, starting at the onset of a new selection trial in the calibration runs, are shifted in 3.0 s steps, and finish at the latest when a decoding result was fed back. Decoding accuracies are determined in a cross-validation scheme leaving one run out for testing. The preprocessing and classification is performed analogously to the online experiment. However, resting state detection is not performed with these data, because the aim is to investigate the quality of SSVEP/SSVEF detection. The channel sets are generated as follows. Each initial set consists of only one channel that is selected over the occipital lobe at a position where the signal commonly is expected. Afterwards, the electrode or sensor closest to the seed point is added to the channel set. For EEG data, this is done starting at electrode Oz and involving up to 15 electrodes, while for the MEG channel set up to 80 sensors are used. The decoding accuracy is determined for each channel set separately as well as for all combinations between EEG and MEG channel sets.

5. Experiments for Validation of Approaches for Improved BMI control

5.1 Common Experimental Setting

In this chapter I will introduce three experiments aiming at the realization of the approaches described in the previous chapter. All subjects participated voluntarily and were paid for participation. Each of the studies presented here was approved by the ethics committee of the Medical Faculty of the Otto-von-Guericke University of Magdeburg. All participants gave their written informed consent and received payment for participation. The experiments have the purpose to evaluate the closed-loop BMI implementations on one hand and to acquire data to validate algorithms in an open-loop manner on the other hand. The MEG system used in all experiments was a BTi 4DNeuroimaging system, equipped with 248 magnetometers. Furthermore, a sampling rate of 678.17 Hz was chosen consistently in each of the experiments.

5.2 SSVEF Based Virtual Reality Object Selection

The initial experiment aims at probing the ability to select objects in a virtual environment by decoding brain waves measured with MEG. A total of 22 subjects participated in the experiment. Subjects were seated in a magnetically shielded room, 1 m in front of a rear projection screen. On the screen a virtual scenario was presented showing a table with four objects placed in a square alignment and separated by a visual angle of 8.5° (see Figure 5.1a). The subject's task was to focus one of the objects which was specified before a new run started. When the flicker stimulation started, their gaze was required to sustain at the circular region surrounding the target object. One stimulation trial ended after 5 s, followed by random feedback in training runs and decoded feedback in

<table>
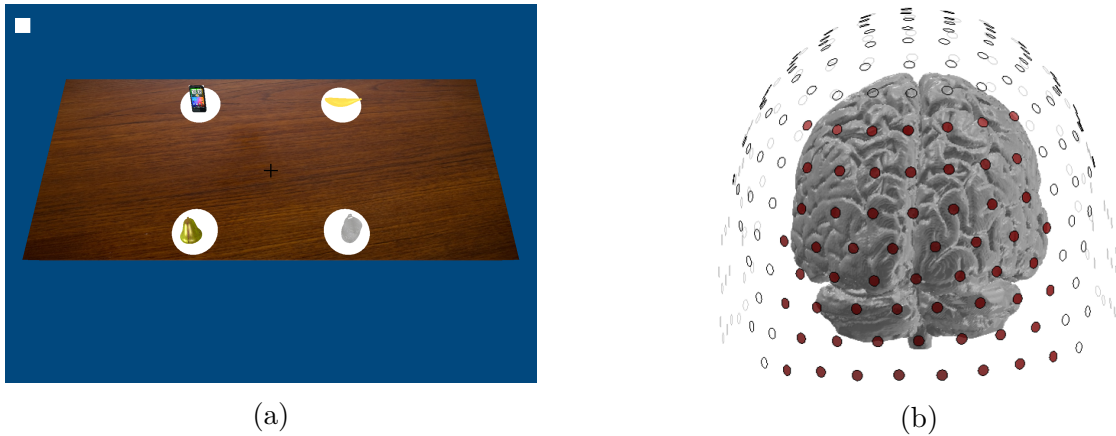<tr><td>(a)</td><td>(b)</td></tr>
</table>

Figure 5.1: (a) Virtual scenario presented to select one of the objects (mobile phone, banana, pear, cup) (b) MEG sensors involved for online decoding of SSVEFs (posterior view).

online runs, respectively. Specifically, the decoded object was marked by a green ring, the remaining objects by a red ring for 1.5 s. Afterwards, objects randomly changed the position and thus were stimulated with different frequencies. The subjects had to track the target object during the entire run, i.e. they had to direct their gaze to the new position of the target object. The time between the repositioning of objects and the next stimulation was of 3 s duration. In total, 32 of such trials were performed per run while subjects performed six to nine runs. Due to incipient system development three subjects did not receive decoded feedback but random feedback. In order to demonstrate the authenticity of the system some subjects performed free selection runs where they chose the target object self-dependent in each single trial. The correctness of the decoded selection they signalized by pressing one button for correct feedback (right index finger) and another button for erroneous feedback (right thumb). The exact number and type of runs performed is listed in Table 5.1. During the experiment MEG signals of the full sensor array were recorded while only 59 posterior sensors, expected to capture magnetic fields of occipital brain regions, were processed for online detection of SSVEFs (see Figure 5.1b). The online processing, designated to determine the item to be selected, was performed as described in Section 4.2.3. Importantly, the classifier was updated after each single trial in runs providing feedback. This procedure provides most recent data and a maximum number of train samples to the decoder. Advanced analyses using the recorded data were performed as described in Section 4.2.4.

5.3 P300 Based Virtual Reality Object Selection

In a second experiment a different strategy of reading the users intention from brain waves was pursued. In total, 17 subjects participated in this experiment which was based on the oddball paradigm (see Section 4.3.1) and utilizes the detection of event related potentials denoted as P300 potentials. Again, the brain-controlled selection of

# subjects	instructed selection		free selection
	random feedback	decoded feedback	
1	7	-	-
1	8	-	-
1	9	-	-
1	2	4	-
1	4	4	-
2	4	3	1
1	2	3	1
1	2	5	2
4	2	5	1
9	2	4	2

Table 5.1: Number of subjects performing different combinations of run types.

virtual objects was aimed with this BMI implementation but there are several advantages compared to the first experiment. The main advantage is the independence of eye gaze which was achieved by instructing the subjects to focus a central fixation cross during the whole experiment. Furthermore, fixation was visually controlled by monitoring eye movements. An important upgrade of the virtual environment software was the integration of a grasping robot able to pick up and put down the selected objects. Another gain of the paradigm is a higher number of alternatives that can be selected with that approach. Here, six objects were used due to constraints of the robot's work space. Figure 5.2a depicts the scenario used in this experiment. However, compared to the first experiment, the length of one selection trial is doubled to 10 s. The MEG was recorded and immediately processed in order to provide a feedback of the currently decoded intention. The task of the subjects was to direct their attention to the background intensifications of one of the objects while visually focussing a fixation cross. They had to ignore all background intensifications different from that of the target object. To ensure that their attention maintained on the stimulus stream, they were instructed to count the number of intensifications of the target object. The target object was cued as described in Section 4.3.2 for instructed selections. Instructed selections were required to collect training data and to evaluate the systems reliability. However, additionally to instructed selection runs subjects were permitted to freely select an object, proving the authenticity of the system. Finally, a demonstration of an intelligent grasping algorithm developed at Fraunhofer IFF was shown by performing an autonomous grasp to the selected object. Feedback was generated according to the processing pipeline described in Section 4.3.3. The sensors involved in the decoding approach are shown in Figure 5.2b. The classifier was trained after each run conducted in instructed selection mode, starting with the second run. The number and type of runs performed by subjects varied and is summarized in Table 5.2. All subjects performed at least seven runs each consisting of 18 selection trials. Virtual grasping of freely selected objects was tested by twelve subjects whereas only six trials were performed due to limited time and the slow movement of the grasping robot. In runs where subjects were free to select the target

(a)

(b)
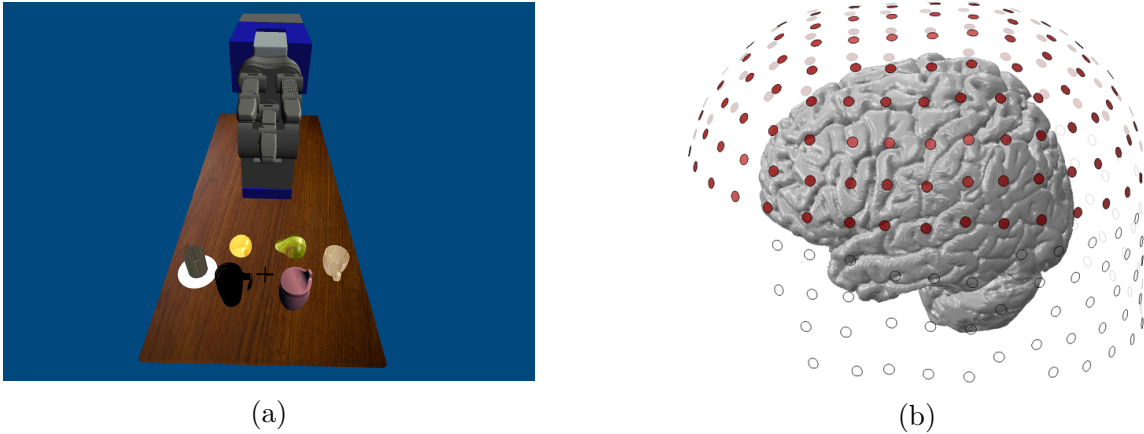
Figure 5.2: (a) Virtual scenario presented to select one of six objects for grasping (b) MEG sensors involved for online decoding of P300 potentials.

object, they indicated a wrong decoding result by saying "no" but gave no response for a correct decoding result. This information is important to determine the decoding accuracy also in free selection mode but insufficient to perform offline analysis, because the subject's true intention is still unknown.

# subjects	instructed selection		free selection	grasp selection
	random feedback	decoded feedback		
1	2	5	-	-
1	3	4	-	-
1	2	4	2	-
1	4	4	1	-
1	2	5	2	-
1	3	3	2	1
3	3	4	1	1
8	2	4	2	1

Table 5.2: Number of subjects performing different combinations of run types.

5.4   Asynchronous Control of a Grasping Device

In a final experiment, the functionality of the system was further extended by facilitating asynchronous control of the robot. The usability was also improved by adding the option to voluntary initiate go and stop commands as well as permitting resting intervals. The demonstrator was tested by eight subjects who were seated in a magnetically shielded room, 1 m in front of a screen. The sensor array which was used for online decoding of SSVEFs comprised 59 occipital sensors, identical to the array used in first experiment (5.1b). In parallel to the MEG, the EEG was registered at 30 electrode sites for offline analysis. Impedance was kept below $5\,\mathrm{k\Omega}$. The visual scene and the

control environment as well as the decoding approach used in this experiment were described in Section 4.4.2. The task of subjects was to initiate control commands by overtly focusing the stimulation marker of a control item. At each point in time the subjects were aware of the current decoding state of the system. The experiment started with 3–4 calibration runs, in which the to be selected item was cued by a black ring. Selectable items were four objects, two buttons and the fixation cross. The online feedback was presented in calibration runs but the robot didn't move in order to rapidly collect training data. In the first run the resting interval was generally fed back as correct selected, because the confidence thresholds could be determined only with a sufficient amount of training data. The classifier was trained after each calibration run. Afterwards, 3–4 runs were performed in robot-control mode, where the to be selected control commands were instructed to the subject prior to the start of a run. The subjects had to select, grasp, and pick up an object and afterwards replace the object and retract the gripper. The experimenter determined the order of objects to be grasped. If the system was doing an undesired action, the subjects had to initiate the respective command to continue the desired action. In robot-control mode a high amount of resting intervals were required, because the robot moved relatively slow and subjects had to prevent undesired commands.

6. Results of Experimental Investigations

6.1 Online Decoding Results for Object Selection

As shown in Table 5.1, the number of runs used for training, for decoding of instructed selections and for decoding of free selections varied over subjects. Accordingly, 19 subjects were presented with feedback resulting from SSVEF decoding, either after selecting a previously instructed object or after freely selecting an arbitrary object. Importantly, all subjects performed the task well above the chance level of 25%. On average, in 74.4% (std: 16.6%) of all trials the decoded object was identical with the actually selected object. A total of 78 runs were performed in instructed selection mode, with an average decoding accuracy of 72.0% (std: 16.7%). Runs in free selection mode were performed after the runs in which target objects were instructed, 27 in total over all subjects. Free selection permitted an average decoding accuracy of 81.3% (std: 14.3%). A Wilcoxon rank sum test proved that the decoding accuracy in free selection runs was significantly higher than in instructed selection runs ($p_{rs} < 0.01$). It is important to note that free selection always proceeded in later runs. Possibly, therefore, the advanced performance is induced by a superiorly trained classifier and subject's increasing experience. A more detailed demonstration of the relationship between decoding accuracy and the experiment's progress is depicted in Figure 6.1. The average decoding accuracy varying as a function of the number of the current run is indicated by black squares, where error bars indicate the standard error of the mean. Although the accuracy tends to increase progressively, the correlation is not significant. To further demonstrate the predominant performance in free selection runs, average accuracies are also shown separately for instructed selection runs (red crosses) and free selection runs (blue asterisks). Concerning the speed of the BMI, the information transfer rate is the commonly used measure in this field. The timing and decoding

accuracy of the proposed BMI gives an average information transfer rate of 10.0 bit/min, ranging from 1.4 to 17.4 bit/min for individual subjects.
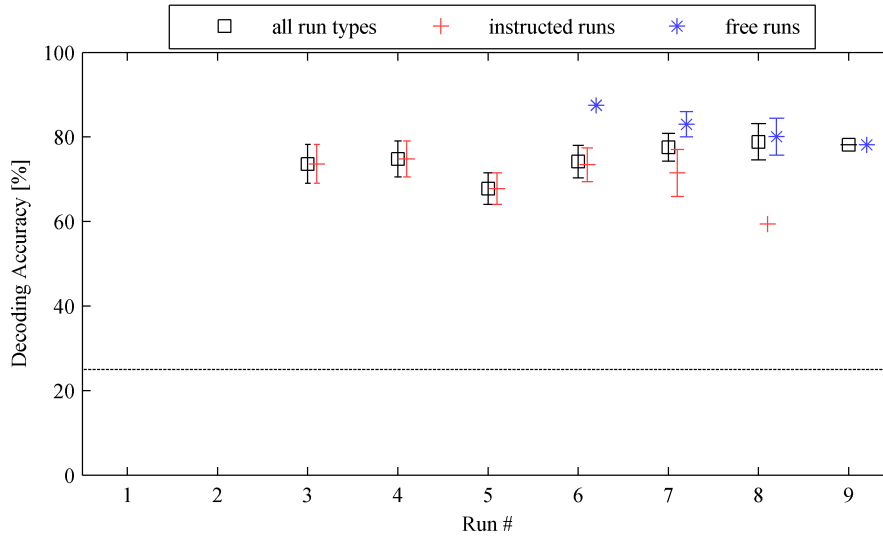
Figure 6.1: Decoding accuracy per run averaged across subjects. Red crosses and blue asterisks show the performance of instructed selection runs and free selection runs, respectively. The dotted line indicates the chance level.

6.2 Optimizing Detection of Steady State Visual Evoked Magnetic Fields

In an offline analysis the recorded MEG data were analyzed by applying different parameters (5 feature extraction methods, 9 interval lengths, 3 numbers of harmonics, and 6 types of classifiers). Data from all 22 participants were involved in the analysis. The validation was performed for each parameter combination described in Section 4.2.4 resulting in one decoding accuracy value per parameter set. Before a detailed analysis of the results was done, statistically significant differences of the obtained decoding accuracies were analyzed by means of a 4-way analysis of variance (ANOVA). Significant difference was determined for all factors which were "feature space" ($F_{4,16037} = 2897.3$, $p = 0.0$), "interval length" ($F_{8,16037} = 2706.3$, $p = 0.0$), "harmonics involvement" ($F_{2,16037} = 37.8$, $p = 0.0$) and "classifier" ($F_{5,16037} = 803.3$, $p = 0.0$). Multiple comparisons adjusted by a Bonferroni correction revealed a statistically significant difference for all pairs of feature spaces except FT and CSP as well as CCA and MEC, for all combinations of interval length, between one and two as well as one and three harmonics involved, and between all pairs of classifiers except the combinations of LDA, nBayes and nCentroid. Additional findings will be explained subsequently using nonparametric statistical testing methods. In these analyses, single parameters are investigated while other parameters are kept as used in the online experiment.

In a first step the impact of feature extraction methods was investigated. In the offline validation scheme, the average decoding accuracy was 72.3% (std: 16.6%) using a

Fourier transform and regularized logistic regression, similar to the methods performed in the online experiment. Because the trials involved in classifier training and in testing for classification was not identical to the closed-loop BMI experiment, the offline validation result deviates from the online results but the difference is not statistically significant ($p_{rs} = 0.76$). Using the same classifier method and the same interval length of 4.5 s, but different feature extraction methods facilitates significantly different results. While the CSP method revealed a non-significantly lower ($p_{sr} = 0.45$) average decoding accuracy of 70.5% (std: 16.4%), the performance of CCA, MEC and MCC was significantly higher ($p < 0.001$) with accuracies of 92.3% (std: 7.9%), 92.7% (std: 6.6%) and 91.2% (std: 7.3%), respectively.

A second parameter of interest was the length of the interval used to convert the time series into the feature space. With shorter analysis intervals the decoding accuracy decreases for all feature extraction methods. The decrease is statistically significant with interval lengths of 2.5 s and shorter, as indicated by a Bonferroni corrected multiple comparison test of an one-way ANOVA with the factor "interval length" ($F_{8,593} = 196.6, p < 0.05$). Consequently, an interval length of 3.0 s could be used for faster control of the system without significant loss of accuracy. See Figure 6.2 for dependence of the performance from the analysis interval for several feature extraction methods. Importantly, CCA, MEC and MCC show no statistically significant difference for all intervals except for the interval of length 0.5 s ($F_{2,65} = 4.8, p < 0.05$). Although CCA appears to perform better for this short interval, the accuracy is quite low for BMI control. In accordance with the results obtained with the 4.5 s interval, CCA, MEC and MCC reveal significantly higher decoding accuracies than Fourier features for all interval lengths ($p_{rs} < 0.05$) except the 0.5 s interval. Similarly, CSP reveals a slightly lower decoding accuracy but the difference becomes significant only with interval length 0.5 s, where accuracy is weak anyway.
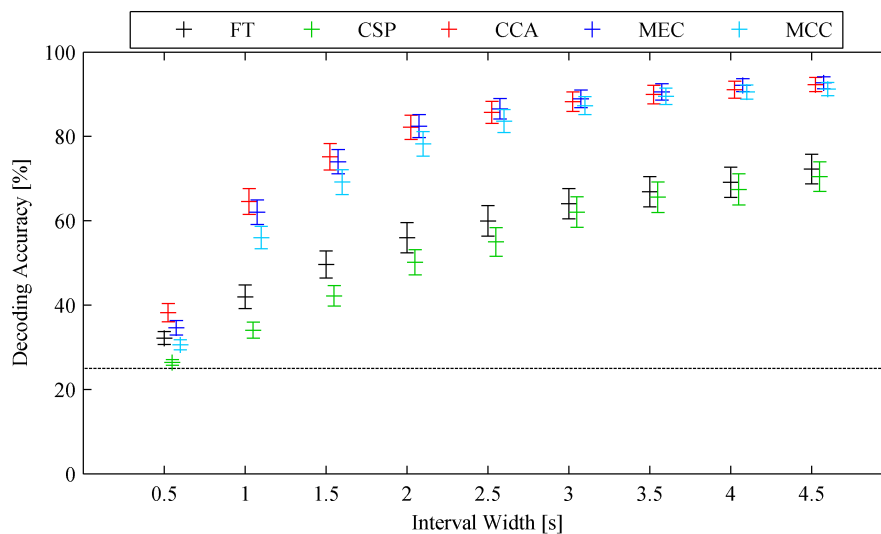

Figure 6.2: Decoding accuracy for different interval sizes achieved with different methods averaged over subjects. The dotted line indicates the chance level.

A higher degree of spectral information was achieved by adding the second and third harmonic of each stimulation frequency to the input space of each feature extraction method. Considering all methods and interval lengths using the rLR classifier, the harmonics show a statistically significant effect ($F_{2,2969} = 3.2, p < 0.05$). However, none of the methods provide statistically significant higher decoding accuracy at any interval length, as shown by performing a Wilcoxon rank sum test, although a trend of slightly improved performance is present in average values. In contrast, a Wilcoxon sign rank test performs pairwise comparisons and reveals the interval width and feature extraction method combinations showing significant improvement by adding harmonics. Significant improvements for all combinations of feature extraction methods and window lengths are shown in Table 6.1. Single asterisks indicate $p_{sr} < 0.05$ and double asterisks indicate $p_{sr} < 0.01$. Involvement of harmonics has no effect on MCC features. For some parameter combinations involvement of two additional harmonics is more advantageous than adding only one harmonic. Generally, involvement of harmonics has the highest impact for Fourier, CSP and CCA features while being also beneficial for MEC features.

[s]	0.5	1.0	1.5	2.0	2.5	3.0	3.5	4.0	4.5
Fourier	-/-	-/-	*/**	*/**	**/*	**/**	**/**	**/**	**/**
CSP	-/-	-/**	-/**	**/**	**/**	-/**	*/**	**/**	**/**
CCA	-/-	*/-	**/**	**/**	*/*	*/*	-/*	*/**	**/**
MEC	-/-	-/*	**/**	*/*	-/-	-/-	-/-	-/-	*/**
MCC	-/-	-/-	-/-	-/-	-/-	-/-	-/-	-/-	-/-

Table 6.1: Significance of harmonics involvement. First item indicates significant improvement when involving the 2nd harmonic, second item indicate significance of involvement of 2nd and 3rd harmonic.

Finally, the effect different classifiers had on discriminating SSVEFs in the different feature space representations was investigated. The CCA, MEC and MCC feature extraction methods can be considered first. A special property of the feature spaces generated with these methods is that each stimulation frequency is associated with one feature, i.e. the feature space is four dimensional in this case. Furthermore, the features represent a direct measure for the amount a frequency is present in the signals, meaning that higher feature values indicate a higher probability that the frequency is the target frequency. With this background a quite simple classifier can be applied to those feature spaces, namely the argmax classifier which selects the frequency that provides the highest feature value. Interestingly, this classifier performs equally well compared to all other classifiers ($F_{4,329} = 1.0$, $p = 0.41$). The average decoding accuracy for the argmax classifier is 91.1% (std: 9.7%), 92.5% (std: 6.6%), 91.1% (std: 7.6%) for CCA, MEC and MCC, respectively. Comparing rLR pairwise with other classifiers for the three feature extraction methods, all classifiers except LDA for CCA features and all classifiers except argmax for MEC and MCC features show a significant difference ($p_{paired} < 0.05$) of decoding accuracy.

In contrast to the direct frequency-feature representations, the FT and the CSP reveal higher dimensional feature spaces due to the involvement of multiple channels (and harmonics). As pointed out in the beginning of this section, these two methods showed significantly lower performance than direct frequency-feature methods. Here, the decoding accuracies achieved with different types of classifiers significantly varies when applying the FT feature space ($F_{4,109} = 2.6, p < 0.05$) but not with CSP features ($F_{4,109} = 0.42, \ p = 0.8$). Note that the initially chosen classifier used in the online experiment reveals the highest accuracies. It can be seen with pairwise comparisons of classifier accuracy that LDA performs significantly lower with FT features and CSP features, whereas nBayes, kNN and nCentroid perform significantly lower only with FT features but not with CSP features, indicated by $p_{sr} < 0.05$ in signed rank tests. The LDA and kNN classifiers show the highest loss in accuracy when using higher dimensional features spaces as with FT and CSP. An overview of achieved decoding accuracies with different classifiers and methods is shown in Figure 6.3.
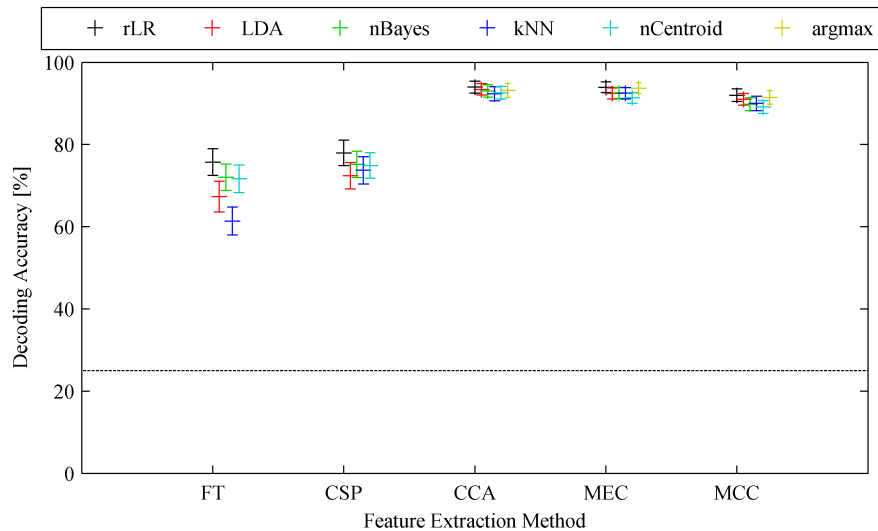
Figure 6.3: Decoding accuracy for different feature extraction methods achieved with different classifiers, averaged over subjects. Chance level is indicated by the dotted line.

In summary, the highest decoding accuracies were achieved by extracting features with the CCA method and classifying the data by a rLR classifier, even though MEC and MCC were comparably accurate and all classifiers performed comparably well on these three feature spaces. Section 4.2.4 states that the reliability of the frequency decomposition increases with longer stimulation intervals. This is confirmed by the experimental data in which highest accuracy is achieved with time intervals of 4.5 s (c.f. Figure 6.2). However, long decision times permit the initiation of only a few commands in a given time. Thus, the information transfer rate was calculated from the decoding accuracy values, given the respective time interval (Equation 4.9). As a result it is apparent that the highest ITR averaged over subjects is found at 1.5 s intervals, using two harmonics in the CCA method and classifying by means of rLR. The bit-rate was 40.0 bit/min on average with this parameter set whereas the best subject would have achieved 75.3 bit/min

using a 1.5 s interval and even 87.9 bit/min with the 1.0 s interval. For more detailed results on other interval sizes and other feature extraction methods see Figure 6.4. Note that the ITR measure is a theoretical value, estimated from temporally separated signal intervals which were cut out from the initial, actually longer stimulation interval.
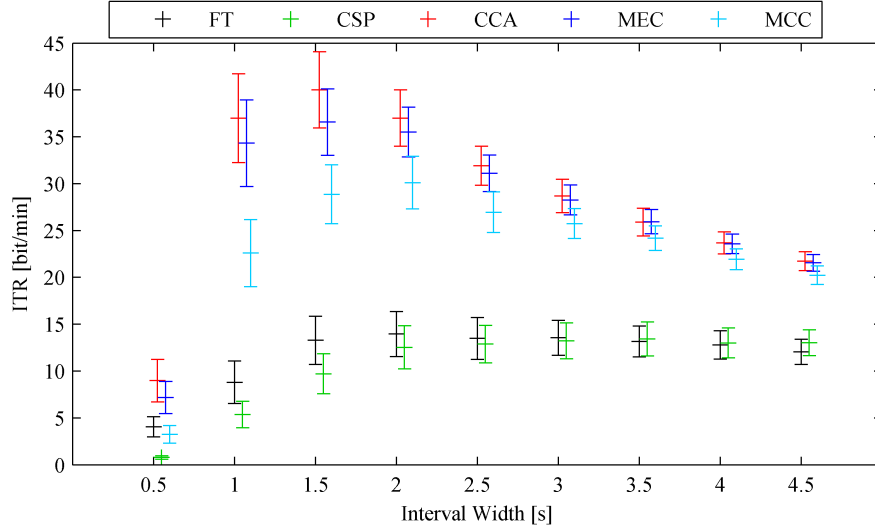
Figure 6.4: Information transfer rate for different interval sizes achieved with different methods, averaged over subjects.

6.3   Online Decoding Results for Grasp Initiation of a Selected Object

The performance achieved by subjects in the experiment based on the oddball paradigm was 78.2% (std: 12.6%) on average across subjects and across all runs which provided decoded feedback. With respect to the number of objects that were available for selection the guessing level is 16.7%, which implies that the achieved decoding accuracy ranging from 55.6% to 92.1% for individual subjects was well above chance level. Distinguishing the runs where selections were instructed or a free choice was made, the average decoding accuracy of 73.9% was lower for instructed selections compared to free selections where it was 85.9% on average. A Wilcoxon rank sum test indicates that this performance difference is statistically significant ($p_{rs} = 0.03$). Importantly, when virtual grasping rather than visual indication was presented as feedback, the average accuracy was even higher at 91.2%. Eight of the twelve subjects who performed grasping runs, achieved perfect control, meaning that the virtual robot grasped the selected objects in all six trials correctly. The decoding accuracy of each run is depicted in Figure 6.5. Given the trial length and decoding accuracies, the ITR is 8.1 bit/min on average, ranging from 3.4 to 12.0 bit/min for individual subjects.
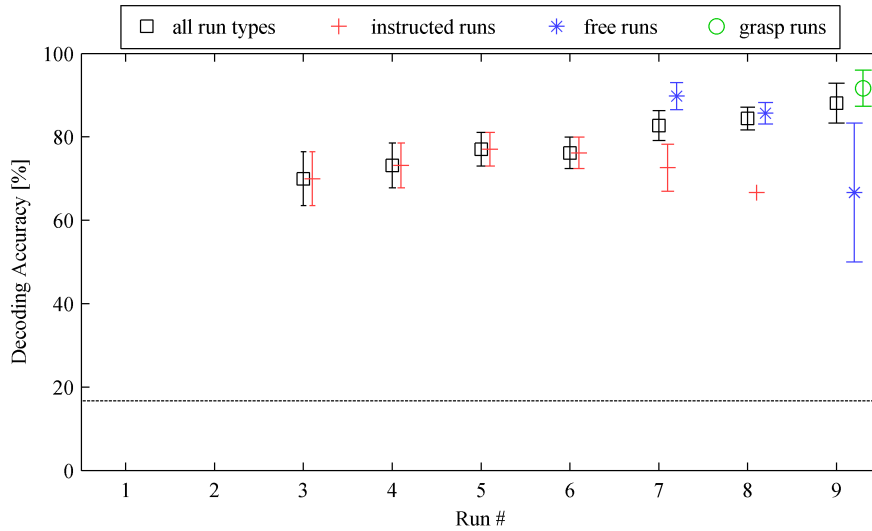
Figure 6.5: Decoding accuracy per run averaged over subjects. Red crosses show the performance of instructed selection runs, blue asterisks indicate free selection runs and the green circle indicates the grasping run. The dotted line indicates the chance level.

6.4 Optimizing Detection of P300 Potentials Evoked in the MEG

In the online decoding of the P300-guided object selections, hypothetical assumptions derived from relevant EEG studies defined the parameter set used to extract the feature space for the classifier. Presumably, the chosen set of parameters was suboptimal for the high density MEG data. Thus, some parameter variations are investigated to find a potentially more suited processing chain for the proposed BMI based on MEG. For each combination of the parameters interval length, high-pass cutoff frequency, number of channels initially involved, and pooling method the classification was repeated offline. The obtained decoding accuracies were tested by means of a 4-way ANOVA to determine significant effects of the parameters. No differences were found for the factors "size of the analysis interval" ($F_{2,611} = 0.2$, $p = 0.78$) and "size of the sensor array involved" ($F_{1,611} = 0.3$, $p = 0.57$). However, statistically significant differences were found for the factors "high-pass cutoff frequency" ($F_{2,611} = 36.5, p < 0.001$) and "pooling method" ($F_{1,611} = 42.5, p < 0.001$). A post-hoc test for multiple comparisons using Bonferroni adjustment shows that the $0.1\,\text{Hz}$ and the $0.5\,\text{Hz}$ cutoff frequency revealed higher decoding accuracies, significantly different from the initially used $1.0\,\text{Hz}$ high-pass filter. Furthermore, pooling the classifier output as performed in the closed-loop BMI, permits significantly higher accuracy than pooling the MEG epochs before classification.

Using the parameters as chosen for the experiment, a decoding accuracy of 80.8% (std: 10.4%) on average was achieved with the offline analysis. This is not significantly different ($p_{sr} = 0.19$) from the result achieved in the online experiment. The deviation can be explained by the differently varying sets of training data that were involved in online classifier training and with the SOV framework, respectively. The following

analyses investigate the single parameter influence when remaining parameters are kept as initially chosen. Regarding the length of the analysis interval, accuracy was 81.7% (std: 11.0%) on average for 0.8 s and 81.1% (std: 11.6%) for length 0.6 s, which is not statistically significant different from the accuracy obtained with length 1.0 s ($p_{sr} >$ 0.08). Involvement of all available channels also permits a comparably equal ($p_{sr} =$ 0.52) decoding accuracy of 81.1% (std: 12.9%) on average. In contrast, the high-pass cutoff frequency considerably improves decoding accuracy when chosen below 1.0 Hz. A bandpass filter between 0.5 and 12.0 Hz reveals an average decoding accuracy of 87.4% (std: 10.1%), which is significantly higher than the achieved performance using 1.0–12.0 Hz bandpass filtered data ($p_{sr} < 0.001$). A slightly higher averaged accuracy of 88.5% (std: 10.5%) was achieved with the 0.1–12.0 Hz bandpass filter ($p_{sr} < 0.001$) but the improvement is not significant compared to the results obtained with the 0.5 Hz cutoff frequency.

Finally, different decoding accuracies were achieved when pooling the data versus pooling the classifier output of single trials. While the standard approach of pooling epochs is classifying the selections in only 73.0% (std: 13.4%) correctly, the new approach of pooling the real valued classifier output achieves a statistically significantly higher ($p_{sr} < 0.001$) accuracy, compared to the initially reported accuracy of 80.6%. The method of pooling epochs also shows improved accuracy when using a band-pass filter of 0.1–12.0 Hz (84.2%, std: 10.4%) compared to the 1.0–12.0 Hz filter but the method of pooling the real valued classifier output achieves a significantly higher ($p_{sr} < 0.001$) decoding accuracy (88.5%, std: 10.5%) as well. Note, that decoding accuracy is reported as percent correct selection out of six possible items. Since the actual classifier determines binary decisions, it is worth focusing on binary decoding accuracy of the classifier. When epochs are pooled, the classifier input is a noise-reduced signal and less training samples are involved in the classification. The binary decoding accuracy is 84.2% (std: 7.5%) for the 1.0–12.0 Hz filter and 90.3% (std: 6.0%) for the 0.1–12.0 Hz filter. In contrast, pooling the classifier output of single events involves more noisy single epoch signals in the classification scheme. Here the binary decoding accuracy is 72.0% (std: 4.7%) for the 1.0–12.0 Hz filter and 76.9% (std: 4.5%) for the 0.1–12.0 Hz filter. Although the binary classifier accuracy is considerably lower for single epoch classification compared to classifying the previously averaged epochs ($p_{sr} < 0.001$), the summation of five single classifier outputs for each of the six potential targets permits more accurate item selection than directly ranking the six classifier outputs obtained from averaged epochs. Altogether, the results indicate that with the current analysis approach the best performance can be achieved when using the parameters as initially chosen, except when the bandpass filter was selected too conservatively regarding slow potentials, and the lower bound is selected equal to or below 0.5 Hz.

Based on these results, an interval length of 0.8 s and a bandpass filter from 0.1–12.0 Hz appear to be optimal for further analysis regarding spatial filter comparison. Furthermore, pooling the classifier output is retained, but for spatial filtering the full sensor array is used, because all brain signals available may be used to determine the event-related brain responses informative for classification. A 1-way ANOVA was calculated

to determine significant differences between no spatial filtering and the spatial filter methods CSP, Whitening, $CCA_{template}$, $CCA_{average}$, and $CCA_{identity}$. The result confirmed the rejection of the null hypothesis that the decoding accuracies of spatial filter methods have equal mean ($F_{5,101} = 3.1, p < 0.05$). However, Bonferroni-adjusted multiple comparisons of the means showed that only $CCA_{average}$ performs significantly different from applying no spatial filter. Average accuracies were 89.8% (std: 8.1%) without spatial filtering, 91.7% (std: 6.3%) using CSP, 92.4% (std: 5.7%) using spatial Whitening, 92.2% (std: 5.1%) using the template reference function with CCA, 96.1% (std: 3.0%) using trial average as reference function combined with CCA, and 95.7% (std: 3.8%) using zeros and the identity matrix as reference function with CCA. Importantly, the CCA based spatial filtering using the new model of sample point generating reference functions $CCA_{identity}$ and $CCA_{average}$ achieve the highest decoding accuracies. A signed rank test using Bonferroni correction revealed significantly higher accuracy of $CCA_{average}$ compared to all other spatial filters except $CCA_{identity}$ ($p_{sr} < 0.05$). Furthermore, $CCA_{identity}$ shows higher performance compared to no filtering, CSP and $CCA_{template}$. The main results of the P300 detection are summarized in Figure 6.6. Note that for all spatial filtering methods the data were bandpass-filtered (BPF) between 0.1 and 12.0 Hz. In the figure, two reference decoding accuracies are shown: the accuracy achieved with the initial parameter set BPF_{online} comprising a 1.0–12.0 Hz filter and the accuracy achieved with the parameter set determined as optimal but without spatial filtering $BPF_{optimal}$.
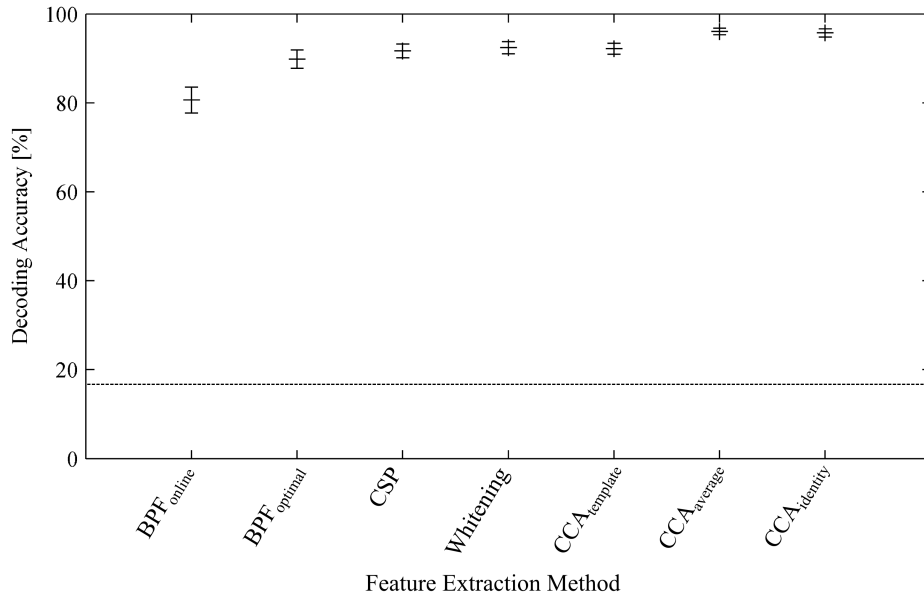

Figure 6.6: Decoding accuracy for several feature extraction methods averaged over subjects. Band-pass filtered (BPF) signals are compared with spatial filter methods. Error bars indicate standard error of the mean, the dotted line indicates the chance level.

6.5 Visualizing Determinant Spatio-temporal Components

Neuroscience does not only focus on discriminating distinctive brain patterns but is also interested in investigating where and when activity occurs. Although detailed analysis and interpretation of brain patterns are out of the scope of this work, I will demonstrate with a few examples how to assess the most important features revealed with the different spatial filtering methods reported in the previous section.

A common property of all spatial filter methods applied in Section 6.4 is that a specific number of channels, regardless of whether selected from the original sensor space or composed as virtual channels, provide the signals that represent the feature space for an SVM classification. Although classifications with most methods rely on more than one component, I will consider only the most prominent component for visualization. Since channel data are normalized and the regularization parameter is determined such that overfitting is circumvented, the weight vector (Equation 2.2) can be interpreted to indicate the importance of specific features. Only the channel that reveals the highest sum of absolute SVM weight values is used to visualize its spatio-temporal distribution, assuming that this component determines the classification result strongest. According to the distributive law, applying the spatial filter $\mathbf{W}$ to averaged signals $\bar{\mathbf{X}}$ is equal to average filtered signals $\hat{\mathbf{X}}$ thus:

$$\bar{\hat{\mathbf{X}}} = \mathbf{W}^{\intercal}\bar{\mathbf{X}}. \tag{6.1}$$

Hence, the mean components for standard and target epochs can easily be determined by multiplying the kth spatial filter with the average signal $\bar{\mathbf{X}}$. Analogising to the calculation of factor loadings in PCA, the correlation of spatially filtered standard and target epochs and original standard and target signals can be determined to evaluate the contribution of a channel to this component:

$$\mathbf{r} = \mathrm{corr}(\bar{\mathbf{X}}, \mathbf{w}_k^{\intercal}\bar{\mathbf{X}}). \tag{6.2}$$

The visualization of $\mathbf{r}$ reveals a topographic distribution of channel involvement and provides an estimate where in the brain the component is generated. However, for a more accurate localization of brain signal components, a source analysis [68] is required. In Figure 6.7 the signal sequences for standard and target epochs, calculated from the spatial filter of the most determinant component (according to the SVM weights) are depicted for one representative subject. The upper left subfigure represents the mean signal across trials using the band-pass filtered epochs (BPF$_{\mathrm{optimal}}$) applying the optimal parameter set as determined in the last paragraph, rather than a spatially filtered component. Assuming the entries of $\mathbf{w}_k$ to be $w_k^i = 0 \forall i \neq k, 1|i = k$ yields equality for $\bar{\mathbf{X}}$ and $\mathbf{w}_k^{\intercal}\bar{\mathbf{X}}$ and implies that $r_k = 1$, given that k is the most determinant channel. The loadings according to Equation 6.2 of the most determinant subcomponent determined from spatial filtering are shown in the remaining subfigures of Figure 6.7, visualized in topographic maps. In the presented case, each of the methods benefits from a component that reveals a relatively slow wave with a positive peak later than $300\,\mathrm{ms}$.

This is a prevalent result when applying oddball paradigms [127]. The topographic maps all show similar patterns of correlations with the strongest components found. The ingoing (red) and outgoing (blue) magnetic fields are distributed over sensors covering tempolateral and parietal brain areas.
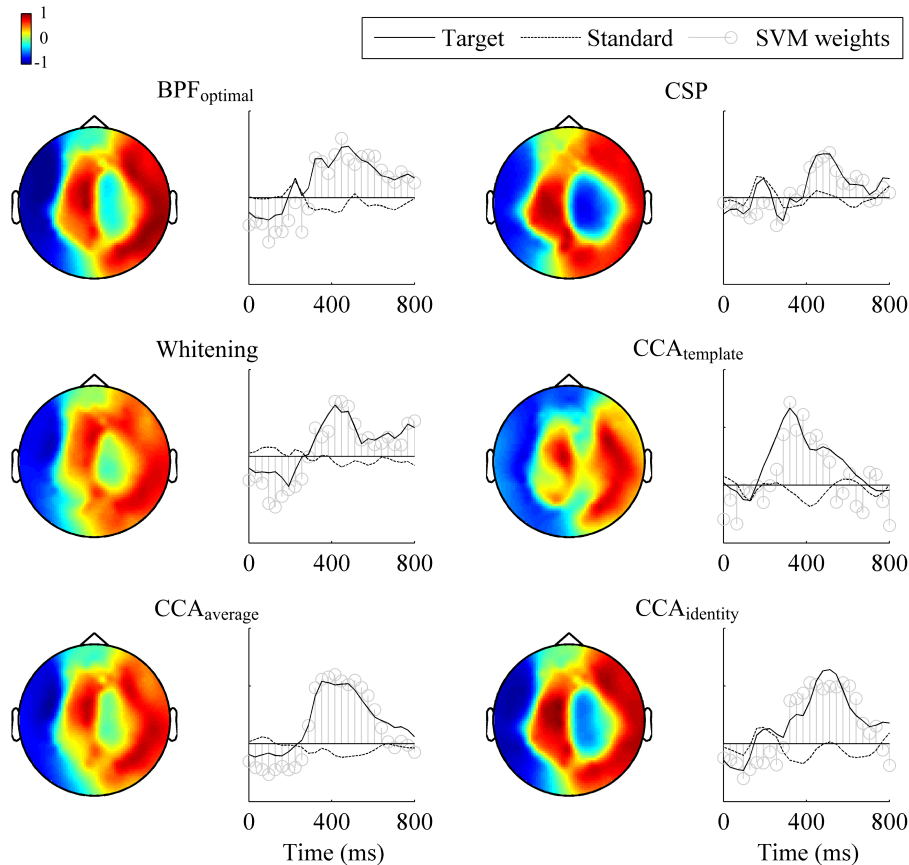
Figure 6.7: Visualization of determinant components for different spatial filter methods, exemplary for one subject.

6.6 Evaluation of a Framework for Asynchronous BMI Control of an Effector

The application of the framework for effective effector control using SSVEF decoding as proposed in Section 4.4 was successfully feasible in all subjects. In calibration runs, the average decoding accuracy was 74% for target trials ($T_{corr}/trials$) and 73% for resting trials ($R_{corr}/trials$). The resting interval predictions of the first run were excluded from the decoding accuracy calculation due to the fake feedback. Considering the seven selectable items, the guessing level was 14%. The time t_{select}, needed until a final selection of an item was generated, was 11.7 s on average. Note that the fastest possible selection was 5 s in respect of the timing used in the asynchronous paradigm. Concerning robot control runs, different evaluation measures were calculated because the real intention of

the user is not always clear in this run mode and the ratio of object selections, button selections and resting intervals is quite different. The first measure used for evaluation is the speed of a complete grasp sequence ($G_{compl}/time$) which was $0.52\ min^{-1}$ on average. Here is important to note that due to a safe gripper control, the movement of the robot was relatively slow (grasping: $28\,$s, picking up: $8\,$s). This circumstance constrained the time required for an optimal complete grasp sequence, without completely retracting the gripper but including selection of the object, to at least $69\,$s, which corresponds to a maximum speed of a complete grasp sequence of $G_{compl}/time = 0.87 min^{-1}$. An important result for the self-paced control of a robotic device is that in this set-up false object selections (S_{err}) occurred reasonably in only 26% of all object selection trials but accidentally initiated robot commands (C_{err}) occurred very rarely (4.7%). Importantly, this reliable detection of resting intervals occurred during long intervals in which the prevention of erroneous selections was required. The results for single subjects are summarized in Table 6.2. Note that the number of trials performed depends on the latency of a final selection and on the number of undesired selections. One of the subjects managed to perfectly control the system, without initiating any erroneous selection.

	Calibration			Robot control		
Subject	T_{corr}	R_{corr}	t_{select}	G_{compl}	C_{err}	S_{err}
#	/trials	/trials	[s]	/time	/trials	/trials
1	56 / 75	18 / 25	12.1	8.2 / 18'04"	3 / 38	3 / 14
2	11 / 27	4 / 10	16.5	7.4 / 24'04"	8 / 44	2 / 13
3	62 / 62	23 / 23	10.9	16.6 / 24'06"	0 / 67	0 / 20
4	40 / 63	15 / 23	10.7	10.2 / 24'23"	2 / 44	6 / 26
5	46 / 64	21 / 23	10.5	12.4 / 24'22"	1 / 50	13 / 33
6	46 / 54	17 / 21	12.8	12.6 / 24'48"	1 / 60	4 / 24
7	60 / 69	16 / 25	9.7	15.0 / 21'39"	1 / 61	14 / 35
8	45 / 67	16 / 23	10.3	10.3 / 23'39"	1 / 53	21 / 38

Table 6.2: Subject performance

6.7 Steady State Magnetic Fields vs. Steady State Potentials

A re-analysis of the data recorded during calibration runs in the asynchronous robot-control experiment was performed to compare the facility of both MEG and EEG to detect steady state visually evoked brain signals from the identical biological source. Furthermore, a potential benefit of combining the two methods that reflect brain activity of complementary sources is investigated. Selecting the maximum value of the channel sets for EEG, MEG and combined EEG/MEG, the combination of EEG and MEG reveals the highest decoding accuracies (72.4% on average, std: 13.1%). Accumulating the performances over subjects, the maximum decoding accuracy is achieved using 6 EEG electrodes and 34 MEG sensors. When using only EEG channels, decoding accuracy was 56.7% on average (std: 19.9%) with 7 electrodes providing the best

accuracy on average. Finally, MEG data permit the correct decoding of the SSVEF in 65.0% on average (std: 16.1%). A Wilcoxon signed rank test revealed that individually achieved EEG/MEG performance is significantly higher than EEG performance ($psr < 0.05$) but not than MEG performance alone. Also, individual SSVEF detection is not better than individual SSVEP detection, although the average value is substantially higher. This is because individual subjects achieve higher accuracy in EEG than in MEG. See Table 6.3 for more detailed results of individually achieved maximum decoding accuracy and the number of channels involved.

	EEG		MEG		EEG+MEG	
Subject #	Acc [%]	# Channels	Acc [%]	# Channels	Acc [%]	# Channels
1	60.6	4	46.6	38	62.9	4+42
2	41.6	5	45.0	42	61.1	8+66
3	83.3	7	91.7	30	91.7	6+20
4	35.9	5	64.6	38	63.2	3+42
5	51.2	6	52.9	46	56.9	6+30
6	74.2	8	71.0	46	82.5	15+20
7	30.8	14	76.7	20	76.1	1+20
8	75.9	15	71.3	20	85.1	14+20

Table 6.3: Maximally achieved accuracy of individual subjects and the number of channels involved.

Picking out the maximum performance achieved with single acquisition modalities and their combination might be too optimistic for comparison, because the optimal number of channels has to be determined experimentally from training data. Thus, in Figure 6.8 decoding accuracies averaged across subjects are shown dependent on the number of channels involved. In addition, the maximum improvement achievable by adding channels of the other modality is shown. A first observation is that beginning with only one channel, the decoding accuracy increases with the number of channels involved and converges with 6 channels of EEG and 20 channels of MEG, respectively. Including more channels doesn't improve accuracy but tends to decrease it. Importantly, adding a reasonable number of MEG channels improves the decoding accuracy significantly compared to using only EEG channels ($psr < 0.05$). Furthermore, adding EEG channels to a set of MEG channels improves the decoding accuracy as well. However, while the involvement of less than 20 MEG channels benefits statistically significantly from additional EEG channels, the maximum average decoding accuracy is at 63.5% (std: 15.8%) using 34 MEG sensors and EEG channel involvement increases the accuracy nonsignificantly to 68.6% (std: 14.3%). The results show that the decoding of SSVEP and SSVEF performs differently between subjects. On average, MEG tends to perform better, involving a higher amount of channels in the analysis. The combination of both modalities provides advantages in terms of decoding accuracy, especially compared to SSVEP decoding using only EEG channels.
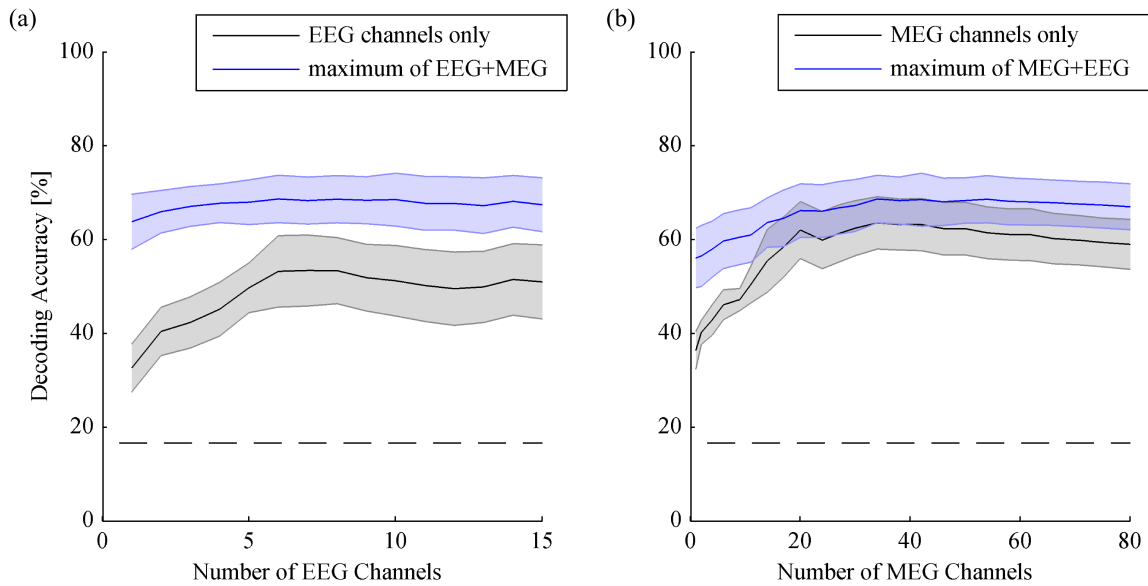
Figure 6.8: Comparison of single modality performance and combined modalities performance. (a) shows decoding accuracy dependent on the number of EEG channels involved and the maximum achieved accuracy when adding MEG channels. (b) shows decoding accuracy dependent on the number of MEG channels involved and the maximum achieved accuracy when adding EEG channels. Thick lines represent average accuracy over subject and the shaded area depicts the standard error of the mean. The dotted line indicates the chance level.

7. Discussion

In the following sections I will discuss which conclusions can be derived from the results obtained with the experiments and the subsequently tested decoding strategies. Common to all the experiments is the modality used to acquire the brain data, i.e. measuring magnetic fields rather than electrical potentials. Using MEG for BCI control has been hardly investigated thus far [31, 128], and not at all in combination with visual stimulation paradigms. The use of MEG permits measurements at a high sampling rate and with a high number of channels, which provide a high amount of potentially informative brain signals. Likewise, a high number of channels creates the additional challenge of finding the relevant information in the high-density data and reducing the input space to a low number of features for classification purposes. This was successfully achieved by means of spatial filtering methods and will be discussed in more detail later in this chapter.

7.1   Pros and Cons for Using MEG

Despite earlier discussions [42, 68], concerning whether or not MEG effectively provides higher spatial resolution than EEG, there is no doubt that MEG provides information originating from supplemental source locations. Bradshaw *et al.* [25, 26] claimed that MEG provides higher spatial resolution than EEG, at least for tangential sources that are not too deep under the scalp surface. Moreover, accuracy of source location, termed as spatial resolution, which is of interest when investigating brain processes, might differ from the so called imaging resolution. In order to decode a brain state, source reconstruction would be a time-consuming transformation of data with a possible loss of information. For BCI control, the ability to distinguish brain responses employing the input data space is important. Thus, image resolution is of significance in the intended use of the signal, since the decoding algorithms are working in the original recording modality, i.e. in sensor space. Additional to the large information content of the signal, due to a high number of sensors available in MEG, there is also the advantage of

short preparation time of the subject or user for a measurement. In fact, the 248 static sensors of the MEG device used in this work provide fast and comfortable access to high-density electrophysiological brain data. The major disadvantage of MEG is the limitation in performing measurements in a laboratory environment. However, there are indications that the development of mobile measurement techniques for MEG is feasible [181, 193], providing the prospect of using this technique in the future. However, even though currently limited to laboratory use, there are also other reasons to go for MEG investigations for BCIs. The superior representation of cortical activity using MEG can be exploited to reveal findings valuable for other modalities such as EEG and ECoG. Algorithm development and uncovering alternative sources could advance the development of EEG-based BCI systems. Furthermore, a more accurate BCI system could provide considerable benefit for locked-in patients to communicate more reliably and faster than with EEG even though limited to occasional sessions in a shielded laboratory. Also, training for demanding neurofeedback applications such as rehabilitation and ADHD treatment could be performed in MEG providing shorter and less annoying preparation and possibly more accurate feedback. In this work, promising algorithms based on spatial filtering were developed to efficiently decode high-density MEG data during specific paradigms, which might be analogously applicable to high-density EEG data as well.

7.2   Comparability of BCI Systems

In general a direct comparison of BCI results is a challenging issue. There are several factors that have considerable impact on the decoding success, being different in almost every study. This applies to the design of the paradigm, e.g. size and timing of the stimulus, or the capability of working independently of gaze, as well as technical issues such as recording modality, amplifier characteristics and number of channels. The various circumstances must be regarded when relating results to different studies.

Even more challenging is the comparison of BCIs that have different purposes or make use of different types of brain signals. To overcome this problem, the information transfer rate (ITR) was introduced as an alternative evaluation measure [222], describing the number of bits that can theoretically be transferred with the system within a specific time. However, the ITR also has its limitations and does not provide a reliable measure to compare between BCI systems. A bit rate should be defined to express the error free transfer of information, which is not sufficiently considered in Equation 4.8. Indeed, the false information is considered in the calculated bit rate, but the receiving system does not know which is the correct and which is the erroneous information. Therefore, error correction is up to the user, which requires further effort that is similarly error-prone. For example, an arbitrarily high number of alternatives and a low latency yields high information transfer rates using Equation 4.8, even if half of the commands are incorrect. A user-guided correction of the error is successful with a probability of 0.5 as well. A reasonable communication would be impossible with such a system, although the ITR is relatively high. Therefore, the most suitable trade-off between accuracy and speed strongly depends on the application.

7.3   Detection of SSVEFs

Using a closed-loop BMI, implemented to decode magnetoencephalographic signals, it was shown for the first time that MEG is well-suited to control a BCI using flickering visual stimuli in a virtual reality environment. The subjects selected the virtual objects on a trial-by-trial basis with relatively high variability, but well above chance level. The decoding accuracy tended to increase over the number of runs but relying on the data presented here it remains unclear whether this was an effect of user training or whether the different selection modes influenced the detection accuracy, as a higher degree of attention could be utilized in the free selection mode.

In order to investigate how other decoding algorithms, timing parameters and features perform when applied to the recorded data, subsequent off-line analyses were performed, representing an open-loop BCI. For feature extraction, several data-driven spatial filter methods were applied.

The common spatial pattern approach known to perform superiorly in the binary classification of motor imagery [23], performed similarly to the Fourier transform approach. This might be the case because CSP is weighting the data such that variance is maximized in one condition and minimized in the other condition and vice versa. Using the variance of a band-pass filtered signal can be considered a kind of spectral representation of the signal, because it represents a measure of the amplitude. CSP basically separates two conditions. Because the maximization of the variance of each condition is achieved by spatial weighting, i.e. an optimal linear combination of the sensors, characteristic frequencies of the different conditions ideally are represented in different channels. However, a spatial separation of different stimulation frequencies in the visual cortex is not expected. Furthermore, in the second condition, representing a baseline condition, stimulation intervals of all three other stimulation frequencies were equally used. Therefore, in this framework CSP seems to act as a feature extraction method revealing features in a frequency domain providing similar accuracy to a Fourier transform. This result supports the findings of a study [75] which found that CSP increases classification accuracy of SMR in EEG measurements but not in MEG.

In contrast, the remaining three spatial filter methods, CCA, MEC and MCC showed a significant increase in performance. Their comparably high decoding accuracies might be due to the fact that the three methods similarly optimize the spatial filter weights for one frequency, independent of the other frequencies. Therefore, even largely overlapping spatial patterns of different frequencies do not affect the feature values obtained. Each of the methods provides exactly one value for each stimulation frequency where the height of the value is a representation of the amplitude's strength. The advantage over Fourier and CSP is the independent optimal weighting of channels, which enhances the signal according to sinusoidal model functions and reduces the noise.

For a rapid communication with BCIs, short trial lengths are recommended. However, a shorter interval of data provides less reliable information and thus reveals less accurate decoding results. In order to express a trade-off between communication speed and

accuracy, the information transfer rate could provide an alternative evaluation measure to determine the optimal analysis window. As expected, a smaller interval size decreases the decoding accuracy. However, when considering the information transfer rate, the highest rate is achieved with 1.5 s intervals. According to the shortcomings of ITR described previously, the corresponding decoding accuracy can be rated as too low for controlling a BCI and a longer duration for selections should be accepted. A nonsignificant loss of accuracy compared to the accuracy achieved at 4.5 s interval length was found at an analysis window size of 3.0 s.

In SSVEP detection, the involvement of harmonics could provide additional information to a classifier, as it was evaluated by Müller-Putz *et al.* [141]. The current work showed an improvement for the detection of SSVEFs when involving harmonics as well, in particular when Fourier features were used. Although Bin *et al.* [13] did not find such a benefit detecting SSVEP using CCA, in SSVEF detection an improvement in combination with CCA decoding could be shown.

A final analysis of the SSVEF data was performed to investigate the outcome of different classifier methods applied with the several feature spaces. In total, all classifiers performed comparably well. In particular, the low dimensional feature spaces based on spatial filtering show similar results with all classification approaches, presumably due to the well-structured input space derived from effective feature extraction. The features that represent all stimulation frequencies have a high value if the frequency is consciously perceived by the subjects shifting their attention to the stimulator. Thus, well-structured clusters are formed in the input space which is supported by the fact that the argmax classifier shows excellent performance with the four dimensional feature spaces obtained with advanced spatial filter methods. In higher dimensional feature spaces, as represented with the Fourier transformed data and the common spatial pattern, the variation of the classifiers' performance is higher. Here the LDA and the kNN classifier generalize worse than rLR, nBayes and nCentroid, despite a marginal significance level.

The first experiment showed that visual brain responses, measured with MEG, can be decoded to control a BMI in a virtual reality environment. So far, MEG was used in BCI scenarios solely by detection of motor activity [31, 128]. The accuracy of the algorithms applied for feedback generation showed notable performance on the level of comparable EEG experiments [140]. However, in a new BCI implementation the prior predefinition of parameters and algorithms is probably suboptimal. The subsequent analysis of the data showed that advanced data-driven spatial filtering methods have a considerable positive impact on the decoding accuracy. Importantly, with these spatial filters a straightforward classification by determining the maximum feature is possible, and elaborate classifiers cannot contribute to further improving the discrimination. Also in EEG experiments CCA, MEC and MCC showed superior performance [13, 59, 118, 217]. These methods benefit from the fact that information of the target signal is distributed across multiple sensors. Since the algorithms are working on a single trial basis, the variation of signal-to-sensor mapping (e.g. due to head movement in MEG) - a known issue in electrophysiological recordings - may not impact classification

results at all. Importantly, the rLR classifier used for determining feedback online during the experiment was the best choice, given the Fourier feature set used. Hence, for future experiments that use SSVEFs to control a BCI, one can conclude that a feature extraction based on CCA, MEC or MCC might be recommended. Furthermore, although longer intervals tend to be more accurate, for a faster information transfer it appears to be sufficient to use shorter stimulation intervals and analysis windows, respectively.

7.4 Detection of P300 Potentials

The second experiment, implemented to act as a closed-loop BMI in MEG as well, made use of a different brain signal and employed an advanced version of the virtual reality scenario in which a robot was simulating a grasp to the selected object. Importantly, the detection of the user's attentional shift was achieved from brain signals that were generated independently from eye movements, as it is often argued that it is required in the target group of users. Only a few studies take this requirement into account [6, 121, 207] although it was shown that focusing the target has a considerable positive impact on decoding accuracy [29], because visual components bias the detection of the target ERP [11, 57]. The current work presents the first experiment that tested the ability to control a BCI by performing an oddball paradigm and detecting magnetic field P300 responses. The subjects' training time, in which calibration data are acquired, was only about ten minutes. On average, the decoding accuracies increased with the number of runs performed. This suggests that user training is beneficial for the performance of the BMI. However, the learning process is likely bilateral, i. e. the classifier improves with a higher amount of training samples and the users improve with the time they use the system [47]. Interestingly, the user's sense of agency [69] also appears to have an impact on the performance because when the subjects were free to select the objects, the performance increased compared to when target objects were instructed. The simulation of the grasping gesture to the selected object increased the accuracy of the system even further, supporting the notion that increased attention provides more reliable control. Note that this observation is speculative, because the impact of learning and the impact of the sense of agency cannot be separated with the present study.

The decoding accuracy achieved with this experiment was well above guessing level and is on a relatively high level, given the gaze-independence condition. Nevertheless, similar to the first experiment, more optimal results may be achieved by reasonable parameter selection and advanced processing algorithms. The open-loop analysis revealed that shorter analysis intervals did not significantly change the accuracy, which indicates that features representing the first 600 ms after the stimulus occurred are sufficient to determine the non-standard stimulus with comparable accuracy. Furthermore, involving the full array of channels did not change the performance significantly, indicating that task specific information is sufficiently represented in the preselected sensor array. However, the high-pass cutoff frequency was selected too conservatively, since permitting lower fluctuations significantly improved the decoding accuracy. This indicates

that in the MEG data of the oddball paradigm slow fluctuations play an important role in characterizing brain response to a deviant stimulus. For example, when the latency of the P300 potential exceeds 500 ms, a 1 Hz cutoff is inadequate. Furthermore, slow wave potentials are known to accompany visual oddball stimuli, although primarily when inter stimulus intervals are long (in the range of seconds) [202]. Possibly, the importance of slow potentials is specific to MEG, since a comparable study [82] using the same number of selectable items but using EEG achieves superior results with the band-pass filter used in the closed-loop experiment. Also, in a study on P300-spelling [114] a high-pass cutoff frequency of 1 Hz has led to considerable accuracy.

Deviating from other P300 BCIs, in the present closed-loop implementation segments of MEG data were classified individually and a real-valued classifier output was summed to identify the target item. This is in contrast to the common method of first averaging the segments and then determining the most probable selection. An open-loop comparison of both approaches showed that the first approach achieves higher prediction rates.

The findings of the parameter search were adopted to investigate more advanced feature extraction algorithms. All algorithms were based on spatial filtering methods, determining the contribution of channels in a data-driven manner. As an important result, all spatial filter methods improved the decoding accuracy. This indicates that spatial filters estimated from the data contribute to a superior signal. Although CSP is primarily suited to discriminating oscillating signals, the features generated with the current approach reveal reasonable decoding. A similar result was also found by Krusienski *et al.* [102]. However, CSP reveals only slightly higher accuracies as compared to no spatial filtering, confirming the lack of performance boost in MEG as it was already shown from EEG based SMR decoding [75]. In a study investigating processing methods, the analysis step of Whitening was suggested to be the best practice to decoding ERPs [53]. Although this method also provided accurate results, it did not perform best. Instead, the highest impact was presented by spatial filtering based on CCA. Interestingly, the different reference functions applied in this work showed that unbiased reference functions appear to be advantageous over reference functions representing hypothetical assumptions, such as the evolution of potential peaking at 300 ms. In the current experiment, the selection of reference functions as suggested by Spüler *et al.* [199] showed the best performance but was equally well performing like the new model for ERP recognition, recently introduced in an own publication [170]. The latter approach provides a further advantage, which is the interpretation of ERP subcomponents obtained by an unbiased method. In the results section an exemplary component and the corresponding topographic map is shown for each of the spatial filter methods. The figure suggests that a relatively late component peaking around 400 ms contributes to the ERP discrimination at most. Although the exact time course varies with the different spatial filter methods, the general shape is quite similar. This is also reflected in the topographic maps showing the correlation of averaged target intervals in the sensor space with the respective subcomponent. The figure demonstrates that all feature extraction methods basically find the discriminating features from a set of training data and that the extracted patterns are stable throughout methods.

Furthermore, it is important to note that the template reference function restricts the extracted component to the hypothetical evolution of the potential. Most likely this is the reason for the highest deviation of the topographic pattern and the lowest, although still high, accuracy across CCA methods. This demonstrates the advantages of data-driven spatial filtering involving a minimum of hypotheses. The patterns which were obtained in Figure 6.7 suggest the localization of at least two dipole sources. The first is located parietally as expected from EEG and MEG studies [54, 159], indicated by posterior-central ingoing and outgoing magnetic field lines. The second source appears to be reverse oriented and located in deeper brain structures, which is in line with previous findings of hippocampal [67] and thalamic activity [84, 127]. Note that the figure shows only the most prominent component of one subject but demonstrates the plausibility and consistency of the decoding approaches.

7.5 Asynchronous Control of a Robot

The constraining of dependent BCIs to only transmit a command when the system expects to receive one of several commands at a defined point in time makes such a system extremely inflexible. Only a few BCI developments address this problem aiming to obtain an asynchronous, self-paced control [36, 61, 85, 116, 130, 140, 147, 221]. With the current experiment another important step towards this development was accomplished. Importantly, it was demonstrated that noninvasive measurement techniques can be used, with the help of intelligent robot control, to perform complex tasks, required in the daily life of severely paralyzed patients. However, the time needed to submit a command is relatively long, which is particularly critical when emergency stops are required. An extension of the system to a hybrid approach, e.g. in combination with eye tracking or detection of eye blinks could help to address those safety issues. Although the accuracy of performed selections is not perfect, it is on a level which permits successful control of the system, which also is achieved by the feasibility of correcting erroneous actions immediately. The lack of decoding accuracy is probably caused by the narrow arrangement of selectable items, which effects a superposition of stimulation frequencies in a small area of the visual field. Furthermore, the short time window, which was chosen to allow for fast selections, decreases the accuracy of frequency decomposition and consequently causes a decreased decoding accuracy as shown in Section 4.2.4. Importantly, the erroneous selections primarily apply to the selections of the objects to be grasped and rarely to the initiation or cancellation of the grasp. Again, this might be caused by the advantageous positioning of the respective buttons, but also by the disabled visual stimulation of objects during the robot activity which effects less potentially superimposing stimuli and provides a smaller number of selectable alternatives. A further, extremely important issue of self-paced BCI control is the ability of the system to function in an idle mode, which permits the user to rest [221]. This requirement is often neglected in asynchronous BCIs but is particularly necessary in the control of prostheses. In the experiment presented here, the relative long duration of the robot's actions allowed the reliability of the system to be proven in withholding unintended commands.

7.6   Comparison of Modalities

The potential advantage of MEG over EEG is a long debated and insufficiently resolved topic [68, 120]. In the past, the primary question of investigations referred to the spatial resolution of either modality. This was approached by determining the localization accuracy of reconstructed sources [42]. With the classification of single trial data, a different view on the signal quality assessment has emerged. The decoding accuracy achieved with a specific modality provides a measurable value of information content, which can be extracted from the recordings. A study on binary classification of ERD [75] suggested that MEG permits higher performances in channel space compared to EEG, but that EEG considerably improves with the CSP method achieving the same level as channel-based MEG classification. However, in this study, data were acquired in different sessions and from different subjects who even performed different imagery tasks, which are critical constraints for comparing two recording techniques. In the current work, measurements of EEG and MEG were performed simultaneously, acquiring their signals from the same activity. Similar to decoding accuracy in classification, the correlation coefficient provides a direct measure in regression for comparison of modalities. A recently published work [99] showed that reconstructed trajectories of hand motion from MEG and EEG data generate significantly higher correlations for MEG, but the amount of this difference was not considered critical by the authors.

In the present study, the recorded data were compared using the same algorithms for both modalities. The CCA method used to estimate the optimal spatial filter is well suited for combining both signals to a common feature space. A grid search strategy was used to determine the optimal set of channels, spread over the visual cortex. It turns out that the superior modality depends on the subject. On average, MEG achieved higher accuracies, but due to the individual variation not significantly higher. Additionally, EEG channels do not significantly improve the accuracy of MEG. However, adding MEG channels increases the accuracy of EEG channels significantly. The number of involved channels considerably affects the performance. This suggests that using several channels rather than only one hypothetically placed channel improves the signal-to-noise ratio if adequate spatial filters are applied. However, the accuracy enhancement rapidly converges with increasing number of involved channels, which indicates that a few channels close to the source are sufficient to extract the available information from the noisy signal. The individual difference between the performance achieved with EEG and MEG might be caused by distinct distortions of either signal. While EEG is more sensitive to muscle activity and eye movements, MEG is more sensitive to environmental distortions, even when the source is far outside the recording chamber. Furthermore, single EEG channels might suffer from weakening conductivity over ongoing recording time. In contrast, the MEG sensor array is fixed while the subject is not, which can lead to a shifting of the signal to other channels if the subject moves. Another important issue is that EEG measured in a shielded room does not represent the conditions of EEG in a natural environment which BCI control is faced with.

The analysis showed that MEG tends to provide a signal that permits a more accurate decoding of SSVEP signals than EEG. This might be caused by the denser distribu-

tion of channels over the relevant brain areas, which supports the notion that MEG provides a higher spatial resolution. Furthermore, using MEG as an additional modality to EEG improved the performance, which illustrates evidence that MEG provides complementary information. In traditional approaches for comparing both modalities, neural generators are determined and the localization accuracy is evaluated. In those studies, improved reconstruction accuracy with combined EEG/MEG was evident as well [60, 120]. The authors likewise argued that the improvement was due to the complementary nature of both modalities.

8. Summary and Future Work

8.1 Summary

In this work I investigated a new approach for instantiating complex movement of a prosthetic device useful for people who suffer from severe disabilities. The movement is planned and performed by an intelligent robot. A potential user controls the robot by the selection of control elements merely by an attentional task. The BMI system decodes the brain activity measured as magnetic field variation and detects the intended control command. The approach was particularly designed to exploit low information transfer, which is possible using brain signals measured with conventional noninvasive recording techniques. To simulate a real world scenario, a virtual reality environment was used, presenting visual stimuli and visualizing the robot movement, grasping an object. It was shown that the system can be controlled relatively accurately by self-paced commands. Importantly, withholding unwanted commands, which only a minority of BMI implementations can account for, was reliably detected by the system.

In accomplishing this final system, initial experiments were conducted, as with BMI systems. Two types of brain signals were used to investigate the performance of selecting an item under circumstances that were insufficiently or not yet researched, i.e. using a virtual environment and decoding from MEG signals. In both paradigms, the first detecting SSVEP signals, and the second detecting ERPs evoked in an oddball paradigm, comparable information transfer rates were achieved. Notably, the oddball paradigm comprises advantageous features such as eye movement independence and less interfering visual stimulation. The achieved performance was comparable to other implementations in the closed-loop BMI experiments and in subsequent open-loop analyses advanced processing and decoding algorithms were investigated in order to identify the most suitable decoding technique. It turned out that spatial filter methods have a considerable impact on the decoding accuracy of high-density channel data as represented by MEG. A statistical approach known as canonical correlation analysis showed superior results for both paradigms. Furthermore, classification algorithms marginally affect

the results if low dimensional feature spaces are used. An important factor influencing decoding accuracy was constituted by the hypotheses involved in data preprocessing, such as band-pass filtering the signal.

In the final experiment, EEG activity was recorded simultaneously to MEG. This permitted the direct comparison of either technique, clarifying potential advantages of MEG, which is assumed to be topographically more sensitive. For the decoding of steady-state responses affected by narrowly arranged visual stimulators, MEG shows only a slight advantage over EEG on average. An even higher accuracy is achieved when EEG and MEG channels are combined, where, in combination with CCA-based spatial filtering, a data-driven selection of channels is required for best results.

The proposed system is the first BMI implementation which decodes MEG signals to asynchronously control an autonomously grasping virtual robot. A main feature of the approach is the simplification of actuator control by reducing the control to selecting targets and initiating commands, respectively. This requires reliably functioning, intelligent robots. Developing such systems is also a challenging task but provides much better perspectives than the prospect of enormously improved noninvasive measurement of neural activity.

8.2   Outlook and Critique

For the realization of the BMI experiments the MEG was used. This technique has strong limitations regarding the mobility of the system and depends on a shielded environment without local disturbances. A closing door or a passing car within several meters of the lab can produce large artifacts. Therefore, a transfer of the approach to use high density EEG electrode arrays is a recommendable next step. The compatibility of the signal characteristics was demonstrated using data from the final experiment, but this is not a general proof. Rather, comparison of both acquisition modalities using other paradigms is required to assess the advantages of either technique. Furthermore, since the EEG recordings provided a much lower number of channels compared to MEG, the constraints for comparison are unequal. A denser array of EEG electrodes would potentially improve the accuracy. A weakness, typical in neuroimaging studies, is the small number of subjects involved. For a more reliable evaluation more subjects are required.

Although the proof-of-principle of asynchronous robot control was demonstrated, there are several shortcomings to be solved. First of all, the accuracy of the final system has potential for improvements. The accuracy probably suffered from the short distances between areas of visual stimuli, which was required due to the limited working area of the robotic gripper used. Narrow projection of stimuli on the retina induce a strong overlap of stimulation frequencies in the visual cortex. Thus, an improved design of stimuli size and position could potentially improve the accuracy of the system. A second issue is the speed of the system. On the one hand, the time needed to select a command is relatively long. On the other hand, the virtual robot used performs the

grasping movements relatively slowly, because the algorithms implement collision detection and are developed to work with the virtual robot's real counterpart. The challenge in autonomous robotics is to perform reliable movements and meet safety issues at the same time. Thus, further improvements in the grasping algorithm and intelligent obstacle avoidance may also help to achieve a more reliable BMI-based grasping device.

The VR environment requires the user to look at a computer display. Thus, another important step is the transfer of visual stimulation to real-world displays, e.g. LED arrays which could be placed in the vicinity of potential target objects. Furthermore, an anthropomorphic robotic arm or prosthesis is required, which is able to perform grasping movements that are similar to human actions and which is capable of performing useful tasks. The existing grasp planning algorithms also might be extended to expand the manipulator's facilities and simultaneously exclude any risk of accidental violation or damage.

8.3 Conclusions

The BMI demonstrator developed in this work illustrated that asynchronous online control of an intelligent robotic gripper is possible using MEG signals. In contrast to experiments based on noninvasively measured motor potentials this approach facilitates grasping in many degrees of freedom, requiring a very low information transfer rate. Importantly, the independence of external cues allows spontaneous use of the system. The subsequent comparison of MEG and EEG data as BMI source signals showed only a marginal difference of decoding success between the modalities, with MEG slightly superior to EEG. The combination of both modalities showed the highest performance. This suggests that MEG provides a supplementary information channel which enhances the detection accuracy of SSVEPs.

To date a prosthesis reliably driven only by the human brain is a vision of many researchers. The findings of this work represent important steps towards the development of prosthetic devices controlled by noninvasive BMIs. Furthermore, the evaluation of spatial filtering methods for both SSVEP and ERP detection provides valuable findings that most likely can be transferred to EEG analysis which is the currently preferred technique for BMI design.

List of Abbreviations

ADHD Attention Deficit Hyperactivity Disorder

BCI Brain-Computer Interface

BMI Brain-Machine Interface

BOLD Blood Oxygenation Level Dependent

BPF Band-pass Filter

CAR Common Average Reference

CCA Canonical Correlation Analysis

CSP Common Spatial Pattern

ECoG Electrocorticogram / Electrocorticography

EEG Electroencephalogram / Electroencephalography

ERD Event-related Desynchronization

ERP Event-related Potential

ERS Event-related Synchronization

fMRI Functional Magnetic Resonance Imaging

HRF Hemodynamic Response Function

ITR Information Transfer Rate

kNN k-Nearest Neighbor

LDA Linear Discriminant Analysis

LFP Local Field Potential

MCC Maximum Contrast Combination

MEC Minimum Energy Combination

MEG Magnetoencephalogram / Magnetoencephalography

MR Magnetic Resonance

MUA Multi Unit Activity

NIRS Near Infrared Spectroscopy

P300 Positive Deflection 300 ms After Stimulus Onset

PCA Principal Component Analysis

rLR Regularized Logistic Regression

SCP Slow Cortical Potentials

SMR Sensorimotor Rhythms

SNR Signal-to-Noise Ratio

SOV Simulated Online Validation

SQUID Superconducting Quantum Interference Devices

SSVEF Steady-state Visual Evoked (magnetic) Field

SSVEP Steady-state Visual Evoked (electrical) Potential

SUA Single Unit Activity

SVM Support Vector Machine

VEP Visual Evoked Potential

VR Virtual Reality

Bibliography

[1] L. Acqualagna, S. Bosse, A. K. Porbadnigk, G. Curio, K.-R. Müller, T. Wiegand, and B. Blankertz. EEG-based classification of video quality perception using steady state visual evoked potentials (SSVEPs). *J Neural Eng*, 12(2):026012, Apr 2015.

[2] F. Akram, S. M. Han, and T.-S. Kim. An efficient word typing P300-BCI system using a modified T9 interface and random forest classifier. *Comput Biol Med*, 56:30–36, Jan 2015.

[3] B. Z. Allison, C. Brunner, C. Altstätter, I. C. Wagner, S. Grissmann, and C. Neuper. A hybrid ERD/SSVEP BCI for continuous simultaneous two dimensional cursor control. *J Neurosci Methods*, 209(2):299–307, Aug 2012.

[4] B. Z. Allison, C. Brunner, V. Kaiser, G. R. Müller-Putz, C. Neuper, and G. Pfurtscheller. Toward a hybrid brain-computer interface based on imagined movement and visual attention. *J Neural Eng*, 7(2):26007, Apr 2010.

[5] B. Z. Allison, D. J. McFarland, G. Schalk, S. D. Zheng, M. M. Jackson, and J. R. Wolpaw. Towards an independent brain-computer interface using steady state visual evoked potentials. *Clin Neurophysiol*, 119(2):399–408, Feb 2008.

[6] F. Aloise, P. Aricò, F. Schettini, A. Riccio, S. Salinari, D. Mattia, F. Babiloni, and F. Cincotti. A covert attention P300-based brain-computer interface: Geospell. *Ergonomics*, 55(5):538–551, 2012.

[7] W. Andrä and H. Nowak. *Magnetism in medicine: a handbook*. John Wiley & Sons, 2007.

[8] A. Bashashati, M. Fatourechi, R. K. Ward, and G. E. Birch. A survey of signal processing algorithms in brain-computer interfaces based on electrical brain signals. *J Neural Eng*, 4(2):R32–R57, Jun 2007.

[9] J. D. Bayliss, S. A. Inverso, and A. Tentler. Changing the P300 brain computer interface. *Cyberpsychol Behav*, 7(6):694–704, Dec 2004.

[10] H. Berger. Über das Elektrenkephalogramm des Menschen. *European Archives of Psychiatry and Clinical Neuroscience*, 87(1):527–570, 1929.

[11] L. Bianchi, S. Sami, A. Hillebrand, I. P. Fawcett, L. R. Quitadamo, and S. Seri. Which physiological components are more suitable for visual ERP based brain-computer interface? a preliminary MEG/EEG study. *Brain Topogr*, 23(2):180–185, Jun 2010.

[12] G. Bin, X. Gao, Y. Wang, Y. Li, B. Hong, and S. Gao. A high-speed BCI based on code modulation VEP. *Journal of neural engineering*, 8(2):025015, 2011.

[13] G. Bin, X. Gao, Z. Yan, B. Hong, and S. Gao. An online multi-channel SSVEP-based brain-computer interface using a canonical correlation analysis method. *J Neural Eng*, 6(4):046002, Aug 2009.

[14] N. Birbaumer and L. G. Cohen. Brain-computer interfaces: communication and restoration of movement in paralysis. *J Physiol*, 579(Pt 3):621–636, Mar 2007.

[15] N. Birbaumer, N. Ghanayim, T. Hinterberger, I. Iversen, B. Kotchoubey, A. Kübler, J. Perelmouter, E. Taub, and H. Flor. A spelling device for the paralysed. *Nature*, 398(6725):297–298, Mar 1999.

[16] N. Birbaumer, A. R. Murguialday, and L. Cohen. Brain-computer interface in paralysis. *Curr Opin Neurol*, 21(6):634–638, Dec 2008.

[17] N. Birbaumer, L. E. Roberts, W. Lutzenberger, B. Rockstroh, and T. Elbert. Area-specific self-regulation of slow cortical potentials on the sagittal midline and its effects on behavior. *Electroencephalogr Clin Neurophysiol*, 84(4):353–361, 1992.

[18] C. M. Bishop. *Pattern recognition and machine learning*, volume 1 of *Information Science and Statistics*. Springer New York, 2006.

[19] B. Blankertz, G. Dornhege, S. Lemm, M. Krauledat, G. Curio, and K.-R. Müller. The Berlin brain-computer interface: Machine learning based detection of user specific brain states. *J. UCS*, 12(6):581–607, 2006.

[20] B. Blankertz, G. Dornhege, C. Schäfer, R. Krepki, J. Kohlmorgen, K.-R. Müller, V. Kunzmann, F. Losch, and G. Curio. Boosting bit rates and error detection for the classification of fast-paced motor commands based on single-trial EEG analysis. *IEEE Trans Neural Syst Rehabil Eng*, 11(2):127–131, Jun 2003.

[21] B. Blankertz, S. Lemm, M. Treder, S. Haufe, and K.-R. Müller. Single-trial analysis and classification of ERP components–a tutorial. *Neuroimage*, 56(2):814–825, May 2011.

[22] B. Blankertz, C. Sannelli, S. Halder, E. M. Hammer, A. Kübler, K.-R. Müller, G. Curio, and T. Dickhaus. Neurophysiological predictor of SMR-based BCI performance. *Neuroimage*, 51(4):1303–1309, Jul 2010.

[23] B. Blankertz, R. Tomioka, S. Lemm, M. Kawanabe, and K.-R. Müller. Optimizing spatial filters for robust EEG single-trial analysis. *IEEE Signal Processing Magazine*, 25(1):41–56, 2008.

[24] J. Bortz. *Statistik: Für Human- und Sozialwissenschaftler*. Springer-Verlag, 2005.

[25] L. A. Bradshaw, R. S. Wijesinghe, and J. Wikswo, Jr. Spatial filter approach for comparison of the forward and inverse problems of electroencephalography and magnetoencephalography. *Ann Biomed Eng*, 29(3):214–226, Mar 2001.

[26] L. A. Bradshaw and J. Wikswo, Jr. Spatial filter approach for evaluation of the surface laplacian of the electroencephalogram and magnetoencephalogram. *Ann Biomed Eng*, 29(3):202–213, Mar 2001.

[27] C. Brunner, B. Z. Allison, D. J. Krusienski, V. Kaiser, G. R. Müller-Putz, G. Pfurtscheller, and C. Neuper. Improved signal processing approaches in an offline simulation of a hybrid brain-computer interface. *J Neurosci Methods*, 188(1):165–173, Apr 2010.

[28] C. Brunner, R. Scherer, B. Graimann, G. Supp, and G. Pfurtscheller. Online control of a brain-computer interface using phase synchronization. *IEEE Trans Biomed Eng*, 53(12 Pt 1):2501–2506, Dec 2006.

[29] P. Brunner, S. Joshi, S. Briskin, J. R. Wolpaw, H. Bischof, and G. Schalk. Does the 'P300' speller depend on eye gaze? *J Neural Eng*, 7(5):056013, Oct 2010.

[30] P. Brunner, A. L. Ritaccio, J. F. Emrich, H. Bischof, and G. Schalk. Rapid communication with a "P300" matrix speller using electrocorticographic signals (ECoG). *Front Neurosci*, 5:5, 2011.

[31] E. Buch, C. Weber, L. G. Cohen, C. Braun, M. A. Dimyan, T. Ard, J. Mellinger, A. Caria, S. Soekadar, A. Fourkas, and N. Birbaumer. Think to move: a neuromagnetic brain-computer interface (BCI) system for chronic stroke. *Stroke*, 39(3):910–917, Mar 2008.

[32] A. Buttfield, P. W. Ferrez, and J. d. R. Millán. Towards a robust BCI: error potentials and online learning. *IEEE Trans Neural Syst Rehabil Eng*, 14(2):164–168, Jun 2006.

[33] G. Buzsáki, C. A. Anastassiou, and C. Koch. The origin of extracellular fields and currents–EEG, ECoG, LFP and spikes. *Nat Rev Neurosci*, 13(6):407–420, Jun 2012.

[34] J. M. Carmena, M. A. Lebedev, R. E. Crist, J. E. O'Doherty, D. M. Santucci, D. F. Dimitrov, P. G. Patil, C. S. Henriquez, and M. A. L. Nicolelis. Learning to control a brain-machine interface for reaching and grasping by primates. *PLoS Biol*, 1(2):E42, Nov 2003.

[35] J. Castillo, S. Muller, E. Caicedo, and T. Bastos. Feature extraction techniques based on power spectrum for a SSVEP-BCI. In *Industrial Electronics (ISIE), 2014 IEEE 23rd International Symposium on*, pages 1051–1055, 2014.

[36] H. Cecotti. A self-paced and calibration-less SSVEP-based brain-computer interface speller. *IEEE Trans Neural Syst Rehabil Eng*, 18(2):127–133, Apr 2010.

[37] H. Cecotti and A. Gräser. Convolutional neural networks for P300 detection with application to brain-computer interfaces. *IEEE Trans Pattern Anal Mach Intell*, 33(3):433–445, Mar 2011.

[38] J. K. Chapin, K. A. Moxon, R. S. Markowitz, and M. A. Nicolelis. Real-time control of a robot arm using simultaneously recorded neurons in the motor cortex. *Nat Neurosci*, 2(7):664–670, Jul 1999.

[39] C.-H. Chen, M.-S. Ho, K.-K. Shyu, K.-C. Hsu, K.-W. Wang, and P.-L. Lee. A noninvasive brain computer interface using visually-induced near-infrared spectroscopy responses. *Neurosci Lett*, 580:22–26, Sep 2014.

[40] P. Cipresso, L. Carelli, F. Solca, D. Meazzi, P. Meriggi, B. Poletti, D. Lulé, A. C. Ludolph, V. Silani, and G. Riva. The use of P300-based BCIs in amyotrophic lateral sclerosis: from augmentative and alternative communication to cognitive assessment. *Brain Behav*, 2(4):479–498, Jul 2012.

[41] D. Cohen. Magnetoencephalography: detection of the brain's electrical activity with a superconducting magnetometer. *Science*, 175(4022):664–666, Feb 1972.

[42] D. Cohen, B. N. Cuffin, K. Yunokuchi, R. Maniewski, C. Purcell, G. R. Cosgrove, J. Ives, J. G. Kennedy, and D. L. Schomer. MEG versus EEG localization test using implanted sources in the human brain. *Ann Neurol*, 28(6):811–817, Dec 1990.

[43] D. D. Cox and R. L. Savoy. Functional magnetic resonance imaging (fMRI) "brain reading": detecting and classifying distributed patterns of fMRI activity in human visual cortex. *Neuroimage*, 19(2 Pt 1):261–270, Jun 2003.

[44] N. E. Crone, D. Boatman, B. Gordon, and L. Hao. Induced electrocorticographic gamma activity during auditory perception. brazier award-winning article, 2001. *Clin Neurophysiol*, 112(4):565–582, Apr 2001.

[45] N. E. Crone, D. L. Miglioretti, B. Gordon, and R. P. Lesser. Functional mapping of human sensorimotor cortex with electrocorticographic spectral analysis. ii. event-related synchronization in the gamma band. *Brain*, 121 (Pt 12):2301–2315, Dec 1998.

[46] N. E. Crone, D. L. Miglioretti, B. Gordon, J. M. Sieracki, M. T. Wilson, S. Uematsu, and R. P. Lesser. Functional mapping of human sensorimotor cortex with electrocorticographic spectral analysis. i. alpha and beta event-related desynchronization. *Brain*, 121 (Pt 12):2271–2299, Dec 1998.

[47] E. A. Curran and M. J. Stokes. Learning to control brain activity: a review of the production and control of EEG components for driving brain-computer interface (BCI) systems. *Brain Cogn*, 51(3):326–336, Apr 2003.

[48] B. Dal Seno, M. Matteucci, and L. Mainardi. Online detection of P300 and error potentials in a BCI speller. *Computational intelligence and neuroscience*, 2010:11, 2010.

[49] C. Davatzikos, K. Ruparel, Y. Fan, D. G. Shen, M. Acharyya, J. W. Loughead, R. C. Gur, and D. D. Langleben. Classifying spatial patterns of brain activity with machine learning methods: application to lie detection. *Neuroimage*, 28(3):663–668, Nov 2005.

[50] P. F. Diez, V. A. Mut, E. M. Avila Perona, and E. Laciar Leber. Asynchronous BCI control using high-frequency SSVEP. *J Neuroeng Rehabil*, 8:39, 2011.

[51] G. Dornhege. *Toward brain-computer interfacing*. MIT press, 2007.

[52] E. Edwards, S. S. Nagarajan, S. S. Dalal, R. T. Canolty, H. E. Kirsch, N. M. Barbaro, and R. T. Knight. Spatiotemporal imaging of cortical activation during verb generation and picture naming. *Neuroimage*, 50(1):291–301, Mar 2010.

[53] J. Farquhar and N. J. Hill. Interactions between pre-processing and classification methods for event-related-potential classification: best-practice guidelines for brain-computer interfacing. *Neuroinformatics*, 11(2):175–192, Apr 2013.

[54] L. A. Farwell and E. Donchin. Talking off the top of your head: toward a mental prosthesis utilizing event-related brain potentials. *Electroencephalogr Clin Neurophysiol*, 70(6):510–523, Dec 1988.

[55] S. Fazli, J. Mehnert, J. Steinbrink, G. Curio, A. Villringer, K.-R. Müller, and B. Blankertz. Enhanced performance by a hybrid NIRS-EEG brain computer interface. *Neuroimage*, 59(1):519–529, Jan 2012.

[56] P. W. Ferrez and J. del R Millan. Error-related EEG potentials generated during simulated brain-computer interaction. *IEEE Trans Biomed Eng*, 55(3):923–929, Mar 2008.

[57] S. Frenzel, E. Neubert, and C. Bandt. Two communication lines in a 3×3 matrix speller. *J Neural Eng*, 8(3):036021, Jun 2011.

[58] I. Fried, G. A. Ojemann, and E. E. Fetz. Language-related potentials specific to human language cortex. *Science*, 212(4492):353–356, Apr 1981.

[59] O. Friman, I. Volosyak, and A. Graser. Multiple channel detection of steady-state visual evoked potentials for brain-computer interfaces. *IEEE Trans Biomed Eng*, 54(4):742–750, 2007.

[60] M. Fuchs, M. Wagner, H. A. Wischmann, T. Köhler, A. Theissen, R. Drenck-hahn, and H. Buchner. Improving source reconstructions by combining bioelectric and biomagnetic data. *Electroencephalogr Clin Neurophysiol*, 107(2):93–111, Aug 1998.

[61] F. Galán, M. Nuttin, E. Lew, P. W. Ferrez, G. Vanacker, J. Philips, and J. D. R. Millán. A brain-actuated wheelchair: asynchronous and non-invasive brain-computer interfaces for continuous control of robots. *Clin Neurophysiol*, 119(9):2159–2169, Sep 2008.

[62] X. Gao, D. Xu, M. Cheng, and S. Gao. A BCI-based environmental controller for the motion-disabled. *IEEE Trans Neural Syst Rehabil Eng*, 11(2):137–140, Jun 2003.

[63] D. Garrett, D. A. Peterson, C. W. Anderson, and M. H. Thaut. Comparison of linear, nonlinear, and feature selection methods for EEG signal classification. *IEEE Trans Neural Syst Rehabil Eng*, 11(2):141–144, Jun 2003.

[64] C. Guger, G. Edlinger, W. Harkam, I. Niedermayer, and G. Pfurtscheller. How many people are able to operate an EEG-based brain-computer interface (BCI)? *IEEE Trans Neural Syst Rehabil Eng*, 11(2):145–147, Jun 2003.

[65] I. Guyon, J. Weston, S. Barnhill, and V. Vapnik. Gene selection for cancer classification using support vector machines. *Machine learning*, 46(1-3):389–422, 2002.

[66] S. Halder, M. Rea, R. Andreoni, F. Nijboer, E. Hammer, S. Kleih, N. Birbaumer, and A. Kübler. An auditory oddball brain–computer interface for binary choices. *Clinical Neurophysiology*, 121(4):516–523, 2010.

[67] E. Halgren, N. K. Squires, C. L. Wilson, J. W. Rohrbaugh, T. L. Babb, and P. H. Crandall. Endogenous potentials generated in the human hippocampal formation and amygdala by infrequent events. *Science*, 210(4471):803–805, Nov 1980.

[68] M. Hämäläinen, R. Hari, R. J. Ilmoniemi, J. Knuutila, and O. V. Lounasmaa. Magnetoencephalography – theory, instrumentation, and applications to noninvasive studies of the working human brain. *Reviews of modern Physics*, 65(2):413, 1993.

[69] P. Haselager. Did i do that? brain–computer interfacing and the sense of agency. *Minds and Machines*, 23(3):405–418, 2013.

[70] J. V. Haxby, M. I. Gobbini, M. L. Furey, A. Ishai, J. L. Schouten, and P. Pietrini. Distributed and overlapping representations of faces and objects in ventral temporal cortex. *Science*, 293(5539):2425–2430, Sep 2001.

[71] J.-D. Haynes and G. Rees. Predicting the stream of consciousness from activity in human visual cortex. *Curr Biol*, 15(14):1301–1307, Jul 2005.

[72] C. S. Herrmann. Human EEG responses to 1–100 hz flicker: resonance phenomena in visual cortex and their potential correlation to cognitive phenomena. *Experimental brain research*, 137(3-4):346–353, 2001.

[73] P. Heuschmann, O. Busse, M. Wagner, M. Endres, A. Villringer, J. Röther, P. Kolominsky-Rabas, and K. Berger. Schlaganfallhäufigkeit und Versorgung von Schlaganfallpatienten in Deutschland. *Aktuelle Neurologie*, 37(07):333–340, Sep 2010.

[74] N. Hill, T. Lal, M. Schroder, T. Hinterberger, B. Wilhelm, F. Nijboer, U. Mochty, G. Widman, C. Elger, B. Scholkopf, A. Kubler, and N. Birbaumer. Classifying EEG and ECoG signals without subject training for fast BCI implementation: comparison of nonparalyzed and completely paralyzed subjects. *IEEE Trans N*, 14(2):183–186, 2006.

[75] N. J. Hill, T. N. Lal, M. Schröder, T. Hinterberger, G. Widman, C. E. Elger, B. Schölkopf, and N. Birbaumer. Classifying event-related desynchronization in EEG, ECoG and MEG signals. In *Pattern Recognition*, pages 404–413. Springer, 2006.

[76] S. A. Hillyard and M. Kutas. Electrophysiology of cognitive processing. *Annu Rev Psychol*, 34:33–61, 1983.

[77] T. Hinterberger, A. Kübler, J. Kaiser, N. Neumann, and N. Birbaumer. A brain-computer interface (BCI) for the locked-in: comparison of different EEG classifications for the thought translation device. *Clin Neurophysiol*, 114(3):416–425, Mar 2003.

[78] L. R. Hochberg, D. Bacher, B. Jarosiewicz, N. Y. Masse, J. D. Simeral, J. Vogel, S. Haddadin, J. Liu, S. S. Cash, P. van der Smagt, and J. P. Donoghue. Reach and grasp by people with tetraplegia using a neurally controlled robotic arm. *Nature*, 485(7398):372–375, May 2012.

[79] L. R. Hochberg, M. D. Serruya, G. M. Friehs, J. A. Mukand, M. Saleh, A. H. Caplan, A. Branner, D. Chen, R. D. Penn, and J. P. Donoghue. Neuronal ensemble control of prosthetic devices by a human with tetraplegia. *Nature*, 442(7099):164–171, Jul 2006.

[80] U. Hoffmann, G. Garcia, J. Vesin, K. Diserens, and T. Ebrahimi. A boosting approach to P300 detection with application to brain-computer interfaces. In *Neural Engineering, 2005. Conference Proceedings. 2nd International IEEE EMBS Conference on*, pages 97–100, 2005.

[81] U. Hoffmann, J.-M. Vesin, and T. Ebrahimi. Spatial filters for the classification of event-related potentials. In *Proceedings of ESANN 2006*, number LTS-CONF-2006-010, 2006.

[82] U. Hoffmann, J.-M. Vesin, T. Ebrahimi, and K. Diserens. An efficient P300-based brain-computer interface for disabled subjects. *J Neurosci Methods*, 167(1):115–125, Jan 2008.

[83] J. Höhne, M. Schreuder, B. Blankertz, and M. Tangermann. A novel 9-class auditory ERP paradigm driving a predictive text entry system. *Front Neurosci*, 5:99, 2011.

[84] T. Horiguchi, K. Ohta, and T. Nishikawa. An MEG study of P300 activity during a color discrimination task 2: source localization study. *Brain Dev*, 25(4):241–244, Jun 2003.

[85] P. Horki, C. Neuper, G. Pfurtscheller, and G. Müller-Putz. Asynchronous steady-state visual evoked potential based BCI control of a 2-DoF artificial upper limb. *Biomed Tech (Berl)*, 55(6):367–374, Dec 2010.

[86] P. Horki, T. Solis-Escalante, C. Neuper, and G. Müller-Putz. Combined motor imagery and SSVEP based BCI control of a 2 DoF artificial upper limb. *Med Biol Eng Comput*, 49(5):567–577, May 2011.

[87] H. Hotelling. The most predictable criterion. *Journal of educational Psychology*, 26(2):139, 1935.

[88] C. Hummel, A. Genow, G. Scheler, R. Hopfengartner, and H. Stefan. Differences between source localizations from MEG and EEG. In *Biomag*, pages 238–9, 2002.

[89] C. I. Hung, P. L. Lee, Y. T. Wu, L. F. Chen, T. C. Yeh, and J. C. Hsieh. Recognition of motor imagery electroencephalography using independent component analysis and machine classifiers. *Ann Biomed Eng*, 33(8):1053–1070, Aug 2005.

[90] J. Jin, B. Z. Allison, E. W. Sellers, C. Brunner, P. Horki, X. Wang, and C. Neuper. An adaptive P300-based control system. *J Neural Eng*, 8(3):036006, Jun 2011.

[91] Y. Kamitani and F. Tong. Decoding seen and attended motion directions from activity in the human visual cortex. *Curr Biol*, 16(11):1096–1102, Jun 2006.

[92] M. Kamrunnahar and A. Geronimo. Motor imagery task discrimination using wide-band frequency spectra with Slepian tapers. In *Engineering in Medicine and Biology Society (EMBC), 2010 Annual International Conference of the IEEE*, pages 3349–3352, 2010.

[93] E. R. Kandel, J. H. Schwartz, T. M. Jessell, et al. *Principles of neural science*, volume 4. McGraw-Hill New York, 2000.

[94] A. A. Karim, T. Hinterberger, J. Richter, J. Mellinger, N. Neumann, H. Flor, A. Kübler, and N. Birbaumer. Neural internet: Web surfing with brain potentials for the completely paralyzed. *Neurorehabil Neural Repair*, 20(4):508–515, Dec 2006.

[95] K. N. Kay, T. Naselaris, R. J. Prenger, and J. L. Gallant. Identifying natural images from human brain activity. *Nature*, 452(7185):352–355, Mar 2008.

[96] T. Kayikcioglu and O. Aydemir. A polynomial fitting and k-NN based approach for improving classification of motor imagery BCI data. *Pattern Recognition Letters*, 31(11):1207–1215, 2010.

[97] S. P. Kelly, E. C. Lalor, R. B. Reilly, and J. J. Foxe. Visual spatial attention tracking using high-density SSVEP data for independent brain-computer communication. *IEEE Trans Neural Syst Rehabil Eng*, 13(2):172–178, Jun 2005.

[98] M. Kennel, C. Reichert, U. Schmucker, H. Hinrichs, and J. W. Rieger. A robot for brain-controlled grasping. In *Proceedings of the Human-Robot Interaction Workshop*, March 2014.

[99] Y. Kim, S. Park, H. Yeom, M. Bang, J. Kim, C. Chung, and S. Kim. A study on a robot arm driven by three-dimensional trajectories predicted from non-invasive neural signals. *BioMedical Engineering Online*, 14(1), 2015. cited By 0.

[100] D. S. Klobassa, T. Vaughan, P. Brunner, N. Schwartz, J. Wolpaw, C. Neuper, and E. Sellers. Toward a high-throughput auditory P300-based brain–computer interface. *Clinical Neurophysiology*, 120(7):1252–1261, 2009.

[101] M. Krauledat, M. Tangermann, B. Blankertz, and K.-R. Müller. Towards zero training for brain-computer interfacing. *PLoS One*, 3(8):e2967, 2008.

[102] D. Krusienski, E. Sellers, and T. Vaughan. Common spatio-temporal patterns for the P300 Speller. In *Neural Engineering, 2007. CNE '07. 3rd International IEEE/EMBS Conference on*, pages 421–424, 2007.

[103] D. J. Krusienski, D. J. McFarland, and J. R. Wolpaw. An evaluation of autoregressive spectral estimation model order for brain-computer interface applications. *Conf Proc IEEE Eng Med Biol Soc*, 1:1323–1326, 2006.

[104] D. J. Krusienski, G. Schalk, D. J. McFarland, and J. R. Wolpaw. A mu-rhythm matched filter for continuous control of a brain-computer interface. *IEEE Trans Biomed Eng*, 54(2):273–280, Feb 2007.

[105] J. Kubánek, K. J. Miller, J. G. Ojemann, J. R. Wolpaw, and G. Schalk. Decoding flexion of individual fingers using electrocorticographic signals in humans. *J Neural Eng*, 6(6):066001, Dec 2009.

[106] A. Kübler and N. Birbaumer. Brain-computer interfaces and communication in paralysis: extinction of goal directed thinking in completely paralysed patients? *Clin Neurophysiol*, 119(11):2658–2666, Nov 2008.

[107] A. Kübler, B. Kotchoubey, T. Hinterberger, N. Ghanayim, J. Perelmouter, M. Schauer, C. Fritsch, E. Taub, and N. Birbaumer. The thought translation device: a neurophysiological approach to communication in total motor paralysis. *Exp Brain Res*, 124(2):223–232, Jan 1999.

[108] A. Kübler, F. Nijboer, J. Mellinger, T. M. Vaughan, H. Pawelzik, G. Schalk, D. J. McFarland, N. Birbaumer, and J. R. Wolpaw. Patients with ALS can use sensorimotor rhythms to operate a brain-computer interface. *Neurology*, 64(10):1775–1777, May 2005.

[109] T. N. Lal, M. Schröder, T. Hinterberger, J. Weston, M. Bogdan, N. Birbaumer, and B. Schölkopf. Support vector channel selection in BCI. *IEEE Trans Biomed Eng*, 51(6):1003–1010, Jun 2004.

[110] R. M. Leahy, J. C. Mosher, M. E. Spencer, M. X. Huang, and J. D. Lewine. A study of dipole localization accuracy for MEG and EEG using a human skull phantom. *Electroencephalogr Clin Neurophysiol*, 107(2):159–173, Aug 1998.

[111] H. Lee and S. Choi. PCA+HMM+SVM for EEG pattern classification. In *Signal Processing and Its Applications, 2003. Proceedings. Seventh International Symposium on*, volume 1, pages 541–544. IEEE, 2003.

[112] R. Leeb, D. Friedman, G. R. Müller-Putz, R. Scherer, M. Slater, and G. Pfurtscheller. Self-paced (asynchronous) BCI control of a wheelchair in virtual environments: a case study with a tetraplegic. *Comput Intell Neurosci*, page 79642, 2007.

[113] R. Leeb, H. Sagha, R. Chavarriaga, and J. D. R. Millán. A hybrid brain-computer interface based on the fusion of electroencephalographic and electromyographic activities. *J Neural Eng*, 8(2):025011, Apr 2011.

[114] A. Lenhardt, M. Kaper, and H. J. Ritter. An adaptive P300-based online brain-computer interface. *IEEE Trans Neural Syst Rehabil Eng*, 16(2):121–130, Apr 2008.

[115] E. C. Leuthardt, K. J. Miller, G. Schalk, R. P. N. Rao, and J. G. Ojemann. Electrocorticography-based brain computer interface–the Seattle experience. *IEEE Trans Neural Syst Rehabil Eng*, 14(2):194–198, Jun 2006.

[116] E. Lew, R. Chavarriaga, S. Silvoni, and J. D. R. Millán. Detection of self-paced reaching movement intention from EEG signals. *Front Neuroeng*, 5:13, 2012.

[117] C. G. Lim, T. S. Lee, C. Guan, D. S. S. Fung, Y. Zhao, S. S. W. Teng, H. Zhang, and K. R. R. Krishnan. A brain-computer interface based attention training program for treating attention deficit hyperactivity disorder. *PLoS One*, 7(10):e46692, 2012.

[118] Z. Lin, C. Zhang, W. Wu, and X. Gao. Frequency recognition based on canonical correlation analysis for SSVEP-based BCIs. *IEEE Trans Biomed Eng*, 53(12):2610–2614, 2006.

[119] D. E. J. Linden. The P300: where in the brain is it produced and what does it tell us? *Neuroscientist*, 11(6):563–576, Dec 2005.

[120] A. K. Liu, A. M. Dale, and J. W. Belliveau. Monte Carlo simulation studies of EEG and MEG localization accuracy. *Hum Brain Mapp*, 16(1):47–62, May 2002.

[121] Y. Liu, Z. Zhou, and D. Hu. Gaze independent brain-computer speller with covert visual search tasks. *Clin Neurophysiol*, 122(6):1127–1136, Jun 2011.

[122] J. Long, Y. Li, T. Yu, and Z. Gu. Target selection with hybrid feature for BCI-based 2-D cursor control. *IEEE Trans Biomed Eng*, 59(1):132–140, 2012.

[123] F. Lotte, M. Congedo, A. Lécuyer, F. Lamarche, and B. Arnaldi. A review of classification algorithms for EEG-based brain-computer interfaces. *J Neural Eng*, 4(2):R1–R13, Jun 2007.

[124] W. Q. Malik, W. Truccolo, E. N. Brown, and L. R. Hochberg. Efficient decoding with steady-state Kalman filter in neural interface systems. *IEEE Trans Neural Syst Rehabil Eng*, 19(1):25–34, Feb 2011.

[125] D. J. McFarland, W. A. Sarnacki, and J. R. Wolpaw. Electroencephalographic (EEG) control of three-dimensional movement. *J Neural Eng*, 7(3):036007, Jun 2010.

[126] D. J. McFarland and J. R. Wolpaw. Sensorimotor rhythm-based brain-computer interface (BCI): model order selection for autoregressive spectral analysis. *J Neural Eng*, 5(2):155–162, Jun 2008.

[127] A. Mecklinger, B. Maess, B. Opitz, E. Pfeifer, D. Cheyne, and H. Weinberg. A MEG analysis of the P300 in visual discrimination tasks. *Electroencephalogr Clin Neurophysiol*, 108(1):45–56, Jan 1998.

[128] J. Mellinger, G. Schalk, C. Braun, H. Preissl, W. Rosenstiel, N. Birbaumer, and A. Kübler. An MEG-based brain-computer interface (BCI). *Neuroimage*, 36(3):581–593, Jul 2007.

[129] J. D. R. Millán, M. Franzé, J. Mouriño, F. Cincotti, and F. Babiloni. Relevant EEG features for the classification of spontaneous motor-related tasks. *Biol Cybern*, 86(2):89–95, Feb 2002.

[130] J. d. R. Millán, F. Galán, D. Vanhooydonck, E. Lew, J. Philips, and M. Nuttin. Asynchronous non-invasive brain-actuated control of an intelligent wheelchair. *Conf Proc IEEE Eng Med Biol Soc*, 2009:3361–3364, 2009.

[131] J. d. R. Millán, F. Renkens, J. Mouriño, and W. Gerstner. Noninvasive brain-actuated control of a mobile robot by human EEG. *IEEE Trans Biomed Eng*, 51(6):1026–1033, Jun 2004.

[132] J. d. R. Millán, R. Rupp, G. R. Müller-Putz, R. Murray-Smith, C. Giugliemma, M. Tangermann, C. Vidaurre, F. Cincotti, A. Kübler, R. Leeb, C. Neuper, K.-R. Müller, and D. Mattia. Combining brain-computer interfaces and assistive technologies: State-of-the-art and challenges. *Front Neurosci*, 4, 2010.

[133] K. J. Miller, E. C. Leuthardt, G. Schalk, R. P. N. Rao, N. R. Anderson, D. W. Moran, J. W. Miller, and J. G. Ojemann. Spectral changes in cortical surface potentials during motor movement. *J Neurosci*, 27(9):2424–2432, Feb 2007.

[134] M. Mishkin, L. G. Ungerleider, and K. A. Macko. Object vision and spatial vision: two cortical pathways. *Trends in neurosciences*, 6:414–417, 1983.

[135] T. M. Mitchell, R. Hutchinson, R. S. Niculescu, F. Pereira, X. Wang, M. Just, and S. Newman. Learning to decode cognitive states from brain images. *Machine Learning*, 57(1-2):145–175, 2004.

[136] E. Mugler, M. Bensch, S. Halder, W. Rosenstiel, M. Bogdan, N. Birbaumer, and A. Kübler. Control of an internet browser using the P300 event related potential. *International Journal of Bioelectromagnetism*, 10(1):56–63, 2008.

[137] K.-R. Müller, M. Krauledat, G. Dornhege, G. Curio, and B. Blankertz. Machine learning techniques for brain-computer interfaces. *Biomedical Engineering (Biomedizinische Technik)*, 49(1):11–22, 2004.

[138] K.-R. Müller, M. Tangermann, G. Dornhege, M. Krauledat, G. Curio, and B. Blankertz. Machine learning for real-time single-trial EEG-analysis: from brain-computer interfacing to mental state monitoring. *J Neurosci Methods*, 167(1):82–90, Jan 2008.

[139] T. Müller, T. Ball, R. Kristeva-Feige, T. Mergner, and J. Timmer. Selecting relevant electrode positions for classification tasks based on the electro-encephalogram. *Med Biol Eng Comput*, 38(1):62–67, Jan 2000.

[140] G. R. Müller-Putz and G. Pfurtscheller. Control of an electrical prosthesis with an SSVEP-based BCI. *IEEE Trans Biomed Eng*, 55(1):361–364, Jan 2008.

[141] G. R. Müller-Putz, R. Scherer, C. Brauneis, and G. Pfurtscheller. Steady-state visual evoked potential (SSVEP)-based communication: impact of harmonic frequency components. *J Neural Eng*, 2(4):123–130, Dec 2005.

[142] G. R. Müller-Putz, R. Scherer, G. Pfurtscheller, and C. Neuper. Temporal coding of brain patterns for direct limb control in humans. *Front Neurosci*, 4, 2010.

[143] F. Nijboer, E. W. Sellers, J. Mellinger, M. A. Jordan, T. Matuz, A. Furdea, S. Halder, U. Mochty, D. J. Krusienski, T. M. Vaughan, J. R. Wolpaw, N. Birbaumer, and A. Kübler. A P300-based brain-computer interface for people with amyotrophic lateral sclerosis. *Clin Neurophysiol*, 119(8):1909–1916, Aug 2008.

[144] D. P. Nowlis and J. Kamiya. The control of electroencephalographic alpha rhythms through auditory feedback and the associated mental activity. *Psychophysiology*, 6(4):476–484, Jan 1970.

[145] S. Ogawa, T.-M. Lee, A. S. Nayak, and P. Glynn. Oxygenation-sensitive contrast in magnetic resonance image of rodent brain at high magnetic fields. *Magnetic resonance in medicine*, 14(1):68–78, 1990.

[146] R. Ortner, B. Z. Allison, G. Korisek, H. Gaggl, and G. Pfurtscheller. An SSVEP BCI to control a hand orthosis for persons with tetraplegia. *IEEE Trans Neural Syst Rehabil Eng*, 19(1):1–5, Feb 2011.

[147] S. Parini, L. Maggi, A. C. Turconi, and G. Andreoni. A robust and self-paced BCI system based on a four class SSVEP paradigm: algorithms and protocols for a high-transfer-rate direct brain communication. *Comput Intell Neurosci*, page 864564, 2009.

[148] L. C. Parra, C. D. Spence, A. D. Gerson, and P. Sajda. Response error correction–a demonstration of improved human-machine performance using real-time EEG monitoring. *IEEE Trans Neural Syst Rehabil Eng*, 11(2):173–177, Jun 2003.

[149] L. C. Parra, C. D. Spence, A. D. Gerson, and P. Sajda. Recipes for the linear analysis of EEG. *Neuroimage*, 28(2):326–341, Nov 2005.

[150] B. N. Pasley, S. V. David, N. Mesgarani, A. Flinker, S. A. Shamma, N. E. Crone, R. T. Knight, and E. F. Chang. Reconstructing speech from human auditory cortex. *PLoS Biol*, 10(1):e1001251, Jan 2012.

[151] S. Perdikis, R. Leeb, N. Liboni, M. Tangermann, and J. d. R. Millán. TOBI project: BCI for enhancing communication and control capabilities of disabled people. BBCI Workshop Berlin 2009, 2009.

[152] S. Perdikis, R. Leeb, J. Williamson, A. Ramsay, M. Tavella, L. Desideri, E.-J. Hoogerwerf, A. Al-Khodairy, R. Murray-Smith, and J. D. R. Millán. Clinical evaluation of BrainTree, a motor imagery hybrid BCI speller. *J Neural Eng*, 11(3):036003, Jun 2014.

[153] G. Pfurtscheller, C. Guger, G. Müller, G. Krausz, and C. Neuper. Brain oscillations control hand orthosis in a tetraplegic. *Neurosci Lett*, 292(3):211–214, Oct 2000.

[154] G. Pfurtscheller, P. Linortner, R. Winkler, G. Korisek, and G. Müller-Putz. Discrimination of motor imagery-induced EEG patterns in patients with complete spinal cord injury. *Comput Intell Neurosci*, page 104180, 2009.

[155] G. Pfurtscheller and F. H. Lopes da Silva. Event-related EEG/MEG synchronization and desynchronization: basic principles. *Clinical neurophysiology*, 110(11):1842–1857, 1999.

[156] G. Pfurtscheller, C. Neuper, A. Schlögl, and K. Lugger. Separability of EEG signals recorded during right and left motor imagery using adaptive autoregressive parameters. *IEEE Trans Rehabil Eng*, 6(3):316–325, Sep 1998.

[157] J. Pineda, B. Allison, and A. Vankov. The effects of self-movement, observation, and imagination on μ rhythms and readiness potentials (RP's): toward a brain-computer interface (BCI). *IEEE Trans Rehabil Eng*, 8(2):219–222, 2000.

[158] T. Pistohl, T. Ball, A. Schulze-Bonhage, A. Aertsen, and C. Mehring. Prediction of arm movement trajectories from ECoG-recordings in humans. *J Neurosci Methods*, 167(1):105–114, Jan 2008.

[159] J. Polich. Updating P300: an integrative theory of P3a and P3b. *Clin Neurophysiol*, 118(10):2128–2148, Oct 2007.

[160] V. S. Polikov, P. A. Tresco, and W. M. Reichert. Response of brain tissue to chronically implanted neural electrodes. *J Neurosci Methods*, 148(1):1–18, Oct 2005.

[161] P. Poryzala and A. Materka. Cluster analysis of CCA coefficients for robust detection of the asynchronous SSVEPs in brain–computer interfaces. *Biomedical Signal Processing and Control*, 10:201–208, 2014.

[162] G. Prasad, P. Herman, D. Coyle, S. McDonough, and J. Crosbie. Applying a brain-computer interface to support motor imagery practice in people with stroke for upper limb recovery: a feasibility study. *J Neuroeng Rehabil*, 7:60, 2010.

[163] Y. Punsawad, Y. Wongsawat, and M. Parnichkun. Hybrid EEG-EOG brain–computer interface system for practical machine control. In *Engineering in Medicine and Biology Society (EMBC), 2010 Annual International Conference of the IEEE*, pages 1360–1363, 2010.

[164] F. Quandt, C. Reichert, H. Hinrichs, H. J. Heinze, R. T. Knight, and J. W. Rieger. Single trial discrimination of individual finger movements on one hand: A combined MEG and EEG study. *Neuroimage*, 59(4):3316–3324, Feb 2012.

[165] F. Quandt, C. Reichert, B. Schneider, S. Dürschmid, D. Richter, H. Hinrichs, and J. Rieger. Fundamentals and application of brain-machine interfaces (BMI) [Grundlagen und Anwendung von Brain-Machine Interfaces (BMI)]. *Klinische Neurophysiologie*, 43 (02):158–167, 2012.

[166] A. Ramos-Murguialday, M. Schürholz, V. Caggiano, M. Wildgruber, A. Caria, E. M. Hammer, S. Halder, and N. Birbaumer. Proprioceptive feedback and brain computer interface (BCI) based neuroprostheses. *PLoS One*, 7(10):e47048, 2012.

[167] H. Ramoser, J. Müller-Gerking, and G. Pfurtscheller. Optimal spatial filtering of single trial EEG during imagined hand movement. *IEEE Trans Rehabil Eng*, 8(4):441–446, 2000.

[168] S. Ray, N. E. Crone, E. Niebur, P. J. Franaszczuk, and S. S. Hsiao. Neural correlates of high-gamma oscillations (60-200 Hz) in macaque local field potentials and their potential implications in electrocorticography. *J Neurosci*, 28(45):11526–11536, Nov 2008.

[169] D. Regan. Some characteristics of average steady-state and transient responses evoked by modulated light. *Electroencephalogr Clin Neurophysiol*, 20(3):238–248, Mar 1966.

[170] C. Reichert, S. Dürschmid, R. Kruse, and H. Hinrichs. Efficient recognition of event-related potentials in high-density MEG recordings. In *Computer Science and Electronic Engineering Conference (CEEC), 2015 7th*, pages 81–86, Sept 2015.

[171] C. Reichert, R. Fendrich, J. Bernarding, C. Tempelmann, H. Hinrichs, and J. W. Rieger. Online tracking of the contents of conscious perception using real-time fMRI. *Front Neurosci*, 8:116, 2014.

[172] C. Reichert, M. Kennel, R. Kruse, H.-J. Heinze, U. Schmucker, H. Hinrichs, and J. W. Rieger. Robotic grasp initiation by gaze independent brain controlled selection of virtual reality objects. In *NEUROTECHNIX 2013 - Proceedings of the International Congress on Neurotechnology, Electronics and Informatics*, pages 5–12. SciTePress, 2013.

[173] C. Reichert, M. Kennel, R. Kruse, and H. Hinrichs. An asynchronous BMI for autonomous robotic grasping based on SSVEF detection. In *Proceedings of the 6th Brain-Computer Interface Conference 2014*, 2014.

[174] C. Reichert, M. Kennel, R. Kruse, H. Hinrichs, and J. W. Rieger. Efficiency of SSVEF Recognition from the Magnetoencephalogram - A Comparison of Spectral Feature Classification and CCA-based Prediction. In *NEUROTECHNIX 2013 - Proceedings of the International Congress on Neurotechnology, Electronics and Informatics*, pages 233–237. SciTePress, 2013.

[175] J. W. Rieger, C. Reichert, K. R. Gegenfurtner, T. Noesselt, C. Braun, H.-J. Heinze, R. Kruse, and H. Hinrichs. Predicting the recognition of natural scenes from single trial MEG recordings of brain activity. *Neuroimage*, 42(3):1056–1068, Sep 2008.

[176] B. Rivet, A. Souloumiac, V. Attina, and G. Gibert. xDAWN algorithm to enhance evoked potentials: application to brain-computer interface. *IEEE Trans Biomed Eng*, 56(8):2035–2043, Aug 2009.

[177] S. E. Robinson. Environmental noise cancellation for biomagnetic measurements. In *Advances in biomagnetism*, pages 721–724. Springer, 1989.

[178] B. Rockstroh. *Slow cortical potentials and behaviour*. Urban & Schwarzenberg, 1989.

[179] S. Ruiz, K. Buyukturkoglu, M. Rana, N. Birbaumer, and R. Sitaram. Real-time fMRI brain computer interfaces: self-regulation of single brain regions to networks. *Biol Psychol*, 95:4–20, Jan 2014.

[180] E. Sadeghian and M. Moradi. Continuous detection of motor imagery in a four-class asynchronous BCI. In *Engineering in Medicine and Biology Society, 2007. EMBS 2007. 29th Annual International Conference of the IEEE*, pages 3241–3244, 2007.

[181] T. H. Sander, J. Preusser, R. Mhaskar, J. Kitching, L. Trahms, and S. Knappe. Magnetoencephalography with a chip-scale atomic magnetometer. *Biomed Opt Express*, 3(5):981–990, May 2012.

[182] G. Schalk, J. Kubánek, K. J. Miller, N. R. Anderson, E. C. Leuthardt, J. G. Ojemann, D. Limbrick, D. Moran, L. A. Gerhardt, and J. R. Wolpaw. Decoding two-dimensional movement trajectories using electrocorticographic signals in humans. *J Neural Eng*, 4(3):264–275, Sep 2007.

[183] G. Schalk and E. C. Leuthardt. Brain-computer interfaces using electrocorticographic signals. *IEEE Rev Biomed Eng*, 4:140–154, 2011.

[184] G. Schalk, K. J. Miller, N. R. Anderson, J. A. Wilson, M. D. Smyth, J. G. Ojemann, D. W. Moran, J. R. Wolpaw, and E. C. Leuthardt. Two-dimensional movement control using electrocorticographic signals in humans. *J Neural Eng*, 5(1):75–84, Mar 2008.

[185] G. Schalk, J. R. Wolpaw, D. J. McFarland, and G. Pfurtscheller. EEG-based communication: presence of an error potential. *Clin Neurophysiol*, 111(12):2138–2144, Dec 2000.

[186] R. Scherer, F. Lee, A. Schlögl, R. Leeb, H. Bischof, and G. Pfurtscheller. Toward self-paced brain–computer communication: Navigation through virtual worlds. *IEEE Trans Biomed Eng*, 55(2):675–682, 2008.

[187] R. Scherer, G. R. Müller, C. Neuper, B. Graimann, and G. Pfurtscheller. An asynchronously controlled EEG-based virtual keyboard: improvement of the spelling rate. *IEEE Trans Biomed Eng*, 51(6):979–984, Jun 2004.

[188] M. Schreuder, T. Rost, and M. Tangermann. Listen, you are writing! Speeding up online spelling with a dynamic auditory BCI. *Front Neurosci*, 5:112, 2011.

[189] S. Schröer, I. Killmann, B. Frank, M. Volker, L. Fiederer, T. Ball, and W. Burgard. An autonomous robotic assistant for drinking. In *Robotics and Automation (ICRA), 2015 IEEE International Conference on*, pages 6482–6487, 2015.

[190] E. W. Sellers and E. Donchin. A P300-based brain-computer interface: initial tests by ALS patients. *Clin Neurophysiol*, 117(3):538–548, Mar 2006.

[191] E. W. Sellers, D. J. Krusienski, D. J. McFarland, T. M. Vaughan, and J. R. Wolpaw. A P300 event-related potential brain–computer interface (BCI): the effects of matrix size and inter stimulus interval on performance. *Biological psychology*, 73(3):242–252, 2006.

[192] H. Serby, E. Yom-Tov, and G. F. Inbar. An improved P300-based brain-computer interface. *IEEE Trans Neural Syst Rehabil Eng*, 13(1):89–98, Mar 2005.

[193] D. Sheng, S. Li, N. Dural, and M. V. Romalis. Subfemtotesla scalar atomic magnetometry using multipass cells. *Phys Rev Lett*, 110(16):160802, Apr 2013.

[194] J. D. Simeral, S.-P. Kim, M. J. Black, J. P. Donoghue, and L. R. Hochberg. Neural control of cursor trajectory and click by a human with tetraplegia 1000 days after implant of an intracortical microelectrode array. *J Neural Eng*, 8(2):025027, Apr 2011.

[195] K. M. Spencer, J. Dien, and E. Donchin. Spatiotemporal analysis of the late ERP responses to deviant stimuli. *Psychophysiology*, 38(2):343–358, Mar 2001.

[196] M. Spüler. A brain-computer interface (BCI) system to use arbitrary windows applications by directly controlling mouse and keyboard. In *In Proceedings of 37th Annual International Conference of the IEEE Engineering in Medicine and Biology Society (EMBC'15)*, pages 1087–1090, 08 2015.

[197] M. Spüler, M. Bensch, S. Kleih, W. Rosenstiel, M. Bogdan, and A. Kübler. Online use of error-related potentials in healthy users and people with severe motor impairment increases performance of a P300-BCI. *Clinical Neurophysiology*, 123(7):1328–1337, 2012.

[198] M. Spüler, W. Rosenstiel, and M. Bogdan. Online adaptation of a c-VEP brain-computer interface (BCI) based on error-related potentials and unsupervised learning. *PLoS One*, 7(12):e51077, 2012.

[199] M. Spüler, A. Walter, W. Rosenstiel, and M. Bogdan. Spatial filtering based on canonical correlation analysis for classification of evoked or event-related potentials in EEG data. *IEEE Trans Neural Syst Rehabil Eng*, 22(6):1097–1103, Nov 2014.

[200] N. K. Squires, K. C. Squires, and S. A. Hillyard. Two varieties of long-latency positive waves evoked by unpredictable auditory stimuli in man. *Electroencephalogr Clin Neurophysiol*, 38(4):387–401, Apr 1975.

[201] U. Strehl, U. Leins, G. Goth, C. Klinger, T. Hinterberger, and N. Birbaumer. Self-regulation of slow cortical potentials: a new treatment for children with attention-deficit/hyperactivity disorder. *Pediatrics*, 118(5):e1530–e1540, Nov 2006.

[202] D. Strüber and J. Polich. P300 and slow wave from oddball and single-stimulus visual tasks: inter-stimulus interval effects. *Int J Psychophysiol*, 45(3):187–196, Sep 2002.

[203] S. Sutton, M. Braren, J. Zubin, and E. R. John. Evoked-potential correlates of stimulus uncertainty. *Science*, 150(3700):1187–1188, Nov 1965.

[204] K. P. Thomas, C. Guan, C. T. Lau, A. P. Vinod, and K. K. Ang. A new discriminative common spatial pattern method for motor imagery brain-computer interfaces. *IEEE Trans Biomed Eng*, 56(11 Pt 2):2730–2733, Nov 2009.

[205] L. Tonin, T. Carlson, R. Leeb, and J. del Millan. Brain-controlled telepresence robot by motor-disabled people. In *Engineering in Medicine and Biology Society, EMBC, 2011 Annual International Conference of the IEEE*, pages 4227–4230, 2011.

[206] G. Townsend, B. K. LaPallo, C. B. Boulay, D. J. Krusienski, G. E. Frye, C. K. Hauser, N. E. Schwartz, T. M. Vaughan, J. R. Wolpaw, and E. W. Sellers. A novel P300-based brain-computer interface stimulus presentation paradigm: moving beyond rows and columns. *Clin Neurophysiol*, 121(7):1109–1120, Jul 2010.

[207] M. S. Treder and B. Blankertz. (C)overt attention and visual speller design in an ERP-based brain-computer interface. *Behav Brain Funct*, 6:28, 2010.

[208] M. S. Treder, N. M. Schmidt, and B. Blankertz. Gaze-independent brain–computer interfaces based on covert attention and feature attention. *Journal of neural engineering*, 8(6):066003, 2011.

[209] M. van Gerven, A. Bahramisharif, T. Heskes, and O. Jensen. Selecting features for BCI control based on a covert spatial attention paradigm. *Neural Netw*, 22(9):1271–1277, Nov 2009.

[210] M. Velliste, S. Perel, M. C. Spalding, A. S. Whitford, and A. B. Schwartz. Cortical control of a prosthetic arm for self-feeding. *Nature*, 453(7198):1098–1101, Jun 2008.

[211] F.-B. Vialatte, M. Maurice, J. Dauwels, and A. Cichocki. Steady-state visually evoked potentials: focus on essential paradigms and future perspectives. *Prog Neurobiol*, 90(4):418–438, Apr 2010.

[212] I. Volosyak. SSVEP-based Bremen-BCI interface–boosting information transfer rates. *J Neural Eng*, 8(3):036020, Jun 2011.

[213] I. Volosyak, D. Valbuena, T. Lüth, T. Malechka, and A. Gräser. BCI demographics II: how many (and what kinds of) people can use a high-frequency SSVEP BCI? *IEEE Trans Neural Syst Rehabil Eng*, 19(3):232–239, Jun 2011.

[214] M. Wang, I. Daly, B. Z. Allison, J. Jin, Y. Zhang, L. Chen, and X. Wang. A new hybrid BCI paradigm based on P300 and SSVEP. *J Neurosci Methods*, Jul 2014.

[215] Y. Wang, M. Sutherland, L. Sanfratello, and A. Tang. Single-trial classification of ERPs using second-order blind identification (SOBI). In *Machine Learning and Cybernetics, 2004. Proceedings of 2004 International Conference on*, volume 7, pages 4246–4251, 2004.

[216] Y. Wang, R. Wang, X. Gao, B. Hong, and S. Gao. A practical VEP-based brain-computer interface. *IEEE Trans Neural Syst Rehabil Eng*, 14(2):234–240, 2006.

[217] Y.-T. Wang, Y. Wang, and T.-P. Jung. A cell-phone-based brain-computer interface for communication in daily life. *J Neural Eng*, 8(2):025018, Apr 2011.

[218] Z. Wang, A. Gunduz, P. Brunner, A. L. Ritaccio, Q. Ji, and G. Schalk. Decoding onset and direction of movements using electrocorticographic (ECoG) signals in humans. *Front Neuroeng*, 5:15, 2012.

[219] N. Weiskopf. Real-time fMRI and its application to neurofeedback. *Neuroimage*, 62(2):682–692, Aug 2012.

[220] J. Wessberg, C. R. Stambaugh, J. D. Kralik, P. D. Beck, M. Laubach, J. K. Chapin, J. Kim, S. J. Biggs, M. A. Srinivasan, and M. A. Nicolelis. Real-time prediction of hand trajectory by ensembles of cortical neurons in primates. *Nature*, 408(6810):361–365, Nov 2000.

[221] J. J. Williams, A. G. Rouse, S. Thongpang, J. C. Williams, and D. W. Moran. Differentiating closed-loop cortical intention from rest: building an asynchronous electrocorticographic BCI. *J Neural Eng*, 10(4):046001, Aug 2013.

[222] J. Wolpaw, N. Birbaumer, W. Heetderks, D. McFarland, P. Peckham, G. Schalk, E. Donchin, C. Robinson, and T. Vaughan. Brain-computer interface technology: a review of the first international meeting. *IEEE Transactions on Rehabilitation Engineering*, 8(2):164–173, 2000.

[223] J. R. Wolpaw, N. Birbaumer, D. J. McFarland, G. Pfurtscheller, and T. M. Vaughan. Brain-computer interfaces for communication and control. *Clinical Neurophysiology*, 113(6):767–791, Jun 2002.

[224] J. R. Wolpaw and D. J. McFarland. Control of a two-dimensional movement signal by a noninvasive brain-computer interface in humans. *Proc. Natl. Acad. Sci. U. S. A.*, 101(51):17849–17854, Dec 2004.

[225] E. Yin, Z. Zhou, J. Jiang, F. Chen, Y. Liu, and D. Hu. A novel hybrid BCI speller based on the incorporation of SSVEP into the P300 paradigm. *J Neural Eng*, 10(2):026012, Apr 2013.

[226] E. Yin, Z. Zhou, J. Jiang, F. Chen, Y. Liu, and D. Hu. A speedy hybrid BCI spelling approach combining P300 and SSVEP. *IEEE Trans Biomed Eng*, 61(2):473–483, Feb 2014.

[227] N. Yoshimura and N. Itakura. A transient VEP-based real-time brain-computer interface using non-direct gazed visual stimuli. *Electromyogr Clin Neurophysiol*, 49(8):323–335, 2009.

[228] T. O. Zander, M. Gaertner, C. Kothe, and R. Vilimek. Combining eye gaze input with a brain–computer interface for touchless human–computer interaction. *Intl. Journal of Human–Computer Interaction*, 27(1):38–51, 2010.

[229] H. Zhang, C. Guan, and C. Wang. Asynchronous P300-based brain-computer interfaces: a computational approach with statistical models. *IEEE Trans Biomed Eng*, 55(6):1754–1763, Jun 2008.

[230] Y. Zhang, P. Xu, K. Cheng, and D. Yao. Multivariate synchronization index for frequency recognition of SSVEP-based brain-computer interface. *Journal of Neuroscience Methods*, 221:32–40, 2014. cited By (since 1996)3.

[231] D. Zhu, J. Bieger, G. Garcia Molina, and R. M. Aarts. A survey of stimulation methods used in SSVEP-based BCIs. *Comput Intell Neurosci*, page 702357, 2010.

[232] R. Zimmermann, L. Marchal-Crespo, J. Edelmann, O. Lambercy, M.-C. Fluet, R. Riener, M. Wolf, and R. Gassert. Detection of motor execution using a hybrid fNIRS-biosignal BCI: a feasibility study. *J Neuroeng Rehabil*, 10:4, 2013.

Ehrenerklärung

Ich versichere hiermit, dass ich die vorliegende Arbeit ohne unzulässige Hilfe Dritter und ohne Benutzung anderer als der angegebenen Hilfsmittel angefertigt habe; verwendete fremde und eigene Quellen sind als solche kenntlich gemacht. Insbesondere habe ich nicht die Hilfe eines kommerziellen Promotionsberaters in Anspruch genommen. Dritte haben von mir weder unmittelbar noch mittelbar geldwerte Leistungen für Arbeiten erhalten, die im Zusammenhang mit dem Inhalt der vorgelegten Dissertation stehen.

Ich habe insbesondere nicht wissentlich:
-       Ergebnisse erfunden oder widersprüchliche Ergebnisse verschwiegen,
-       statistische Verfahren absichtlich missbraucht, um Daten in ungerechtfertigter Weise zu interpretieren,
-       fremde Ergebnisse oder Veröffentlichungen plagiiert,
-       fremde Forschungsergebnisse verzerrt wiedergegeben.

Mir ist bekannt, dass Verstöße gegen das Urheberrecht Unterlassungs- und Schadensersatzansprüche des Urhebers sowie eine strafrechtliche Ahndung durch die Strafverfolgungsbehörden begründen kann. Die Arbeit wurde bisher weder im Inland noch im Ausland in gleicher oder ähnlicher Form als Dissertation eingereicht und ist als Ganzes auch noch nicht veröffentlicht."

Magdeburg, den 01.12.2016

Christoph Reichert